TABLE DES MATIÈRES

REMERCIEMENTS ..... **iv**

AVANT-PROPOS ..... **v**

RÉSUMÉ ..... **vii**

LISTE DES FIGURES ..... **xii**

LISTE DES ACRONYMES, SIGLES ET SYMBOLES ..... **xiv**

CHAPITRE I
INTRODUCTION GÉNÉRALE **1**

1.1 Mise en contexte : généralités sur les porphyrines et leurs dérivés 1

1.2 Structure des porphyrines 3

1.3 Nomenclature 4

1.4 Propriétés des porphyrines 5

1.4.1 Propriétés optiques 5

1.4.2 Propriétés photochimiques 7

1.5 Intérêts et limites des porphyrines endogènes 9

1.5.1 Applications potentielles 9

1.6 Problème 12

1.7 Revue de la littérature sur les différentes méthodes de photoprotection des porphyrines naturelles et leurs dérivés 12

1.8 Présentation du projet de thèse 15

1.9 Notions essentielles sur l'augmentation de l'émission de fluorescence d'un fluorophe par un métal 18

1.10 Notions essentielles sur l'augmentation de la production d'oxygène singulet du photosensibilisateur par un métal 21

1.11 Hypothèses de recherche 22

1.12 Objectif général de cette thèse 23

1.13 Objectifs opérationnels 23

1.14 Organisation du document 23

1.15 Références 24

CHAPITRE II
BENEFICIAL ROLE OF GOLD NANOPARTICLES AS PHOTOPROTECTOR OF MAGNESIUM TETRAPHENYLPORPHYRIN..... 32

2.1 Résumé de l'article 32

2.2 Premier article scientifique 33

Abstract 33

Introduction 34

Experimental section 35

Materials and methods 35

Synthesis of Au nanoparticles 35

Photodegradation measurements 36

X-Ray Photoemission Spectroscopy (XPS) 36

Percentage photoprotection 37

Determination of the fraction of the light absorbed by MgTPP (5.3 μM) and AuNPs of varying concentrations (2-130 μM) in the mixture of MgTPP and AuNPs 37

Results and discussion 39

Conclusions 49

Acknowledgments 49

Références 50

CHAPITRE III
ENHANCED PHOTOSTABILITY OF CHLOROPHYLL-*A* USING GOLD NANOPARTICLES AS AN EFFICIENT PHOTOPROTECTOR..... 70

3.1 Résumé de l'article 70

3.2 Deuxième article scientifique 71

Abstract 71

Introduction 72

Materials and methods 73

Materials 73

Synthesis of gold nanoparticles (AuNPs) 73

Photodegradation measurements 74

Absorption and emission spectrometry 74

Transmission electron microscopy (TEM) 74

X-ray photoemission spectroscopy (XPS) 75

Percentage photostability 76

Results 76

Photodegradation of chlorophyll-*a* (Chl*a*) 76

Photoprotective action of gold nanoparticles 77

X-ray photoelectron spectroscopy (XPS) studies 80

Comparison of the photoprotective ability of AuNPs with other Chl*a* photoprotectors 83

Discussion 84

Conclusions 86

Acknowledgments 87

Références 87

CHAPITRE IV
NANO-SILVER COULD USHER IN NEXT GENERATION PHOTOPROTECTIVE AGENTS FOR NATURAL PORPHYRINS 109

4.1 Résumé de l'article 109

4.2 Troisième article scientifique 110

Abstract 110

Experimental Section 122

Acknowledgements 125

References 125

CHAPITRE V
CONCLUSION ET PERSPECTIVES 146

5.1 Conclusion générale 146

5.2 Bilan des résultats 147

5.3 Contribution de la thèse à l'avancement des connaissances 150

5.4 Perspectives 150

5.4.1 Analyser systématiquement l'effet de la taille et de la forme des nanoparticules sur l'efficacité photoprotectrice 151

5.4.2 Examiner si la méthode de photoprotection mise en œuvre dans cette thèse peut être employée pour l'élaboration des nanoparticules fonctionnelles pour des applications médicales 153

5.5 Références 155

ANNEXE A
MÉTHODES EXPÉRIMENTALES, SYNTHÈSE ET INSTRUMENTATION . 157

A.1 Synthèse générale des nanoparticules métalliques en solution 157

A.1.1 Préparation des nanoparticules d'or (AuNPs) 158

A.1.2 Préparation des nanoparticules d'argent (AgNPs) 159

A.2 Caractérisation des nanoparticules 160

A.2.1 Microscopie électronique à transmission (MET) 160

A.2.2 Spectrométrie d'absorption UV-visible 160

A.2.3 Spectroscopie de photoélectrons X (XPS) 161

A.3 Références 161

LISTE DES FIGURES

Figure		Page
1.1	Structure de quelques porphyrines endogènes	2
1.2	Structure chimique de porphyrine : (a) Porphyrine base libre; (b) Porphyrine base métallée ou métallo-porphyrine; (c) Représentation du système de 18 électrons π aromatiques	4
1.3	Système de nomenclature du macrocycle tétrapyrrolique	5
1.4	Spectres d'absorption et d'émission de la porphyrine H_2TPP dans le toluène à 25°C	6
1.5	Diagramme de Jablonski décrivant les transitions non radiatives et radiatives, impliquées lors de l'absorption d'un photon et de sa réémission par luminescence (fluorescence et phosphorescence)	7
1.6	Illustration schématique de la production des dérivés réactifs de l'oxygène par réaction photochimique des porphyrines	8
1.7	Diagramme de Jablonski qui montre qu'on peut inactiver de manière photodynamique les agents pathogéniques	10
1.8	Mécanisme de photodégradation du tétraphénylporphyrine de magnésium (MgTPP) avec formation d'époxyde	15
1.9	Mécanisme de photodégradation des dérivés de la chlorophylle	16
1.10	Représentation de la formation d'un plasmon de surface sur une nanoparticule métallique	19
1.11	Modification du processus d'absorption et de déexcitation par une nanoparticule métallique à proximité d'un fluorophore	21
1.12	Diagramme énergétique de la production d'oxygène singulet photosensibilisée *via* le couplage plasmon surface-photosensibilisateur	22
5.1	Solutions de nanoparticules d'or de différentes tailles. La différence de taille provoque la différence de couleur	152
5.2	Spectres de diffusion de la lumière par des nanoparticules d'argent de différentes formes	152

5.3 Représentation schématique de l'agent photoprotecteur magnétique de structure cœur-coquille Fe_3O_4@Au 154

5.4 Schéma illustrant le ciblage *in vivo* de la tumeur par champ magnétique externe 155

LISTE DES ACRONYMES, SIGLES ET SYMBOLES

Au	Or
Ag	Argent
AgNPs	Nanoparticules d'argent
AuNPs	Nanoparticules d'or
Chl*a*	Chlorophylle-*a*
Chl	Chlorophylle
eV	Électronvolt
HOMO	Niveau énergétique le plus haut occupé
H_2TTP	Tétraphenyl porphyrine base libre
H_2O_2	Peroxyde d'hydrogène
K_{app}	Constante d'association
K_s	Constante de formation
K_{SV}	Constante de Stern-Volmer
mL	Millilitre (10^{-3} L)
mM	Millimole (10^{-3} M)
MEF	Augmentation de l'émission de fluorescence par le métal
ME^1O_2	Augmentation de la génération d'oxygène singulet par le métal
MgTPP	Tétraphénylporphyrine de magnésium
MTPP	Tétraphénylporphyrine métallique
nM	Nanomole (10^{-9} M)
nm	Nanomètre (10^{-9} m)
NIR	Proche infrarouge
NP	Nanoparticule

$O_2^{\cdot -}$	Anion superoxyde
$^1O_2$	Oxygène singulet
$^3O_2$	Oxygène moléculaire
OH·	Radical hydroxyle
OLEDs	Diodes électroluminescentes organiques
OPV	Photovoltaïque organique
PDT	Thérapie photodynamique
^{1}Porp	État fondamental singulet de la porphyrine
^{3}Porp*	Porphyrine en état triplet
^{1}PS	État fondamental singulet du photosensibilisateur
^{1}PS*	État singulet excité du photosensibilisateur
^{3}PS*	État triplet du photosensibilisateur
^{3}Porp*	État triplet de la porphyrine
PS	Photosensibilisateur
R_4N^+	Tétraalkyl ammonium
ROSs	Dérivés réactifs de l'oxygène
TOAB	Bromure de tétraoctylammonium
µL	Microlitre (10^{-6} L)
µM	Micromole (10^{-3} M)
λ	Longueur d'onde

CHAPITRE I

INTRODUCTION GÉNÉRALE

1.1 Mise en contexte : généralités sur les porphyrines et leurs dérivés

Les porphyrines, les métalloporphyrines et leurs dérivés sont parmi les composés hétérocycliques aromatiques les plus étudiés de tous les composés macrocycliques[1]. Ces molécules peuvent être distinguées selon leur origine : soit d'origine endogène, si elles sont synthétisées à l'intérieur d'un organisme animal ou végétal, soit d'origine exogène, si elles ne le sont pas (c'est-à-dire qui proviennent des laboratoires). Les porphyrines entrent dans la composition de nombreux pigments et servent de base dans la formation de certaines molécules chez les organismes vivants. Les porphyrines endogènes participent à de nombreux processus physiologiques essentiels, dans bon nombre de cellules vivantes aussi bien végétales qu'animales (Figure 1.1). À titre d'exemple, l'on peut citer la cyanocobalamine, plus connue sous le nom de vitamine B12, qui est indispensable au bon développement du corps. Combinées à un ion fer, les porphyrines animales forment l'hème, un motif nécessaire à la fonction de nombreuses métalloprotéines : l'hème de l'hémoglobine des globules rouges assure le transport de l'oxygène et du dioxyde de carbone dans le sang. Enfin, liées à un ion magnésium, les porphyrines végétales forment la chlorophylle, indispensable à la photosynthèse. Cette classe de molécules organiques colorées, interagissent avec la lumière et comptant parmi les éléments fondamentaux de la vie, ne cesse de piquer la curiosité des chercheurs. Leur étude nourrit aujourd'hui des applications biotechnologiques innovantes dans des domaines aussi variés que la médecine, l'agronomie, la microélectronique ou l'optoélectronique. Les détails sur leurs potentielles applications sont fournis à la section 1.5.

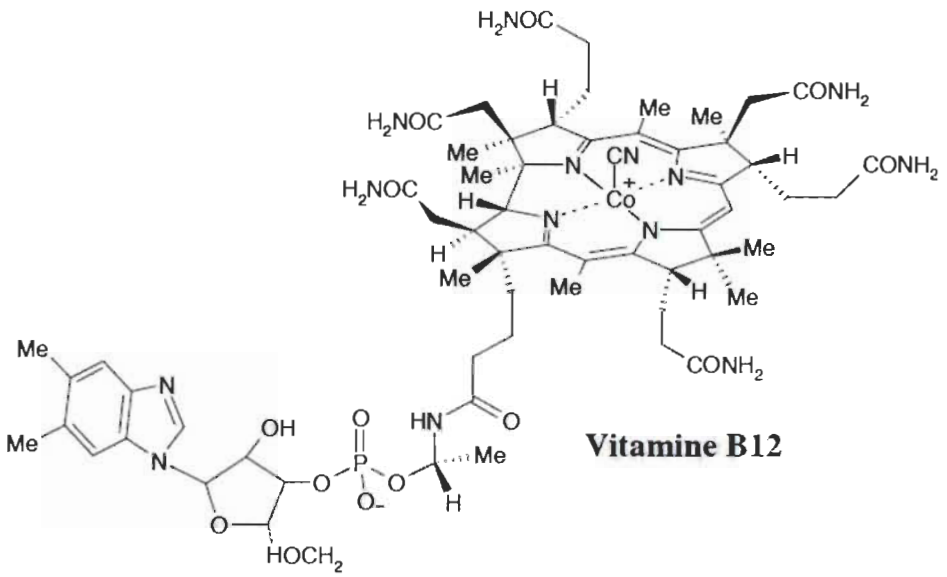

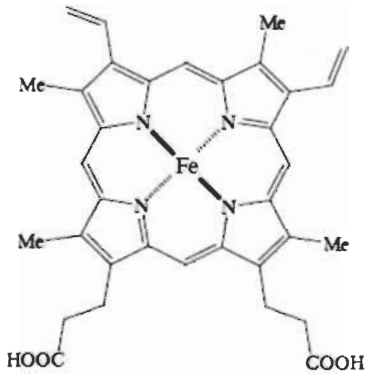

Le groupement hème de l'hémoglobine

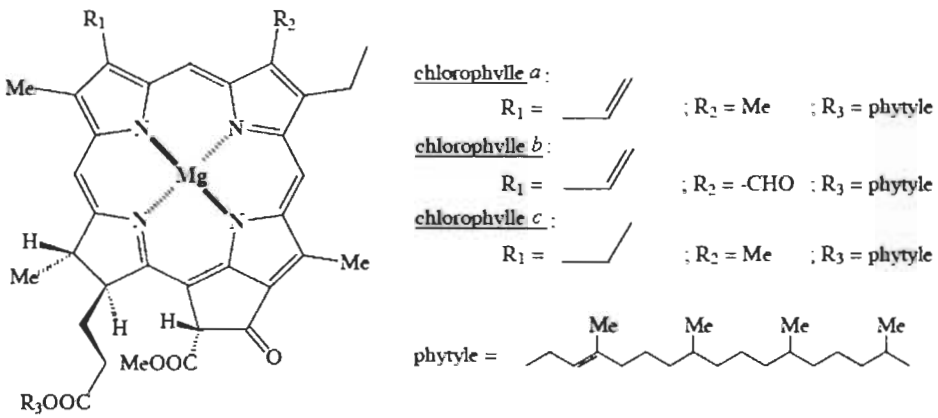

Chlorophylles

Figure 1.1 Structure de quelques porphyrines endogènes.

1.2 Structure des porphyrines

Les porphyrines forment une classe de composés cycliques dans lesquels le macrocycle principal se compose de quatre unités de type pyrrole, reliées entre elles par des ponts de carbone simple (méthine) (Figure 1.2). Ces macrocycliques tétrapyrroliques mesurent environ 9 Å et possèdent une cavité centrale d'environ 4,2 Å de diamètre[2]. La cavité centrale de la porphyrine possède une taille idéale pour être occupée par les métaux de transition de la première série (fer, cobalt, nickel, cuivre, zinc, ect), les ions métalliques plus volumineux sont localisés au-dessus du macrocycle, ce qui oblige la porphyrine à adopter une conformation en forme de dôme. Les porphyrines sont des composés aromatiques possédant 18 électrons π conjugués qui leur confèrent une forte coloration et une fluorescence intrinsèque. Le macrocycle tétrapyrrolique aromatique est stable thermiquement, chimiquement et biologiquement. Ces composés ont également l'avantage d'être non toxiques lorsqu'ils ne sont pas soumis à la lumière[3]. Toutes les molécules issues des porphyrines (l'hème, la chlorophylle ou macrocycles dérivés) sont construites sur le même schéma : un anneau tétrapyrrolique au sein duquel peut être niché un ion métallique (Figure 1.2).

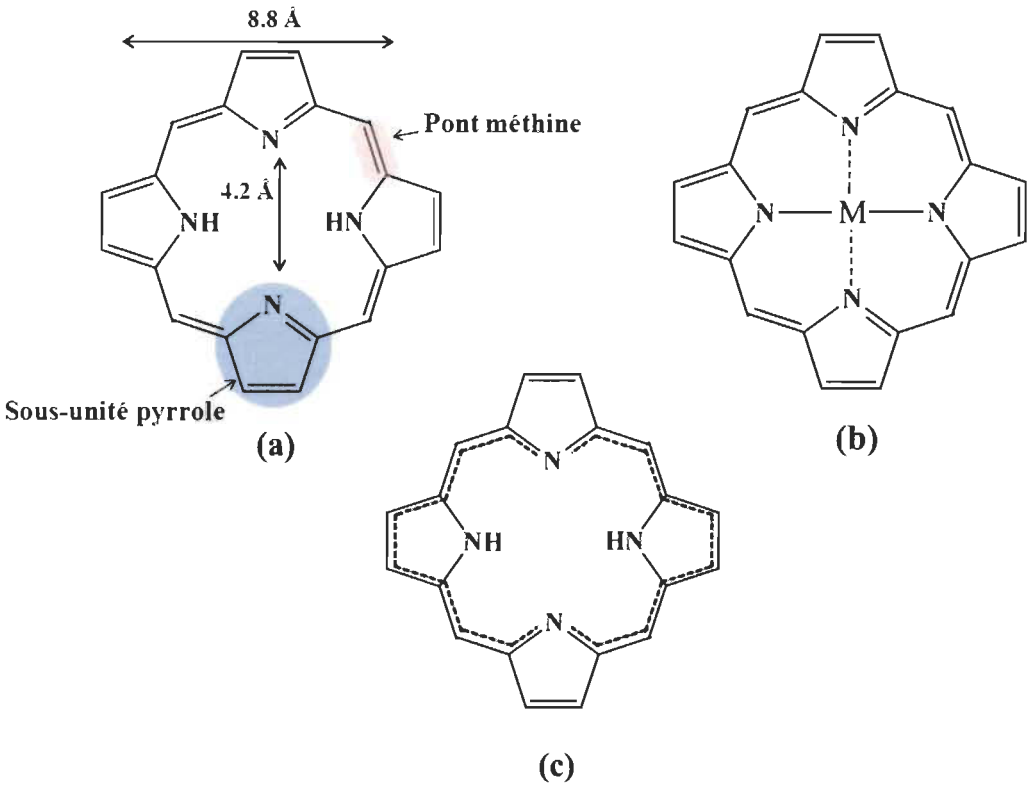

Figure 1.2 Structure chimique de porphyrine : (a) Porphyrine base libre; (b) Porphyrine base métallée ou métallo-porphyrine; (c) Représentation du système de 18 électrons π aromatiques.

1.3 Nomenclature

Le chimiste allemand Hans Fischer, lauréat du Prix Nobel de chimie en 1930 pour ses études sur les porphyrines, proposa un système de nomenclature, basé sur un système de numérotation de 1 à 24, pour désigner les porphyrines substituées sur les positions β–pyrroliques[4]. Dans cette nomenclature, les atomes de carbone des positions méthines, aussi appelés « méso », sont numérotés α, β, γ et δ et les carbones β-pyrroliques sont notés 1, 2, 3, 4, 5, 6, 7 et 8 (Figure 1.3). Par la suite, une numérotation systématique du macrocycle a été adoptée en 1987, afin de simplifier la nomenclature de ces molécules[5]. Ainsi, les carbones *méso* portent alors les numéros 5, 10, 15, 20, les positions α et β des cycles pyrroliques sont notés respectivement 1, 4, 6, 9, 11, 14, 16, 19 et 2, 3, 7, 8, 12, 13, 17, 18 et enfin les numéros 21, 22, 23, 24 ont été attribués aux quatre atomes d'azote (Figure 1.3).

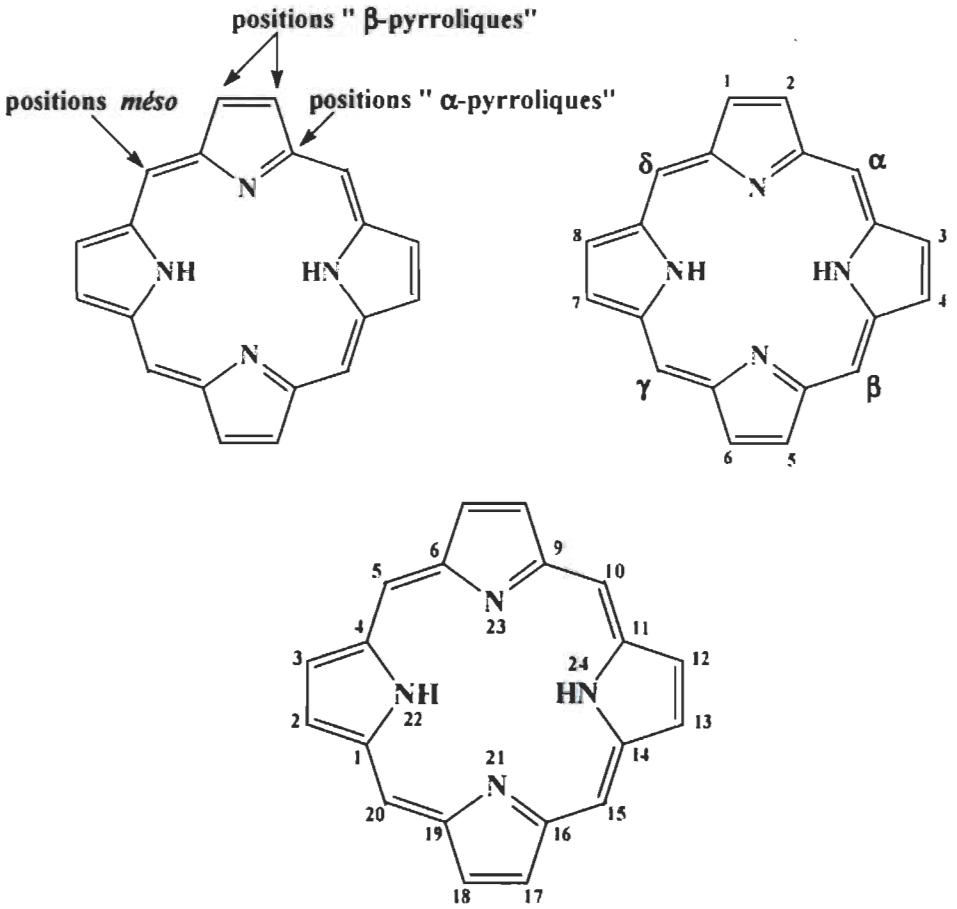

Figure 1.3 Système de nomenclature du macrocycle tétrapyrrolique.

1.4 Propriétés des porphyrines

1.4.1 Propriétés optiques

Les porphyrines présentent des spectres d'absorption et d'émission de fluorescence caractéristiques. À titre d'exemple, les spectres d'absorption et d'émission de fluorescence de la tétraphényl porphyrine base libre (H_2TTP) sont représentés à la figure 1.4[6a]. L'interprétation admise pour expliquer le spectre optique des porphyrines est la suivante : une bande d'absorption très forte est située dans le proche ultraviolet (proche UV) autour de 400 nm (connue sous le nom de bande de Soret ou bande B), correspondant à la transition de l'état électronique fondamental au second état

électronique singulet ($S_2 \leftarrow S_0$). Cette bande disparaît lorsque l'aromaticité du macrocycle est rompue. Dans la région du spectre visible, il existe quatre bandes supplémentaires autour de 500 à 760 nm dénommées bandes Q, responsables de la coloration intense de ces composés. Ces bandes d'absorption sont le résultat de la transition de l'état électronique fondamental au premier état électronique singulet ($S_1 \leftarrow S_0$). L'intensité des bandes Q des porphyrines est généralement sensible aux variations de structures du macrocycle. En effet, les bandes Q voient leur intensité relative varier considérablement, en fonction de la nature et de la position des substituants sur le macrocycle[7]. La plupart des porphyrines naturelles, telles que les chlorophylles, les bactériochlorophylles et leurs dérivés, ont des bandes d'absorption Q dans le proche infrarouge entre 650 et 780 nm et plusieurs ont été étudiées par divers chercheurs[8] pour leur utilisation comme agent photosensibilisateur. Par surcroît, l'excitation des chromophores porphyriques conduit à l'observation de deux fortes bandes d'émission de fluorescence, situées dans le NIR autour de 670 à 720 nm. Les interprétations du comportement photophysique des porphyrines sont résumées sur le diagramme de Jablonski, représenté à la figure 1.5.

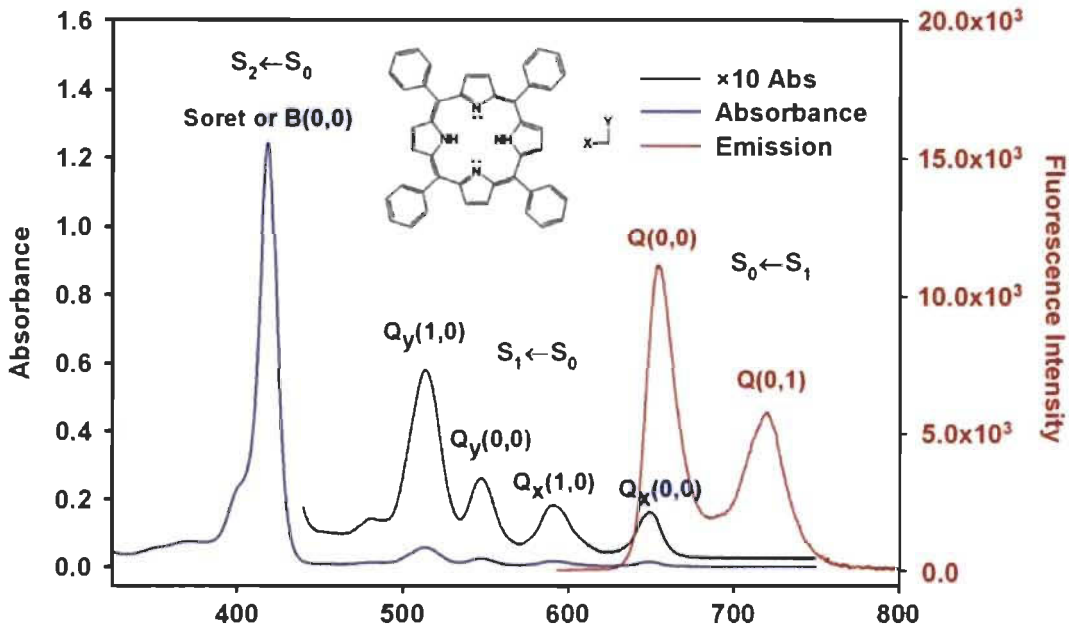

Figure 1.4 Spectres d'absorption et d'émission de la porphyrine H_2TPP dans le toluène à 25°C[6a].

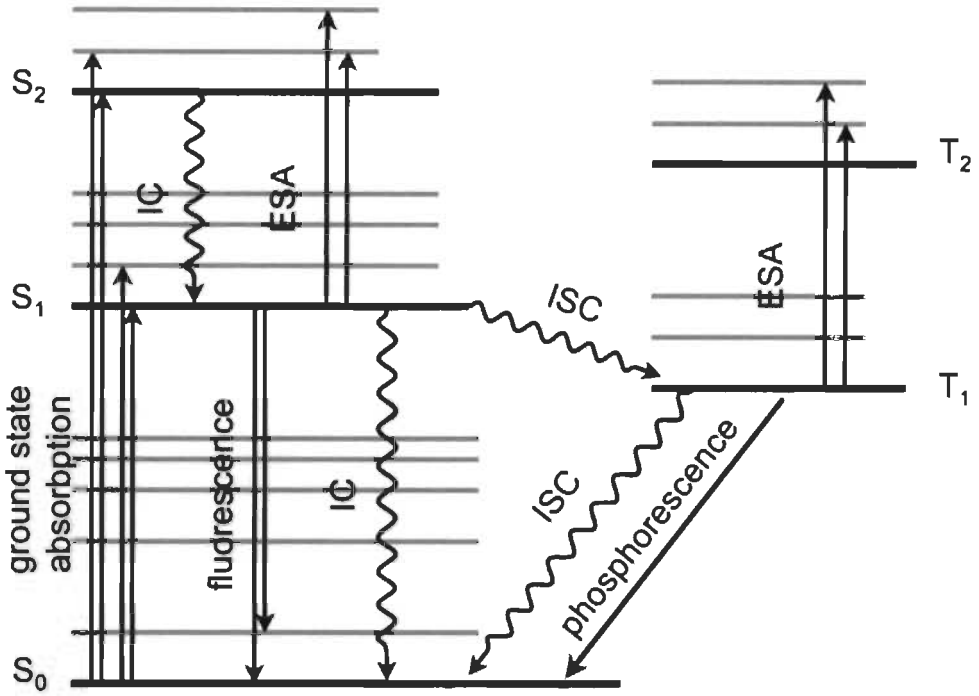

Figure 1.5 Diagramme de Jablonski décrivant les transitions non radiatives et radiatives, impliquées lors de l'absorption d'un photon et de sa réémission par luminescence (fluorescence et phosphorescence) [6b].

1.4.2 Propriétés photochimiques

Non seulement l'excitation des chromophores porphyriques produit généralement de la photoluminescence (fluorescence ou phosphorescence), mais elle permet également la production des dérivés réactifs de l'oxygène (en anglais reactive oxygen species, ROS). comme l'anion superoxyde ($O_2^{\bullet -}$), l'oxygène singulet ($^1O_2$), le radical hydroxyle ($OH^{\bullet}$), le peroxyde d'hydrogène H_2O_2, etc. Lorsque le photosensibilisateur (PS) à l'état fondamental singulet (^1PS) est stimulé par une lumière correspondant à son pic d'absorption, il est promu à son état singulet excité ($^1PS^*$). Dans cet état, plusieurs processus de désexcitation peuvent se produire rapidement, afin de ramener le $^1PS^*$ à son état fondamental ^1PS. Cependant, le processus de désexcitation indispensable à la formation des ROSs est la conversion intersystème (ISC pour intersystem crossing), à l'origine de la formation des PSs à l'état triplet ($^3PS^*$). Cet état triplet est moins énergétique que l'état singulet excité et possède une durée de vie beaucoup plus longue

que celle de l'état singulet excité (micro/millisecondes au lieu de nanosecondes). Le $^3PS^*$ peut revenir à l'état fondamental en émettant son énergie sous forme d'un photon (phénomène de phosphorescence), ou bien il peut interagir avec des molécules abondantes dans son environnement immédiat, tel que l'oxygène. L'interaction du $^3PS^*$ avec l'oxygène peut se produire de deux façons distinctes :

- Soit le $^3PS^*$ transfère directement un électron, parfois de concert avec un don de protons à la molécule d'oxygène pour former $O_2^{\bullet -}$, pouvant par la suite former d'autres ROS comme le $OH^\bullet$ et le H_2O_2 (Figure 1.6). Cette réaction photochimique est appelée réaction de Type I[9].

- Soit le $^3PS^*$ transfère son énergie par collision à la molécule d'oxygène. Compte tenu des règles de sélection qui spécifient que les interactions triplet-triplet sont autorisées, alors que les interactions triplet-singulet sont interdites[10], le $^3PS^*$ peut donc réagir facilement avec l'oxygène moléculaire, $^3O_2$ l'une des rares molécules de la nature dont l'état fondamental est un état triplet[11]. Cette réaction photochimique, connue sous le nom de réaction de Type II, est à l'origine de la formation du $^1O_2$ (Figure 1.6)[9].

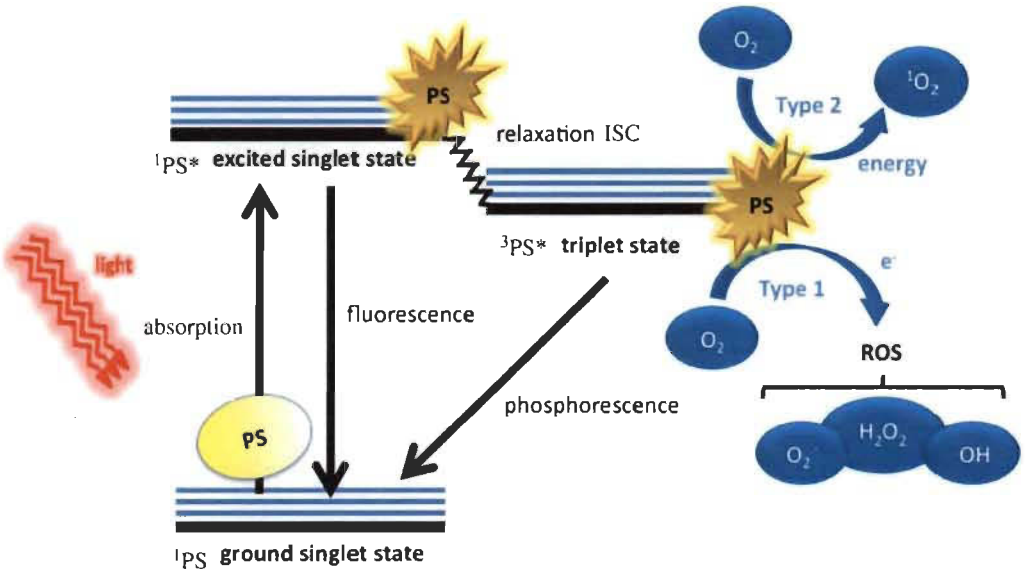

Figure 1.6 Illustration schématique de la production des dérivés réactifs de l'oxygène par réaction photochimique des porphyrines[9].

Les propriétés optiques et photochimiques évoquées ci-dessus incitent aujourd'hui les chercheurs à explorer le potentiel des molécules de porphyrines, en vue de développer des technologies novatrices et performantes pour le génie biomédical, l'optoélectronique, l'environnement, etc.

1.5 Intérêts et limites des porphyrines endogènes

1.5.1 Applications potentielles

Bien que le rôle biologique et physiologique des porphyrines dans leur milieu naturel soit bien connu, leur potentiel d'utilisation dans le développement des biotechnologies commence à peine à être élucidé. Du fait que les maximas des bandes d'absorption et d'émission des porphyrines naturelles sont situés dans la fenêtre thérapeutique (typiquement entre 650 et 900 nm), c'est-à-dire là où l'absorption globale des tissus biologiques est minimale, ils peuvent être utilisés comme agent de contraste pour l'imagerie optique par fluorescence. En effet, Fan et ses collègues ont étudié la possibilité d'utiliser les porphyrines endogènes comme produit de contraste pour l'imagerie médicale[12]. Ils ont démontré que les molécules de chlorophylles, extraites des feuilles de Chimonanthus salicifoliues, pourraient servir à l'imagerie clinique des ganglions sentinelles, c'est-à-dire, les premiers ganglions axillaires les plus proches de la tumeur et donc susceptibles d'être envahis par les cellules cancéreuses. De plus, leurs résultats des tests de cytotoxicité confirment que les molécules de chlorophylles présentent une très faible toxicité. Ceci suggère que ces composés abondants dans nos écosystèmes pourraient potentiellement être utilisés en imagerie médicale.

Il y a également un intérêt croissant pour l'utilisation de photosensibilisateurs (PSs), à base de porphyrine naturelle, comme produit pour le théranostique (c'est-à-dire l'association d'une thérapeutique et d'un test diagnostique). L'idée derrière cette application est de tirer avantage de la fluorescence, dans le proche infrarouge des porphyrines naturelles pour le diagnostic par fluorescence, et de leurs fortes capacités de génération d'oxygène singulet pour la thérapie photodynamique (PDT). La PDT est un

traitement du cancer, cliniquement approuvé, combinant trois ingrédients : un agent photodynamique (activé par la lumière) appelé PS, la lumière et l'oxygène. À cet égard, une équipe de chercheurs de l'Université de Toronto, et leurs collègues de l'Université de Shanghai ont récemment conçu et synthétisé une sonde théranostique à base d'un dérivé de la bactériochlorophylle et un agent de ciblage (peptide)[13]. Ils ont démontré qu'en utilisant une telle sonde, il est possible, par imagerie de fluorescence de la bactériochlorophylle, de différencier les tissus sains des tumeurs. De plus, la capacité qu'a la bactériochlorophylle à générer l'oxygène singulet par photosensibilisation permet de détruire sélectivement les cellules cancéreuses ciblées, tout en épargnant les tissus sains. Ainsi, ces résultats démontrent clairement l'énorme potentiel, encore inexploité des porphyrines endogènes à servir comme agents multifonctionnels, capable de jouer un rôle primordial en thénostique, nouvel espoir dans la lutte contre le cancer.

Par ailleurs, la forte capacité de génération d'oxygène singulet des porphyrines naturelles suscite également un attrait pour le développement de technologies, basées sur le traitement photodynamique, pour éradiquer les agents pathogéniques, tels que les bactéries, les levures, les parasites et les champignons[14] (Figure 1.7).

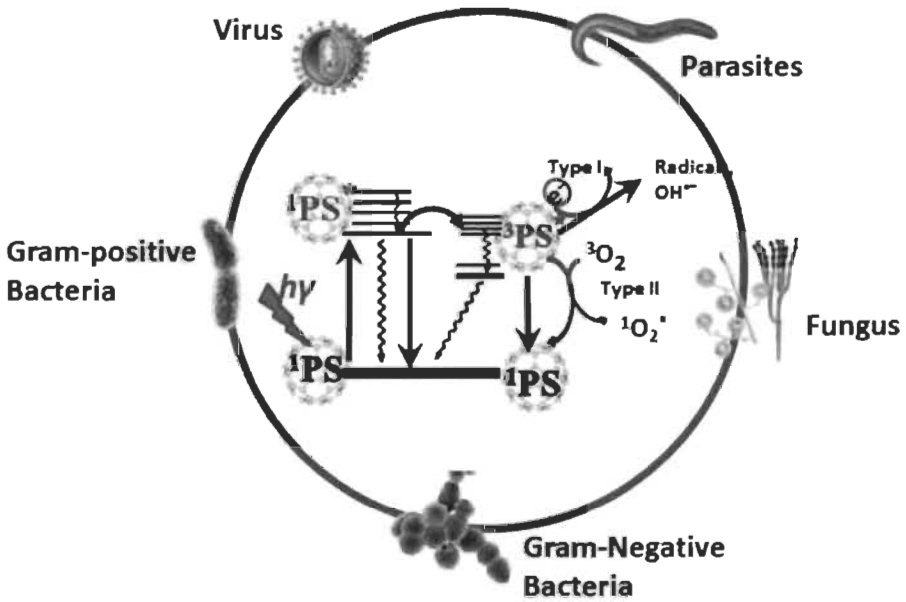

Figure 1.7 Diagramme de Jablonski qui montre qu'on peut inactiver de manière photodynamique les agents pathogéniques[14].

Par exemple, les chercheurs du secteur agricole étudient de nouvelles façons d'éliminer les insectes nuisibles. Étant donné que l'utilisation des pesticides usuels suscite beaucoup d'inquiétudes aujourd'hui, il est plus que nécessaire d'opter pour des solutions de rechange. En effet, en remplacement des pesticides chimiques actuels, représentant un danger aussi bien pour l'environnement que pour notre santé, la recherche s'oriente donc, à juste titre, vers le développement d'insecticides naturels activés par la lumière solaire (plus communément appelé insecticide photodynamique ou photo-insecticide)[15]. Ces types de pesticides ont la capacité de contrôler la population d'insectes nuisibles. Wohllebe et ses collègues ont étudié la possibilité d'utiliser les dérivés de porphyrines naturelles afin d'éliminer les insectes nuisibles. Ils ont démontré que les espèces réactives de l'oxygène, générées par photosensibilisation de la chlorophylline (résultant de la chlorophylle après élimination de la longue queue liposoluble d'hydrocarbures, queue phytol) et la pheophorbide (un produit de la dégradation de la chlorophylline), sont capables de tuer les larves de moustiques et d'autres petits insectes, au bout de quelques heures d'exposition au rayonnement solaire[16]. Cette étude illustre parfaitement que l'emploi des porphyrines naturelles, comme agent de photo-insecticide, constitue une méthode de valorisation économico-environnementale permettant de développer des insecticides efficaces et à faible empreinte écologique.

Enfin, un autre secteur d'activité, et non des moindres, à vouloir tirer profit des propriétés photoniques excellentes des porphyrines naturelles, est celui de la microélectronique et l'optoélectronique. En effet, en 2011, Ohtani et ses collaborateurs de l'Université Doshisha à Kyoto au Japon ont réussi à fabriquer des diodes électroluminescentes organiques utilisant comme ingrédient actif des chlorophylles extraites de feuilles d'épinards[17]. Pareillement, les chercheurs de l'Institut des sciences moléculaires et atomiques de Taiwan ont démontré que la chlorophylle pourrait être intégrée dans un phototransistor afin de créer un interrupteur activé par la lumière[18]. Cet intérêt à utiliser la capacité photoréceptrice des chlorophylles n'est pas surprenant, car leur capacité à absorber la lumière visible est parmi les plus élevées observées pour les composés organiques.

Cependant, avant une possible commercialisation ou mise en oeuvre de telles technologies à base de porphyrines naturelles, des avancées concernant leur photostabilité doivent encore être réalisées. C'est pourquoi les exemples d'applications présentés ci-dessus ne sont que des démonstrations de faisabilité intéressante, qui prouvent que l'exploitation des ressources naturelles, en particulier celle provenant des écosystèmes aquatiques et forestiers, pourrait répondre aux besoins constamment renouvelés en matériaux de pointe utilisés dans plusieurs technologies modernes.

1.6 Problème

En dépit de leurs caractéristiques photoniques plus que favorables, un inconvénient majeur avec les porphyrines d'origine végétale (c'est-à-dire porphyrines de magnésium) est qu'en raison de leurs niveaux d'énergie HOMO (niveau énergétique le plus haut occupé) élevés, les porphyrines de magnésium montrent une mauvaise stabilité, ce qui les rend facilement hydrolysées en solution acide et prompte à la photodégradation (ou photoblanchiment) sous irradiation lumineuse[19,20] s'en suit. Le photoblanchiment est une limite importante des porphyrines naturelles. C'est une réaction chimique photo-induite et irréversible de destruction des liaisons moléculaires, responsables des propriétés intéressantes de ces molécules (la capacité d'absorber la lumière visible, l'émission de fluorescence, la génération d'oxygène singulet, etc.). Il s'agit essentiellement de réactions d'oxydation avec des radicaux libres provenant de l'oxygène (principalement l'oxygène singulet). Cet aspect négatif des porphyrines naturelles fait obstacle à leurs utilisations dans des domaines d'application liés à la photonique et la photomédecine.

1.7 Revue de la littérature sur les différentes méthodes de photoprotection des porphyrines naturelles et leurs dérivés

Il est généralement admis que les porphyrines se dégradent sous l'action des interactions entre la porphyrine en état triplet (^{3}Porp*), qui interagit avec une molécule de $^3O_2$ (oxygène triplet) pour conduire à de l'oxygène singulet ($^1O_2$). C'est ensuite cette

espèce qui réagit avec la molécule de porphyrine à l'état fondamental (^{1}Porp) et cause sa décomposition[21]. Le mécanisme de photodégradation proposé pour expliquer la décomposition des colorants organiques, en particulier celle des porphyrines, est résumé par les équations des réactions photochimiques ci-dessous :

(1) Réaction d'excitation de la porphyrine depuis son état fondamental à son état triplet.

$$^1Porp + h\nu \rightarrow {}^1Porp^* \xrightarrow{ISC} {}^3Porp^*$$

(2) Réaction de la porphyrine état triplet avec oxygène pour produire de l'oxygène singulet.

$$^3Porp^* + {}^3O_2 \longrightarrow {}^1Porp + {}^1O_2$$

(3) Décomposition de la porphyrine par l'oxygène singulet.

$$^1Porp + {}^1O_2 \rightarrow décomposition$$

Au cours des dernières années, de nombreuses approches ont été explorées afin d'améliorer la photostabilité de porphyrines naturelles et leurs dérivés. La méthode la plus courante consiste au remplacement de l'ion central magnésium (Mg^{2+}) par d'autres ions métalliques (par exemple, le palladium), pour former des métalloporphyrines plus stables[22]. Cette méthode de photoprotection est particulièrement intéressante afin d'améliorer non seulement la stabilité, mais aussi la capacité de génération d'oxygène singulet des porphyrines naturelles, puisque certains métaux lourds (métaux diamagnétiques) sont connus pour améliorer la conversion intersystème[23,24]. Cependant, elle a pour inconvénient d'altérer significativement l'émission de fluorescence de ces porphyrines[25]. Autrement dit, elle ne peut être employée pour augmenter la photostabilité des porphyrines naturelles, en vue de les utiliser comme agent de contraste fluorescent pour diagnostiquer un cancer précoce. Il fut également constaté que l'incorporation d'un ou plusieurs groupes attracteurs d'électrons (par exemple, les sulfonate, les cyano, les halogènes, etc.) conduit à une augmentation prononcée de la photostabilité, en raison de la diminution de la densité électronique sur le noyau aromatique, ce qui le rend moins réactif[26-29].

Une autre approche élégante, afin d'améliorer la photostabilité, consiste à incorporer les molécules de porphyrines à l'intérieur d'une nanocapsule (liposome, micelle, polymère, etc.) de type coeur-coquille[30], permettant de conserver la structure chimique originelle des porphyrines et de réduire leurs interactions avec les $^1O_2$. Par contre, cette approche possède, sur le plan pratique, deux inconvénients majeurs : (i) les matériaux constituant la nanocapsule (la coquille) pourraient nuire à l'absorption de photons par les molécules encapsulées[31-33]; (ii) les molécules encapsulées doivent être éjectées de la nanocapsule, afin de pouvoir produire le $^1O_2$. De plus, les $^1O_2$ produites sont susceptibles de réagir avec les matériaux de la coquille, en particulier les matériaux polymères, ce qui se traduit souvent par une efficacité photocytotoxique très inférieure à celle des molécules non encapsulées[34]. La complexation de l'ion central avec un ligand supplémentaire a également été explorée pour améliorer de la photostabilité. En effet, Matsuo et ses collègues ont démontré qu'une coordination axiale de l'ion métallique peut améliorer la photostabilité des porphyrines de magnésium[35]. Enfin, Itoh et ses collaborateurs ont, pour leur part, utilisé de la silice mésoporeuse pour améliorer la photostabilité de chlorophylles[36]. Ces chercheurs ont expliqué que l'effet de la silice mésoporeuse est similaire à celle des protéines dans la photosynthèse, c'est-à-dire qu'il inhibe la formation des espèces réactives de l'oxygène (ROS). Cette méthode n'est donc pas appropriée pour être utilisée dans des applications, comme la thérapie photodynamique, le théranostique et la conception de photo-insecticides.

Bien que ces différentes stratégies afin d'améliorer la photostabilité des porphyrines de magnésium se soient avérées efficaces, par rapport à la stabilité *in vivo* de ces molécules (dans les cellules photosynthétiques), la photostabilité *in vitro* des porphyrines de magnésium est encore très faible. De ce point de vue, de nouvelles méthodes, pour améliorer la photostabilité des porphyrines d'origine naturelle, devraient être développées. C'est dans la poursuite de cet objectif qu'ont été réalisés les travaux décrits dans cette thèse.

1.8 Présentation du projet de thèse

Le mécanisme réactionnel détaillé, de la photodégradation de la tétraphénylporphyrine métallique (MTPP)[37-39] des dérivés de chlorophylle[40,41] et des bactériochlorophylles[42], a été examiné par plusieurs chercheurs. Ces travaux de recherche ont mis en évidence que la photodégradation des porphyrines est initiée par l'ajout d'un $^1O_2$ sur les doubles liaisons C=C d'alcènes riches en électrons (réaction de Diels-Alder, réactions sur les alcènes, 2+2 cyclo-additions) des porphyrines, suivi par l'ouverture du macrocycle porphyrique. En particulier, Matsuura et ses collègues ont avancé que le mécanisme réactionnel de photodégradation du tétraphénylporphyrine de magnésium (MgTPP) passe par la formation d'intermédiaire preroxide zwitterionique 3 ou 4, suivie de la formation d'un époxyde 5, puis de l'ouverture du macrocycle 2 (Figure 1.8)[43]. Toutefois, du fait de leur très courte durée de vie, ils n'ont pu isoler d'intermédiaires réactionnels de la photodégradation pour confirmer ce mécanisme.

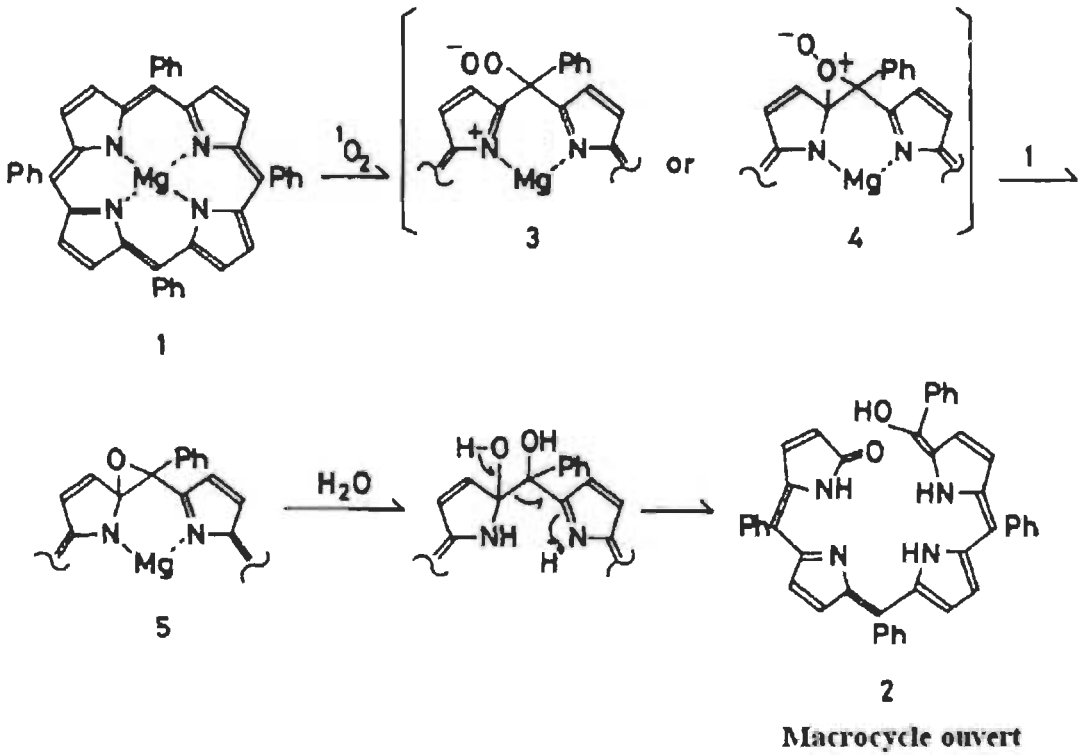

Figure 1.8 Mécanisme de photodégradation du tétraphénylporphyrine de magnésium (MgTPP) avec formation d'époxyde[43].

Pareillement, il faut souligner que le mécanisme réactionnel, proposé par Iturraspe et ses collègues pour expliquer la photodégradation des dérivés de la chlorophylle, passe exactement par les mêmes étapes (Figure 1.9)[44].

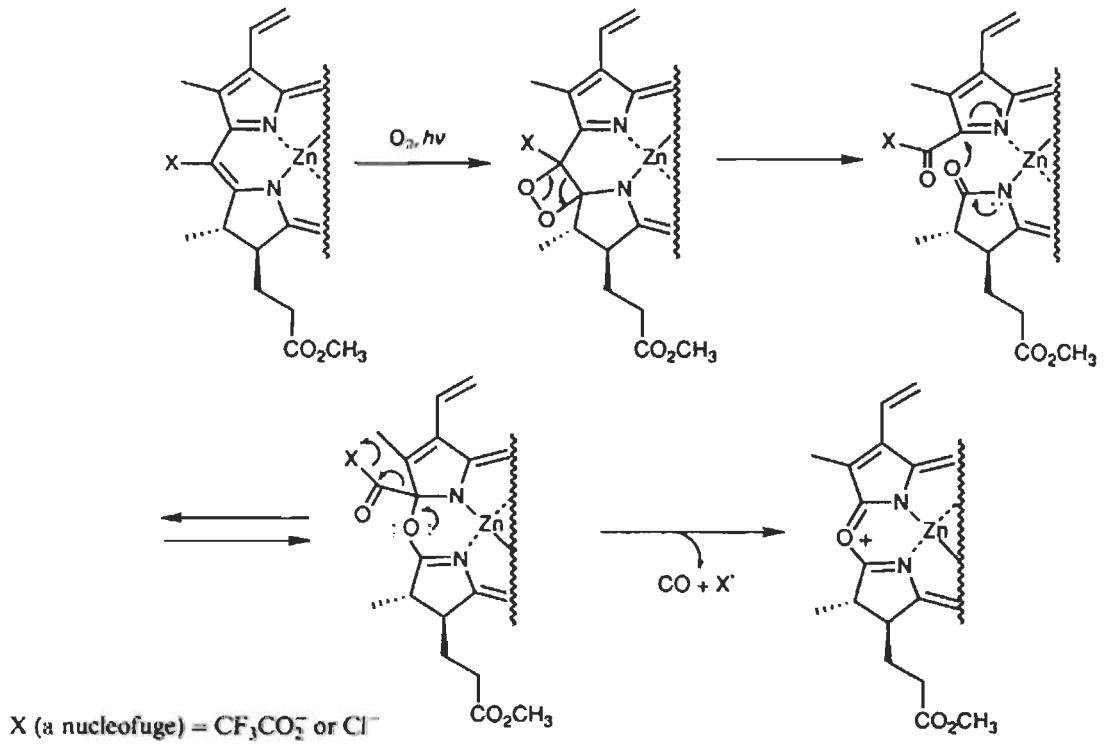

Figure 1.9 Mécanisme de photodégradation des dérivés de la chlorophylle[44].

Dans les deux mécanismes proposés, on peut clairement constater que l'ouverture du macrocycle porphyrique implique la participation des doublets d'électrons libres des atomes d'azote du macrocycle. De plus, de récents travaux sur les propriétés photochimiques du MgTPP ont révélé que la photodégradation du MgTPP passe par la formation d'un intermédiaire MgTPP-O_2, dans lequel une molécule O_2 est liée aux atomes d'azotes du macrocycle porphyrique, *via* des liaisons azote-oxygène (N-O)[45,46]. Pris ensemble, ces résultats suggèrent que les atomes d'azote du macrocycle porphyrique jouent un rôle essentiel dans le processus de photodégradation des porphyrines. D'autre part, et plus fondamentalement, on se questionne à savoir si empêcher le doublet d'électrons libres des atomes d'azote du macrocycle de participer à la réaction de

photodégradation, ou tout au moins empêcher l'oxygène de se lier à ces sites azotés pourrait ralentir la photodégradation. Une réponse affirmative à cette interrogation conduira indubitablement au développement d'une nouvelle stratégie de photoprotection des porphyrines, basé sur l'inhibition des sites azotés du macrocycle par un agent capable de se lier aux atomes d'azote.

Pour ce faire, j'ai opté d'utiliser comme ligand, des nanoparticules de métaux nobles à savoir : les nanoparticules d'or (AuNPs) et d'argent (AgNPS). Parce que les nanoparticules sont extrêmement petites, elles ont un rapport surface/volume très important. En raison de cette surface spécifique élevée, les atomes présents en surface sont plus nombreux et ce sont eux qui participent aux réactions chimiques. De plus, il est bien connu que la vitesse d'une réaction chimique augmente avec l'étendue de la surface de contact. Ainsi, les nanoparticules présentent une importante réactivité chimique, ce qui est l'une des raisons justifiant mon choix d'utiliser ces matériaux. Ma deuxième raison, d'utiliser des AuNPs et AgNPs, vient du fait que ces nanoparticules font l'objet d'un intérêt croissant dans des domaines aussi divers que la nanomédecine (l'application des nanotechnologies au monde médical)[47-49], le photovoltaïque[50], l'électronique[51,52] ou la catalyse[53,54]. Enfin, la troisième et dernière raison, qui explique mon penchant pour les nanoparticules, est que ces matériaux nanométriques ont, dans certaines conditions, la capacité d'augmenter l'émission de fluorescence d'un fluorophore, lorsque celui-ci est situé à proximité de la surface métallique, un phénomène connu sous le nom de l'augmentation de la fluorescence induite par métal[55,56]. De plus, il fut également démontré que la présence des nanoparticules à proximité d'un photosensibilisateur pourrait accroître la génération des espèces réactives de l'oxygène ($^1O_2$ et radicaux libres)[57].

Le tétraphénylporphyrine de magnésium (MgTPP) et la chlorophylle-*a* (Chl*a*) ont été choisis pour cette étude, comme des porphyrines de magnésium modèles, afin de tester l'efficacité de notre approche.

1.9 Notions essentielles sur l'augmentation de l'émission de fluorescence d'un fluorophe par un métal

L'augmentation de l'émission de fluorescence d'un fluorophe par un métal (MEF pour Metal-Enhanced Fluorescence) est un effet physique qui se produit lorsqu'un fluorophore est situé à une distance nanométrique (< 10 nm) d'une surface métallique[58]. Ce processus est caractérisé par un taux d'émission spontanée accrue dans le système fluorophore-métal. Il est généralement admis aujourd'hui que le MEF est dû à au moins un des deux mécanismes suivants : (1) l'augmentation du champ électromagnétique local, lorsque la nanoparticule métallique agit comme un élément concentrateur du champ électrique local de la lumière, ce qui permet au fluorophore d'avoir un meilleur taux d'absorption de photons[59]; (2) l'intense champ électrique autour de la nanoparticule augmente le taux d'émission radiative, en diminuant le temps de vie à l'état excité de la molécule[60].

Le premier mécanisme, soit l'amélioration de l'intensité d'émission, à la suite de l'augmentation du champ incident local sur le fluorophore par le métal, peut être compris comme suit : sous l'influence d'une lumière incidente, le champ électrique est intensifié autour de la nanoparticule métallique. Ainsi, le champ électrique résultant est alors égal à la sommation du champ incident (E) et de l'amplification du champ dû au métal (E_m). Autrement dit, un fluorophore situé à proximité d'une nanoparticule reçoit un champ électrique global amplifié E_T ($E_T = E+E_m$).

Les propriétés électromagnétiques des nanoparticules métalliques peuvent être expliquées de façon intuitive par le modèle de Drude des métaux[61]. Ce modèle traite les métaux sous forme de matrice d'ions chargés positivement et d'un nuage d'électrons se déplaçant à travers le potentiel de ces ions (Figure 1.10). Lorsque soumis à un champ électromagnétique externe, les électrons se déplacent de façon cohérente à l'intérieur du matériau[62]. Le déplacement d'électrons génère des forces de rappel électrostatique, où le nuage d'électrons chargés négativement est attiré vers les ions chargés positivement. La présence de cette force de rappel, pour les petits déplacements de l'équilibre, provoque l'onde de densité de charge qui oscillera dans le métal. Cette oscillation, collective et

cohérente des électrons à la surface d'une nanoparticule métallique, est appelée plasmon de surface. Les oscillations dans des nanoparticules sont, bien sûr, localisées, d'où l'appellation de plasmon de surface localisé (PSLs), et s'accompagnent d'une augmentation du champ électromagnétique près de la surface de la particule. Cette amélioration diminue rapidement avec la distance à partir de la surface.

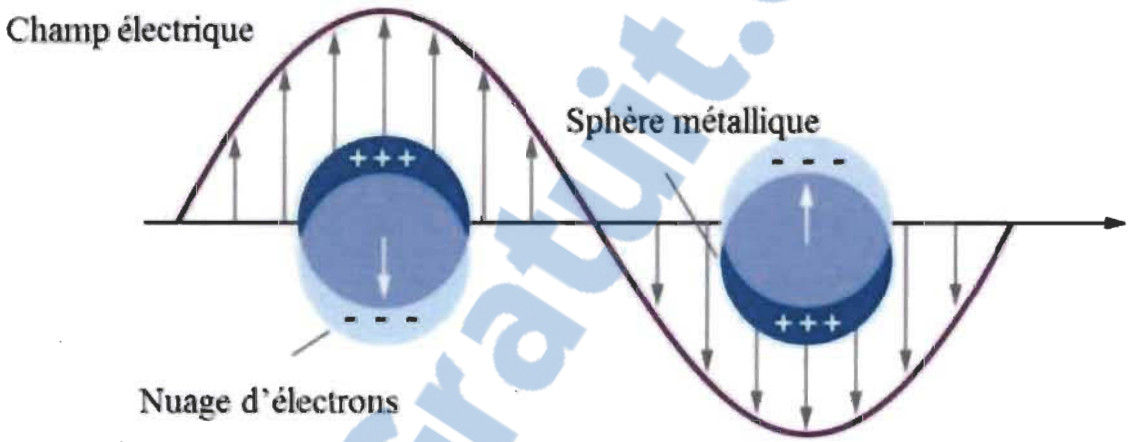

Figure 1.10 Représentation de la formation d'un plasmon de surface sur une nanoparticule métallique[62].

Le champ électrique amplifié localement (E_T) produit l'amélioration locale de fluorescence, en raison du fait que la puissance d'émission de fluorescence ($P_{fluorophore}$) est proportionnelle au flux de photons qui, à son tour, est proportionnel au champ électrique au carré, en supposant qu'il n'y a aucun effet de saturation dans l'état excité. Par conséquent, la puissance d'émission de fluorescence peut être donnée par la formule suivante[63] :

$$P_{fluorophore} = knQ_0$$

et

$$n\alpha|E|^2$$

où k est la section efficace d'absorption du fluorophore, n le flux de photons et Q_0 le rendement quantique du fluorophore.

Par ailleurs, le second mécanisme, soit l'amélioration de l'intensité de fluorescence, suite à l'augmentation du taux d'émission radiative en diminuant le temps de vie à l'état excité du fluorophore (τ), peut être compris comme un moyen de stimuler le taux d'émission radiative. Pour un fluorophore libre, le rendement quantique de fluorescence Q_0 peut être exprimé de la façon suivante :

$$Q_0 = \frac{\Gamma}{\Gamma + K_{nr}}$$

où Γ représente le taux d'émission radiative et K_{nr} le taux d'émission non-radiative. Ce dernier inclut tout ce qui contribue à faire diminuer l'émission de lumière. Le temps de vie à l'état excité du fluorophore libre (τ_0), défini comme le temps moyen que passe la molécule à l'état excité S_1 avant de retourner au niveau fondamental S_0 avec une émission de lumière, peut être donné par la formule suivante :

$$\tau_0 = \frac{1}{\Gamma + K_{nr}}$$

Lorsqu'un fluorophore est localisé près de la nanoparticule métallique, à la fois le taux d'émission radiative (Γ) et celui d'émission non-radiative (K_{nr}) sont modifiés par le substrat métallique[64]. Ainsi, il fut suggéré que, pour un fluorophore localisé près d'un métal, il y ait ajout du terme Γ_m représentant le taux d'émission radiative et K_m désignant le taux d'émission non-radiative en présence de métal. Ces termes sont additifs aux taux de transfert intrinsèques au fluorophore libre (Figure 1.11). De ce fait, en présence d'un métal, le rendement quantique de fluorescence Q_m peut être exprimé de la façon suivante :

$$Q_m = \frac{\Gamma + \Gamma_m}{\Gamma + \Gamma_m + K_m + K_{nr}}$$

Et, le temps de vie à l'état excité du fluorophore, localisé à proximité d'un métal (τ_m), est donné par la formule suivante :

$$\tau_m = \frac{1}{\Gamma + \Gamma_m + K_m + K_{nr}}$$

L'addition d'une composante d'émission non-radiative supplémentaire peut paraître surprenante mais, en fait, il y a toujours compétition entre le quenching et l'effet d'amélioration. Toutefois, la dépendance de distance (métal-fluorophore) pour chaque processus est différente, de sorte que le quenching de fluorescence domine lorsque le fluorophore est très proche (<1 nm) de la surface, tandis que l'amélioration de fluorescence est prépondérante à de plus grandes distances[65,66]. Le diagramme de Jablonski simplifié à la figure 1.11 est une représentation résumant le phénomène d'augmentation de l'émission de fluorescence par un métal.

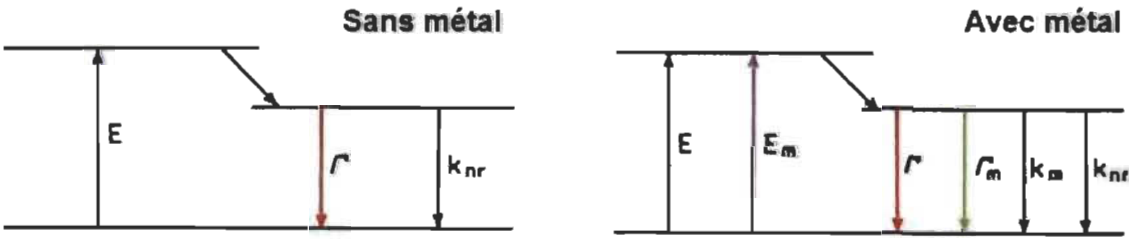

Figure 1.11 Modification du processus d'absorption et de déexcitation par une nanoparticule métallique à proximité d'un fluorophore[64].

1.10 Notions essentielles sur l'augmentation de la production d'oxygène singulet du photosensibilisateur par un métal

Il a été montré que d'amélioration du métal ne se limite pas qu'à la fluorescence : l'amélioration de la production à la fois de l'oxygène singulet ($^1O_2$) et le rendement quantique de phosphorescence ont été observés[67-75]. À ce jour, le mécanisme exact de l'effet d'amélioration du métal sur la production des ROSs est encore sujet à débat, mais il apparaît expérimentalement que l'amplification du champ électromagnétique au

voisinage des NPs peut jouer un rôle important dans l'amélioration de la production des ROSs. En effet, il a été démontré que l'interaction, entre le moment dipolaire du photosensibilisateur et du champ électromagnétique au voisinage des NPs, peut conduire à une formation accrue de l'état triplet du photosensibilisateur[76] et, par le fait même, améliorer la production de $^1O_2$ par photosensibilisation.

Alternativement, les NPs pourraient également améliorer la production de $^1O_2$, en augmentant la constante de vitesse de la transition $^1\Delta_g \rightarrow {}^3\Sigma_g$ (Figure 1.12), résultant en une augmentation du rendement quantique de phosphorescence de l'oxygène singulet[70]. En utilisant cette approche, Toftegaard et ses collègues ont réussi à démontrer une augmentation de la production de $^1O_2$ par un photosensibilisateur au voisinage des nanodisques d'or, pour lequel la bande de plasmon de surface correspond à la phosphorescence de $^1O_2$ à 1270 nm[70].

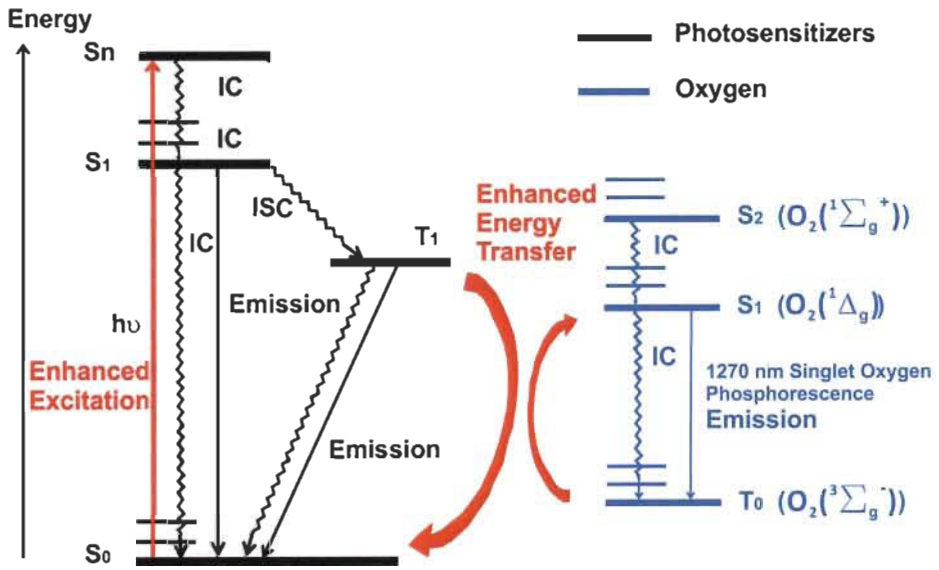

Figure 1.12 Diagramme énergétique de la production d'oxygène singulet photosensibilisée *via* le couplage plasmon surface-photosensibilisateur[75].

1.11 Hypothèses de recherche

Si les sites azotés du macrocycle porphyrique sont bloqués dans l'obscurité avant l'illumination, alors il se produira une augmentation de la photostabilité.

1.12 Objectif général de cette thèse

Le principal objectif de cette thèse de doctorat est de développer une stratégie de photoprotection, reposant sur l'utilisation des nanoparticules de métaux nobles, afin d'améliorer la stabilité des porphyrines de magnésium.

1.13 Objectifs opérationnels

1) Vérifier que l'inhibition des sites azotés du macrocycle porphyrique peut induire une photoprotection.

2) Établir que cette méthode de photoprotection pourrait également permettre d'accroître la stabilité des porphyrines de magnésium, possédant à la fois des doublets d'électrons libres sur les atomes d'azote du macrocycle et sur les groupes fonctionnels périphériques qui ne sont pas conjugués au macrocycle, comme c'est le cas avec les chlorophylles et les bactériochlorophylles.

3) Utiliser cette approche pour démontrer qu'il est possible d'améliorer simultanément la stabilité, l'émission de fluorescence et la capacité de génération d'oxygène singulet des porphyrines de magnésium.

1.14 Organisation du document

Cette thèse comporte en tout cinq chapitres. Suite à la présentation au premier chapitre du contexte, état de l'art sur les différentes stratégies de photoprotection des porphyrines de magnésium et le projet de thèse, le deuxième chapitre fera état de la découverte d'une nouvelle stratégie de photoprotection des porphyrines de magnésium. En effet, dans l'article intitulé « Beneficial role of gold nanoparticles as photoprotector of magnesium tetraphenylporphyrin », il sera démontré que l'inhibition des sites azotés du macrocycle porphyrique peut induire une photoprotection. Le troisième chapitre concernera la possibilité de protéger les porphyrines naturelles par cette méthode. Ainsi, l'article titré « Enhanced photostability of chlorophyll-*a* using gold nanoparticles as an

efficient photoprotector » expliquera les capacités qu'ont les nanoparticules d'or (AuNPs) à protéger les molécules de chlorophylles-*a*, dans les conditions *in vitro*. À cet égard, une attention particulière est portée sur la comparaison entre l'efficacité photoprotectrice des AuNPs et celle des composés antioxydants, lesquelles sont connues comme étant très efficaces pour protéger les chlorophylles dans la nature. Dans le chapitre suivant, dont l'article présenté se nomme « Nanosilver Could Usher in Next-Generation Photoprotective Agents for Magnesium Porphyrins », il sera fait mention d'une possibilité de coaméliorer la photostabilité, l'émission de fluorescence et la génération d'oxygène singulet par photosensibilisation des chlorophylles-*a*. Quant au dernier chapitre, il s'applique à présenter une synthèse des résultats et des contributions scientifiques de l'ouvrage. Nos perspectives sur l'avancement des connaissances et quelques questions laissées ouvertes par la thèse y seront également soumises. À la fin du présent document, une annexe explique les procédures expérimentales de synthèse des nanoparticules développées dans ce travail, ainsi que les méthodes de caractérisation.

1.15 Références

(1) Kadish, K. M.; Smith, K. M.; Guillard, R. The porphyrin handbook. Eds, Academic press: San Diego, **2000**; Vol. 1-10.

(2) Bonnett R.; Chemical Aspects of Photodynamic Therapy, Gordon and Breach Science Publishers, **2000**.

(3) Schaffer, M.; Ertl-Wagner, B.; Schaffer, P. M.; Kulka, U.; Hofstetter, A.; Duhmke, E.; Jori G. Porphyrins as Radiosensitizing Agents for Solid Neoplasms. *Curr. Phar. Des.*, **2003**, 9, 2024-2035.

(4) Fischer, H.; Orth, H. Die Chemie des Pyrrols, vol. I-III. Akademische Verlags-gesellschaft **1934**, M.B.H., Leipzig.

(5) Dixon H. B. F., Cornish-Bowden A., Liebecq C., Loening K. L., Moss G. P., Reedijk J., Velick S. F., Venetianer P., Vliegenthart J. F. G. *et al.* Nomenclature of tetrapyrroles. *Pure Appl. Chem.*, **1987**, 59, 779-832.

(6) (a) Uttamlal, M.; Holmes-Smith, A. S. The excitation wavelength dependent fluorescence of porphyrins. *Chem. Phys. Lett.*, **2008**, 454, 223-228. (b) Zimmermann, J.; Zeug, A.; Röder, B. A generalization of the Jablonski diagram to account for polarization and anisotropy effects in time-resolved experiments. *Phys. Chem. Chem. Phys.*, **2003**, 5, 2964-2969.

(7) Gouterman, M. Spectra of porphyrins *J. Mol. Spectrosc.*, **1961**, 6, 138-163.

(8) (a) Henderson, B.W.; Sumlin, A.B.; Owczarczak, B.L.; Dougherty, T.J. Bacteriochlorophyll-*a* as photosensitizer for photodynamic treatment of transplantable murine tumors. *J. Photochem. Photobiol. B,* **1991**, 10, 303-313. (b) Xodo, L. E.; Rapozzi, V.; Zacchigna, M.; Drioli, S.; Zorzet, S. The Chlorophyll Catabolite Pheophorbide-*a* as a Photosensitizer for the Photodynamic Therapy. *Curr. Med. Chem.*, **2012**, 19, 799-807.

(9) Dai, T.; Fuch, B. B.; Coleman, J. J.; Prates, R. A.; Astrakas, C.; St. Denis, T. G.; Ribeiro, M. S.; Mylonakis, E.; Hamblin, M. R.; Tegos, G. P. Concepts and principles of photodynamic therapy as an alternative antifungal discovery platform. *Front. Microbiol.*, **2012**, 3, article 120, 1-15.

(10) Schweitzer, C.; Schmidt, R. Physical Mechanisms of Generation and Deactivation of Singlet Oxygen. *Chem. Rev.*, **2003**, 103, 1685-1757.

(11) Valeur, B.; Berberan-Santos, M. N. Molecular Fluorescence: Principles and Applications. 2nd Edition, Wiley VCH, **2013**.

(12) Fanl, L.; Wu, Q.; Chu, M. Near infrared fluorescent chlorophyll nanoscale liposomes for sentinel lymph node mapping. *Int. J. Nanomed.*, **2012**, 7, 3071-3080.

(13) Liu, T. W.; Chen, J.; Burgess, L.; Cao, W.; Shi, J.; Wilson, B.C.; Zheng, G. Multimodal Bacteriochlorophyll Theranostic Agent. *Theranostics.*, **2011**, 1, 354-362.

(14) Sperandio, F. F.; Huang, Y-Y.; Hamblin, M. R. Antimicrobial Photodynamic Therapy to Kill Gram-negative Bacteria. *Recent Pat. Antiinfect. Drug Discov.*, **2013**, 8, 108-120.

(15) Alves, E.; Faustino, M. A. F.; Neves, M. G. P. M. S.; Cunha, A.; Nadais, H.; Almeida, A. Potential applications of porphyrins in photodynamic inactivation beyond the medical scope. *Journal of Photochemistry and Photobiology C: Photochem. Rev.*, **2015**, 22, 34-57.

(16) Wohllebe, S.; Richter, R.; Richter, P.; Häder, D. P. Photodynamic control of human pathogenic parasites in aquatic ecosystems using chlorophyllin and pheophorbid as photodynamic substances. *Parasitol. Res.*, **2009**, 104, 593-600.

(17) Ohtani, N.; Kitagawa, N.; Matsuda, T. Fabrication of Organic Light-Emitting Diodes Using Photosynthetic Pigments Extracted from Spinach. *Jpn. J. Appl. Phys.*, **2011**, 50, 01BC08.

(18) Chen, S. Y.; Lu, Y. Y.; Shih, F. Y.; Ho, P. H.; Chen, Y. F.; Chen, C. W.; Chen, Y. T.; Wang, W. H. Biologically inspired graphene-chlorophyll phototransistors with high gain. *Carbon.*, **2013**, 63, 23-29.

(19) Bonnett, R.; Djelal, B. D.; Hamilton, P. A.; Martinez, G.; Wierrani, F.; Photobleaching of 5,10,15,20-tetrakis(m-hydroxyphenyl)porphyrin (m-THPP) and the corresponding chlorin (m-THPC) and bacteriochlorin(m-THPBC). À comparative study. *J. Photochem. Photobiol. B.*, **1999**, 53, 136-143.

(20) Gerola, A. P.; Santana, A.; França, P. B.; Tsubone, T. M.; de Oliveira, H. P.; Caetano, W.; Kimura, E.; Hioka, N. Effects of Metal and the Phytyl Chain on Chlorophyll Derivatives: Physicochemical Evaluation for Photodynamic Inactivation of Microorganisms. *Photochem. Photobiol.*, **2011**, 87, 884-894.

(21) Sinclair, R. S.; Martinez, G., photobleaching of sensitisers used in photodynamic therapy. *Tetrahedron.*, **2001**, 57, 9513-9547.

(22) Fiedor, J.; Fiedor, L.; Kammhuber, N.; Scherz, A.; Scheer, H. Photodynamics of the bacteriochlorophyll-carotenoid system. 2. Influence of central metal, solvent and beta-carotene on photobleaching of bacteriochlorophyll derivatives. *Photochem. Photobiol*, **2002**, *76*, 145-52.

(23) Ball, D. J.; Wood, S. R.; Vernon, D. I.; Griffiths, J.; Dubbelman, T. M. A. R.; Brown, S.B. The characterisation of three substituted zinc phthalocyanines of differing charge for use in photodynamic therapy. A comparative study of their aggregation and photosensitising ability in relation to mTHPC and polyhaematoporphyrin. *J. Photochem. Photobiol. B.*, **1998**, 45, 28-35.

(24) Guldi, D. M.; Mody, T. D.; Gerasimchuk, N. N.; Magda, D.; Sessler, J. L. Influence of large metal cations on the photophysical properties of texaphyrin, a rigid aromatic chromophore. *J. Am. Chem. Soc.*, **2000**, 122, 8289-8298.

(25) Drzewiecka-Matuszeka, A.; Skalna, A.; Karocki, A.; Stochel, G.; Fiedor, L. Effects of heavy central metal on the ground and excited states of chlorophyll. *J. Biol. Inorg. Chem.*, **2005**, 10, 453-62.

(26) Dabrowski, J. M.; Arnaut, L. G.; Pereira, M. M.; Monteiro, C. J. P.; Urbańska, K.; Simoes, S.; Stochel G. New halogenated water-soluble chlorin and bacteriochlorin as photostable PDT sensitizers: synthesis, spectroscopy, photophysics, and in vitro photosensitizing efficacy. *Chem. Med. Chem.*, **2010**, 5, 1770-1780.

(27) Dabrowski, J. M.; Urbanska, K.; Arnaut, L. G.; Pereira, M. M.; Abreu, A. R.; Simoes, S.; Stochel, G. Biodistribution and photodynamic efficacy of a water-soluble, stable, halogenated bacteriochlorin against melanoma. *Chem. Med. Chem.*, **2011**, 6, 465-475.

(28) Dabrowski, J. M.; Arnaut, L. G.; Pereira, M. M.; Urbanska, K.; Simoes, S.; Stochel, G.; Cortes, L. Combined effects of singlet oxygen and hydroxyl radical in photodynamic therapy with photostable bacteriochlorins: evidence from intracellular fluorescence and increased photodynamic efficacy in vitro. *Free Radical Biol. Med.*, **2012**, 52, 1188-1200.

(29) Huang, Y. Y.; Balasubramanian, T.; Yang, E.; Luo, D.; Diers, J. R.; Bocian, D. F.; Lindsey, J. S.; Holten, D.; Hamblin, M. R. Stable synthetic bacteriochlorins for photodynamic therapy: role of dicyano peripheral groups, central metalsubstitution (2H, Zn, Pd), and Cremophor EL delivery. *Chem. Med. Chem.*, **2012**, 7, 2155-2167.

(30) Cao, W.; Ng, K. K.; Corbin, I.; Zhang, Z.; Ding, L.; Chen, J.; Zheng, G.; Synthesis and evaluation of a stable bacteriochlorophyll-analog and its incorporation into high-density lipoprotein nanoparticles for tumor imaging. *Bioconjug. Chem.*, **2009**, 20, 2023-2031.

(31) Huang, P.; Li, Z.; Lin, J.; Yang, D.; Gao, G.; Xu, C.; Bao, L.; Zhang, C.; Wang, K.; Song, H.; Hu, H.; Cui, D. Photosensitizer-conjugated magnetic nanoparticles for in vivo simultaneous magnetofluorescent imaging and targeting therapy. *Biomaterials.*, **2011**, 32, 3447-3458.

(32) Chen, Z.L.; Sun, Y.; Huang. P.; Yang, X. X.; Zhou, X. P. Studies on preparation of photosensitizer loaded magnetic silica nanoparticles and their anti-tumor effects for targeting photodynamic therapy. *Nanoscale Res. Lett.*, **2009**, 4, 400-408.

(33) Liu, F.; Zhou, X.; Chen, Z.; Huang, P.; Wang, X.; Zhou, Y. Preparation of purpurin-18 loaded magnetic nanocarriers in cottonseed oil for photodynamic therapy. *Mater. Lett.*, **2008**, 62, 2844-2847.

(34) Sun, Y.; Chen, Z.; Yang, X.; Huang, P.; Zhou, X.; Du, X. Magnetic chitosan nanoparticles as a drug delivery system for targeting photodynamic therapy. *Nanotechnology.*, **2009**, 20, 135102.

(35) Ichiki, T.; Matsuo, Y.; Nakamura, E. Photostability of a dyad of magnesium porphyrin and fullerene and its application to photocurrent conversion. *Chem. Commun.*, **2013**, 49, 279-281.

(36) Itoh, T.; Yano, K.; Inada, Y.; Fukushima, Y. Photostabilized Chlorophyll a in Mesoporous Silica: Adsorption Properties and Photoreduction Activity of Chlorophyll-a. *J. Am. Chem. Soc.*, **2002**, 124, 13437-13441.

(37) Silva, A. M. S.; Neves, M. G. P. M. S.; Martins, R. R. L.; Cavaleiro, J. A. S; Boschi, T.; Tagliatesta, P. Photo-oxygenation of *meso*-tetraphenylporphyrin derivatives: the influence of the substitution pattern and characterization of the reaction products. *J. Porphyrins.Phthalocyanines.*, **1998**, 2, 45-51.

(38) (a) Smith, K. M; Brown, S. B; Troxler, R. F; Lai, J. J. Photooxygenation of meso-tetraphenylporphyrin metal complexs. *Photochem. Photobiol*, **1982**, 36,147-152; (b) Cavaleiro, J. A. S.; Hewlins, M. J. E.; Jackson, A. H.; Neves, G. P. M. S. Structures of the ring-opened oxidation products from *meso*-tetraphenylporphyrin. *J. Chem. Soc., Chem. Commun.*, **1986**, 142-144.

(39) Cavaleiro, J. A. S.; Neves, M. G. P. S.; Hewlins, M. J. E.; Jackson, A. H. The photo-oxidation of meso-tetraphenylporphyrins. *J. Chem. Soc., Perkin Trans*, **1990**, 1, 1937-1943.

(40) Iturraspe, J.; Gossauer, A. formation of oxoniachlorins on photooxidation of 20-trifluoroactetoxy-and-20-chloro-chlorophyll derivatives. *Photochem. Photobiol.*, **1991**, 54, 43-49.

(41) Iturraspe, J.; Gossauer, A. Dependence of the regioselectivity of photo-oxidative ring opening of the chlorophyll macrocycle on the complexed metal Ion. *Helv. Chim. Acta.*, **1991**, 74, 1713-1717.

(42) (a) Kenner, G. W.; Rimmer, J.; Smith, K. M.; Unsworth, J. F.Pyrroles and related compounds. Part 39. Structural and biosynthetic studies of the *Chlorobium*chlorophylls-660 (bacteriochlorophylls *c*). Incorporations of methionine and porphobilinogen. *J. Chem. Soc. Perkin Trans.*, **1978**, 1, 845-852; (b) Risch, N.; Schormann, A.; Brockmann, H. Photobilin e. Photooxidation von bacteriochlorophyll-e-derivaten. *Tetrahedron. Lett.*, **1984**, 25, 5993-5996; (c) Brown, S. B.; Smith, K. M.; Bisset, G. M. F.; Troxler, R. F. Mechanism of photooxidation of bacteriochlorophyll c derivatives. *J. Biol. Chem.*, **1980**, 255, 8063-8068.

(43) Matsuura, T.; Inoue, K.; Ranade, A. C.; Saito, I. Photooxygenation of magesium meso-tetraphenylporphyrin. *Photochem. Photobiol.*, **1980**, 31, 23-26.

(44) Zhang, J. P.; Zhang, P. Y.; Zhang, Z.; Chen, G. H.; Han, F.; Wei, X. H. Photochemical reaction between magnesium tetraphenyl porphyrin and oxygen. *Chin. Chem. Lett.*, **2008**, 19, 1190-1192.

(45) Zhang, J.; Zhang, P.; Zhang, Z.; Wei, X. Spectroscopic and kinetic studies of photochemical reaction of magnesium tetraphenylporphyrin with oxygen. *J. Phys. Chem. A.*, **2009**, 113, 5367-5374.

(46) Jena, P.; Mohanty, S.; Mallick, R.; Jacob, B.; Sonawane, A. Toxicity and antibacterial assessment of chitosan-coated silver nanoparticles on human pathogens and macrophage cells. *Int. J. Nanomed.*, **2012**, 7, 1805-1818.

(47) Jeyaraj, M.; Sathishkumar, G.; Sivanandhan, G.; MubarakAli, D.; Rajesh, M.; Arun, R.; Kapildev, G.; Manickavasagam, M.; Thajuddin, N.; Premkumar, K.; Ganapathi, A. Biogenic silver nanoparticles for cancer treatment: an experimental report. *Colloids Surf. B.*, **2013**, 106, 86-92.

(48) Arvizo, R.; Bhattacharya, R.; Mukherjee, P. Gold nanoparticles: opportunities and challenges in nanomedicine. *Expert Opin. drug deliv.*, **2010**, 7, 753-763.

(49) Boisselier, E.; Astruc, D. Gold nanoparticles in nanomedicine: preparations, imaging, diagnostics, therapies and toxicity. *Chem. Soc. Rev.*, **2009**, 38, 1759-1782.

(50) Stratakis, E.; Kymakis, E. Nanoparticle-based plasmonic organic photovoltaic devices. *Mater. Today.*, **2013**, 16, 133-146.

(51) Cui, P.; Seo, S.; Lee, J.; Wang, L.; Lee, E.; Min, M.; Lee, H. Nonvolatile memory device using gold nanoparticles covalently bound to reduced graphene oxide. *ACS Nano.*, **2011**, 5, 6826-6833.

(52) Shen, W.; Zhang, X.; Huang, Q.; Xu, Q.; Song, W. Preparation of solid silver nanoparticles for inkjet printed flexible electronics with high conductivity. *Nanoscale.*, **2014**, 6, 1622-1628.

(53) Xia, Y.; Yang, H.; Campbell, C. T. Nanoparticles for Catalysis. *Acc. Chem. Res.*, **2013**, 46, 1671-1672.

(54) Chng, L. L; Erathodiyil, N.; Ying, J. Y. Nanostructured Catalysts for OrganicTransformations. *Acc. Chem. Res.*, **2013**, 46, 1825-1837.

(55) Babu, J.; George, J.; Varma, R. L. Metal-induced fluorescence lifetime enhancement of quinaldine chromophore on gold nanoparticle surface. *New J. Chem.*, **2013**, 37, 2426-2432.

(56) Mishra, H.; Mali, B. L.; Karolin, J.; Dragan, A. I.; Geddes, C. D. Experimental and theoretical study of the distance dependence of metal-enhanced fluorescence, phosphorescence and delayed fluorescence in a single system. *Phys. Chem. Chem. Phys.*, **2013**, 15, 19538-19544.

(57) Karolin, J.; Geddes, C. D. Metal-enhanced fluorescence based excitation volumetric effect of plasmon-enhanced singlet oxygen and super oxide generation. *Phys. Chem. Chem. Phys.*, **2013**, 15, 15740-15745.

(58) Aslan, K.; Leonenko, Z.; Lakowicz, J. R.; Geddes, C. D. Annealed Silver-Island Films for Applications in Metal-Enhanced Fluorescence: Interpretation in Terms of Radiating Plasmons. *J. Fluoresc.*, **2005**, 15, 643-654.

(59) Kümmerlen, J.; Leitner, A.; Brunner, H.; Aussenegg, F.R.; Wokaun, A. Enhanced dye fluorescence over silver island films: analysis of the distance dependence. *Mol. Phys.*, **1993**, 80, 1031-1046.

(60) Gersten, J.; Nitzan, A. Spectroscopic properties of molecules interacting with small dielectric particles. *J. Chem. Phys.*, **1981**, 75, 1139-1152.

(61) F. Xie, Ultra-sensitive protein detection by metal-induced fluorescence enhancement, Macquarie University, **2008**.

(62) Kelly, K. L.; Coronado, E.; Zhao, L. L.; Schatz, G. C. The Optical Properties of Metal Nanoparticles: The Influence of Size, Shape, and Dielectric Environment. *J. Phys. Chem. B.*, **2002**, 107, 668-677.

(63) Le Ru, E. C.; Etchegoin, P. G. Surface-Enhanced Raman Scattering (SERS) and Surface-Enhanced Fluorescence (SEF) in the context of modified spontaneous emission. *arXiv preprint physics/0509154*, **2005**.

(64) Geddes, C. D.; Gryczynski, I.; Malicka, J.; Gryczynski, Z.; Lakowicz,J. R. Metal-enhanced fluorescence: potential applications in HTS. *Comb. Chem. High Throughput Screen.*, **2003**, 6, 109-117.

(65) Anger, P.; Bharadwaj, P.; Novotny, L. Enhancement and Quenching of Single-Molecule Fluorescence. *Phys. Rev. Lett.*, **2006**, 96, 113002-1 à 4.

(66) Feng, A. L.; You, M. L.; Tian, L.; Singamaneni, S.; Liu, M.; Duan, Z.; Lu, T. J.; Xu, F.; M. Lin. Distance-dependent plasmon-enhanced fluorescence of upconversion nanoparticles using polyelectrolyte multilayers as tunable spacers. *Sci. Rep.*, **2015**, 5: 7779, doi:10.1038/srep07779.

(67) Zhang, Y.; Aslan, K.; Previte, M. J. R.; Malyn, S. N.; Geddes, C. D. Metal-enhanced phosphorescence: Interpretation in terms of triplet-coupled radiating plasmons. *J. Phys. Chem. B.*, **2006**, 110, 25108-25114.

(68) Melo, L. S.; Gomes, A. S.; Saska, S.; Nigoghossian, K.; Messaddeq, Y.; Ribeiro, S. J.; Araujo, R. E. Singlet oxygen generation enhanced by silver-pectin nanoparticles. *J. Fluoresc.*, **2012**, 22, 1633-1638.

(69) Toftegaard, R.; Arnbjerg, J.; Cong, H. P.; Agheli, H.; Sutherland, D. S.; Ogilby, P. R. Metal nanoparticle-enhanced radiative transitions: Giving singlet oxygen emission a boost. *Pure Appl. Chem.*, **2011**, 83, 885-898.

(70) Toftegaard, R.; Arnbjerg, J.; Daasbjerg, K.; Ogilby, P. R.; Dmitriev, A.; Sutherland, D. S.; Poulsen, L. Metal-enhanced 1270 nm singlet oxygen phosphorescence. *Angew. Chem. Int. Ed.*, **2008**, 47, 6025-6027.

(71) Zhang, Y.; Aslan, K.; Geddes, C. D. Metal-Enhanced Generation of Oxygen Rich Species. *John Wiley & Sons, Inc., New Jersey.*, **2010**, 277-293.

(72) Zhang, Y.; Aslan, K.; Previte, M. J. R.; Geddes, C. D. Metal-enhanced singlet oxygen generation: A consequence of plasmon enhanced triplet yields. *J. Fluoresc.*, **2007**, 17, 345-349.

(73) Zhang, Y.; Aslan, K.; Previte, M. J. R.; Geddes, C. D. Plasmonic engineering of singlet oxygen generation. *Proc. Natl Acad. Sci.*, **2008**, 105, 1798-1802.

(74) Dragan, A.I.; Geddes, C.D. Metal-enhanced fluorescence: the role of quantum yield, Q_0, in enhanced fluorescence. *Appl. Phys. Lett.*, **2012**,100, p. 093115

(75) Hu, B.; Cao, X.; Nahan, K.; Caruso, J.; Tang, H.; Zhang, P.Surface plasmon-photosensitizer resonance coupling: an enhanced singlet oxygen production platform for broad-spectrum photodynamic inactivation of bacteria. *J. Mater. Chem. B.*, **2014**, 2, 7073-7081.

(76) Pacioni, N. L.; Gonzalez-Bejar, M.; Alarcón, E.; McGilvray, K. L.; Scaiano, J. C. Surface Plasmons Control the Dynamics of Excited Triplet States in the Presence of Gold Nanoparticles. *J. Am. Chem. Soc.*, **2010**, 132, 6298-6299.

CHAPITRE II

BENEFICIAL ROLE OF GOLD NANOPARTICLES AS PHOTOPROTECTOR OF MAGNESIUM TETRAPHENYLPORPHYRIN

Le contenu de ce chapitre a fait l'objet d'une publication en anglais dans la revue : *Journal of Materials Chemistry,* 2012, 22, 2943-2951.

2.1 Résumé de l'article

Le présent article avance l'hypothèse que si les sites azotés du macrocycle porphyrique sont bloqués dans l'obscurité avant l'illumination, alors il se produira une augmentation la photostabilité. Afin de vérifier cette hypothèse, nous avons utilisé des nanoparticules d'or (AuNPs) pour améliorer la photostabilité du tétraphénylporphyrine de magnésium (MgTPP). Nos résultats montrent qu'avec une concentration appropriée de AuNPs, une efficacité de photoprotection d'environ 100 % peut être obtenue. Fait important, la capacité protectrice des AuNPs est le résultat de leur liaison avec les sites azotés du macrocycle porphyrique du MgTPP, inhibant par conséquent l'action des espèces réactives de l'oxygène (ROS) à ces endroits. En outre, la réduction de la formation d'états singulets excités du MgTPP, à la suite de sa liaison avec AuNPs, diminue également la production de ROS, ce qui contribue aussi à l'amélioration de la photostabilité du MgTPP. Par ailleurs, la liaison entre MgTPP et AuNPs peut également être responsable de la photostabilité induite au MgTPP par les AuNPs dans des conditions anaérobies. L'utilisation de nanoparticules d'or nous offre donc une nouvelle stratégie pour améliorer la photostabilité de diverses porphyrines. L'étude présentée dans cet article a été l'aboutissement du premier objectif opérationnel de cette thèse.

2.2 Premier article scientifique

Beneficial role of gold nanoparticles as photoprotector of magnesium tetraphenylporphyrin

Laurent Bekalé, Saïd Barazzouk and Surat Hotchandani*

Groupe de Recherche en Biologie-Végétale, Université du Québec à Trois-Rivières, Trois-Rivières, Qc, G9A 5H7, Canada

* To whom correspondence should be addressed. e-mail: hotchand@uqtr.ca

Abstract

The photoprotection of porphyrins is of immense importance for their utilisation in several photo-related applications. In the present study, we have employed gold nanoparticles (AuNPs) to photoprotect a porphyrin, magnesium tetraphenylporphyrin (MgTPP). Absorption, fluorescence and X-ray photoemission spectroscopic (XPS) studies of MgTPP under illumination in absence and in presence of AuNPs have been carried out to assess their effect on the photostability of MgTPP. The results show that with an appropriate concentration of AuNPs, virtually 100% photoprotection can be provided to MgTPP. The protecting ability of AuNPs is the result of their binding with MgTPP at its nitrogen sites, inhibiting, thus, the binding of reactive oxygen species (ROS) at these sites, known to cause the photodegradation of MgTPP and several other porphyrins under aerobic conditions. Further, the decreased formation of excited singlet states of MgTPP, as a result of its binding with AuNPs, also suppresses the generation of ROS and improves the photostability of MgTPP. The binding between MgTPP and AuNPs may also be responsible for the photoprotection provided to MgTPP by AuNPs under anaerobic conditions too. The use of gold nanoparticles thus offers us a new strategy to photoprotect various porphyrins.

Introduction

Metalloporphyrins, possessing high extinction coefficients in the visible region of solar spectrum and excellent photoconducting and semiconducting properties, have found extensive use in the fabrication of various optoelectronic and solar-energy conversion devices[1-5]. Besides these applications, they have also been employed as photosensitizers in treatment of the tumors (photodynamic therapy)[6-8]. However, as useful as they are in both industrial and medical applications, a major drawback with porphyrins is that many of them tend to photodegrade upon prolonged exposure to illumination. This is quite undesirable especially in their use in photodynamic therapy as the bleaching of the sensitizer during illumination may leave the destruction of the tumor incomplete. Thus for their efficient and durable functioning, it is highly important that their photostability be increased.

The photodegradation of porphyrins under aerobic conditions is known to be a photooxidative process, caused by various reactive oxygen species (ROS), namely, singlet oxygen, superoxide ion and hydrogen peroxide[9-15] which are generated during the illumination of porphyrins. In a recent study, Zhang *et al.*[14,15] reported that during the photochemical degradation of magnesium porphyrin (MgTPP) in air saturated solution, an 1:1 adduct of MgTPP and oxygen, with oxygen bound to the pyrrolenine nitrogen of MgTPP as N-O-Mg, was formed. It is thus reasonable to assume that if one could prevent oxygen from binding to these nitrogen sites, one would slow down the photodegradation or, in other words, increase the photostability of porphyrins. One of the ways to achieve this is to block these nitrogen sites of porphyrins by some harmless ligand before oxygen has a chance to bind with them (nitrogens) and cause photodamage.

To this end, we have employed gold nanoparticles (AuNPs), that possess a high affinity for nitrogen atoms, to photoprotect a porphyrin, MgTPP. We present here in this article, the absorption, fluorescence and X-ray photoemission spectroscopic (XPS) studies of MgTPP under illumination in absence and in presence of AuNPs to assess

their effect on the photostability of MgTPP under ambient conditions. It is seen that AuNPs do provide a huge photoprotection to MgTPP. Further, it should be mentioned that our primary objective is to study the effect of AuNPs on the photostability of MgTPP, we have thus not attempted to analyze and identify the products of degradation, and, therefore, only the comparative study is presented here. To our knowledge, this is the first report on the photoprotection of porphyrins by AuNPs.

Experimental section

Materials and methods

Magnesium tetraphenylporphyrin monohydrate (MgTPP) was purchased from Alfa Aesar Co. Hydrogen tetrachloroaurate trihydrate, sulfuric acid (H_2SO_4), tetraoctylammonium bromide (TOAB), sodium borohydride ($NaBH_4$), sodium sulfate (Na_2SO_4) and toluene, of the purest quality available, were purchased from Aldrich Chemical Co., and were used as received.

Synthesis of Au nanoparticles

The procedure for preparing colloidal gold nanoparticles in an organic medium is a modified version[16] of that proposed by Brust *et al.*[17] Briefly, an aqueous solution of hydrogen tetrachloroaurate (III) hydrate ($(AuCl_4)^-$, 6 mL, 0.04 M) was mixed with a solution of tetraoctylammonium bromide (TOAB) (0.05 M) in 14 mL toluene. The biphasic mixture was vigorously stirred for 30 min until all the $(AuCl_4)^-$ was transferred into the organic layer. An aqueous solution of sodium borohydride (6 mL, 0.4 M) was added dropwise, and the mixture was stirred for 3h. The organic layer was separated off, washed twice with a dilute aqueous solution of H_2SO_4 and then washed five times with deionized water. Finally, the organic layer, containing the colloidal gold nanoparticles, was dried overnight on Na_2SO_4 powder and then filtered. The final concentration of Au nanoparticles, estimated on the basis of atomic concentration, was 13 mM.[18] The TEM micrographs of these Au nanoparticles revealed an average particle diameter of 8 nm.

Photodegradation measurements

The measurements were carried out in a 1-cm path length quartz cuvette. The illumination of MgTPP solution (3 mL, 5.3 μM) in toluene was carried out using collimated light from a 150W xenon lamp that passed through water filter to absorb heat. A cut-off filter which allowed wavelengths greater than 400 nm was used. The light power reaching the sample was ~ 40 mW/cm^2. The solutions were stored in the dark in a refrigerator when not in use. All experiments were carried out in the presence of air. Absorption spectra were recorded with a *Perkin Elmer UV/Vis* spectrophotometer *Lambda 20*. The fluorescence spectra were recorded with a FluoroLog-3 spectrofluorometer.

X-Ray Photoemission Spectroscopy (XPS)

XPS was performed on a *Kratos Axis Ultra* spectrometer (Kratos Analytical Ltd., UK), using a monochromatic Al Kα X-ray source (E = 1486.6 eV) with a power of 225 W, at a take-off angle of 90° relative to the sample surface. 250 μL of the sample was placed on an aluminum substrate and dried in vacuum dissicator overnight to obtain a thin film. The dried sample was then transferred to the XPS sample holder. The measurements were made under a high vacuum of 10^{-9} torr at room temperature. The surface of the sample was ~ 20 mm^2, and the investigated area was typically 1 x 2 mm^2. Survey spectra for each sample over a binding energy range of 0 – 1300 eV were an average of three scans (at three different points) acquired at pass energy of 160 eV and resolution of 1 eV/step (lens in hybrid mode, which assures maximum sensitivity). High-resolution C 1s, N 1s and Au 4f spectra for quantitative measurements of binding energy and atomic concentration were an average of five scans acquired at a pass energy of 40 eV and resolution of 0.1 eV per step. The CasaXPS software was used for background subtraction (Shirley-type), peak integration, fitting and quantitative chemical analysis. The C 1s (C– C) peak at 285 eV was used to calibrate the binding energy scale. Binding energies values are given at ± 0.2 eV. Gaussian peak profiles were used for the deconvolution of XPS spectra. The magnesium metal binding energy was

not recorded due to the poor signal to background counting ratio caused by the low core level cross section of Mg 1s level.

Percentage photoprotection

The percentage photoprotection was calculated using the formula as described by Claes:[19]

$$\frac{E_3 - E_2}{E_1 - E_2} \times 100 \qquad (1)$$

where E_1, E_2, and E_3 are, respectively, the concentration (or absorbance) of MgTPP before irradiation, after irradiation without AuNPs, and after irradiation in the presence of AuNPs.

Determination of the fraction of the light absorbed by MgTPP (5.3 μM) and AuNPs of varying concentrations (2-130 μM) in the mixture of MgTPP and AuNPs

An example of calculation

1) Quantity of incident light absorbed, I_{abs}, by a sample at a given wavelength λ is equal to:

$$i_{abs}^{\lambda} = i_0^{\lambda} \times \left(1 - 10^{-A_\lambda}\right)$$

where i_0^{λ} is the incident illumination intensity at a given wavelength λ and A_λ is the absorbance of the sample at that wavelength.

Thus, the light absorbed by AuNPs (2.27 μM) at λ= 400nm with absorbance of 2.58×10^{-3} is:

$$i_{abs}^{\lambda=400} = i_0^{\lambda=400} \times \left(1 - 10^{-2.58\times10^{-3}}\right) = 5.92 \times 10^{-3} \times i_0^{\lambda=400}$$

2) The total amount of incident light absorbed, $I_{abs(Total)}$, by the sample in the wavelength range (400-900 nm) is thus equal to:

$$I_{abs(Total)} = \int_{A_{\lambda=400}}^{A_{\lambda=900}} i_0^{\lambda} \left(1 - 10^{-A_\lambda}\right) dA_\lambda$$

It should be mentioned that the absorption spectra were recorded with an increment of 0.1 nm, *i.e.*, the number of wavelengths comprised in the wavelength region, 400-900 nm, is exactly 5000. Further, to simplify the calculations, it has been assumed that the power output of the lamp at each wavelength in the range 400-900 nm is constant at a value of i_0. The total illumination intensity incident on the sample is, therefore, 5000 i_0.

Thus the total amount of incident light absorbed, $I_{abs(Total)}$, taking into account the absorbance at each wavelength, by AuNPs (2.17 μM) in the wavelength range of 400-900 nm is:

$$I_{abs(Total)} = i_0 \int_{A_{\lambda=400}}^{A_{\lambda=900}} \left(1 - 10^{-A_\lambda}\right) dA_\lambda = 39 i_0$$

3) By analogy, the total amount of incident light absorbed, $I_{abs(Total)}$, by MgTPP (5.3 μM) in the wevelength range (400-900 nm) is equal to:

$$I_{abs(Total)} = i_0 \times \int_{A_{\lambda=400}}^{A_{\lambda=900}} \left(1 - 10^{-A_\lambda}\right) dA_\lambda = 494 i_0$$

4) The fraction of the incident light absorbed, Fraction $(I_{abs})_{AuNPs}$, by AuNPs (2.17 μM) in the mixture, over a range interval (400-900 nm) is, therefore equal to:

$$\text{Fraction}(I_{abs})_{AuNP} = 100 \times \frac{I_{abs(Total)}(AuNP)}{I_{abs(Total)}(AuNP) + I_{abs(Total)}(MgTPP)} = 100 \times \frac{39\, i_0}{39\, i_0 + 494\, i_0} = 7.3\%$$

And by inference, the fraction of incident light absorbed by MgTPP (5.3 μM) in this mixture over the same wavelength range (400-900 nm) is equal to 92.7%.

It should be mentioned that the assumption of constant i_0 in the wavelengths, 400-900nm, for the sake of calculations does not affect the actual results since it is used for both MgTPP and AuNPs solutions, and, further, in the end, the fractions, as seen above, are evaluated in which i_0 eventually gets cancelled.

In Table S1 (ESI†) are listed the values of the fraction of the light absorbed by AuNPs of varying concentrations in a mixture with MgTPP (5.3 μM), calculated as shown above.

Results and discussion

Figure 1 presents the absorption spectra of MgTPP (5.3 μM) and gold nanoparticles (50 μM) in toluene. The principal absorption peaks of MgTPP (spectrum a), namely, the Soret band at 426 nm and the Q bands at 523, 563 and 602 nm are in agreement with those reported in the literature.[15] The Soret band is quite intense, about 20 times as strong as that for Q bands. The 530 nm absorption band (spectrum b) is characteristic of the surface plasmon band of AuNPs.[20]

Figure 2 displays the absorption spectra of MgTPP in toluene as a function of time of illumination with visible light ($\lambda > 400$ nm) under ambient conditions. The choice of toluene as solvent is due to the fact that AuNPs (to be used for photoprotection studies) have been prepared in toluene. As seen from the figure, the absorbance of MgTPP decreases as illumination time increases. In 45 minutes time, about 50% decrease in the

† Supplementary information

absorbance of the major Soret band at 426 nm was observed. In about 5 hr period, almost 95% MgTPP, based on its absorbance at 426 nm, seems to have degraded. The band at 426 nm has practically all but disappeared and there has appeared a very weak blue-shifted band at 420 nm (spectrum g). The fine structure of Q bands, in the region of 500 to 650 nm, characteristic of MgTPP (inset, spectrum a), is lost, and an increase in the absorption at 462 and 793 nm is also observed in the photodegraded sample (inset, spectrum g). This indicates the formation of a new chemical product. These results are in good agreement with those reported by Zhang *et al.*[15] who studied the photodegradation of air saturated solution of MgTPP in dichloromethane. The photodegradation is due to the reaction of oxygen (ROS) with MgTPP during its illumination.

In order to investigate the role of AuNPs as a photoprotector of MgTPP, the illumination of MgTPP solution (5.3 μM) in the presence of AuNPs in varying concentration (2- 130 μM) was carried out under identical conditions using a 400 nm cut-off filter. The addition of AuNPs, as is clear from Fig. 3, does seem to provide protection to MgTPP against photodegradation. After 45 minutes of illumination, MgTPP has degraded only 15% in presence of the AuNPs (4.3 μM) compared to the 50% photodegradation in absence of AuNPs, as seen from the decrease in the absorbance at 426 nm (Figs. 2 & 3). In 5 hrs, MgTPP alone has photodegraded almost completely, whereas in presence of AuNPs it has degraded only 35%. In other words, a photoprotection of 65% has been provided to MgTPP by 4.3 μM AuNPs. The decrease in photodegradation of MgTPP in presence of AuNPs can also be seen visually in Fig. 4. While the color of MgTPP solution changes from light pink to light green after irradiation, the color of MgTPP admixed with AuNPs remains virtually the same after irradiation, thus indicating clearly the photoprotective action of AuNPs. Further, the photoprotection is dependent upon the AuNPs concentration. The higher the AuNPs concentration, the lower is the photodegradation of MgTPP or the greater is the photoprotection of MgTPP by AuNPs. At AuNPs concentration of 86 μM, almost 100% photoprotection is provided (inset, Fig. 3). The percentage photoprotection was calculated using eq. (1) as described in the Experimental section.

It should be mentioned that the enhanced photoprotection provided to MgTPP with the increase in the concentration of AuNPs is not due to the greater and greater amount of light being absorbed by AuNPs. It is true that AuNPs do absorb light in the wavelength region of 400 nm and onward. For example, in a mixture of 5.3 μM solution of MgTPP and 4.3 μM AuNPs, the relative proportion of the light absorbed by AuNPs is ~10% (Table S1, Supporting information). This value increases, respectively, to 40 and 56% for 43.3 and 65 μM AuNPs in their mixture with 5.3 μM MgTPP. One can, therefore, argue that the protection provided by AuNPs is because AuNPs absorb a portion of incident illumination and thus shield MgTPP from deleterious effect of light.

However, such is not the case; because if it were so, one would have already witnessed a 100% photoprotection of MgTPP with only 22 micromolar solution of AuNPs since it absorbs 3 times as much light as that absorbed by 4.3 μM AuNPs (see Table S1). The results (inset, Fig. 3) show that the photoprotection rendered to MgTPP by 22 μM AuNPs is only 72%, which is comparable to 65% provided by 4.3 μM solution of AuNPs. Further, how can one, based on the absorption of light by AuNPs, explain the same degree of photoprotection, *i.e.*, 88%, provided by both the 43.3 and 65 micromolar solutions of AuNPs even though they absorb different amount, *i.e.*, 40 and 56% of the incident illumination, respectively? Obviously, it is not the optical filter effect of AuNPs, but is rather largely due to the binding between AuNPs and MgTPP that protects MgTPP by keeping oxygen away, as discussed later in the text.

To exclude the possibility that the tetraoctylammonium bromide (TOAB), a stabilizer used in the preparation of AuNPs, had any photoprotective role, MgTPP solution in toluene containing TOAB was irradiated. In this case, MgTPP was not photoprotected, confirming that it is the AuNPs, rather than TOAB, that provide photoprotection to MgTPP. Moreover, AuNPs themselves subjected to the irradiation for same time period (5 hrs) under identical conditions did not show any photochemical changes.

Additionally, AuNPs bring about changes in the absorption spectrum of MgTPP. A decrease in the absorption at 426 nm and an appearance of a new band at 430 nm, as the concentration of AuNPs increases, indicates the formation of a complex between MgTPP and AuNPs (Fig. 5). Similar changes in the bands at 523, 563 and 602 nm are also visible. The changes in the absorption in Soret (430 nm) and Q band (567 and 608 nm) wavelength regions were used to determine the association constant between MgTPP and AuNPs employing Benesi-Hilderbrand method.[21] An average apparent association constant, K_{app}, of 3.95 x 10^4 M^{-1} was obtained from the intercept-to-slope ratio of the double reciprocal plot of $1/\Delta A$ vs 1/[AuNPs] (inset, Figs. 5 A,B). It should be mentioned that since the absorbance of MgTPP is low for Q bands, a higher concentration of MgTPP has been used to observe meaningful spectral changes in it with the addition of AuNPs, and obtain a reliable value of K_{app}. The high value of K_{app} observed in these experiments suggests a strong binding between AuNPs and MgTPP. A similar value, ~10^4 M^{-1}, for association constant has also been obtained from fluorescence quenching experiments of MgTPP in presence of AuNPs (Fig. 6). The high value of the Stern-Volmer constant, K_{SV}, (inset, Fig. 6) suggests that the quenching is of static type, and K_{SV} represents the association constant[22] between MgTPP and AuNPs.

Since, AuNPs possess affinity for the nitrogens, it is reasonable to assume that the complex is formed as a result of the interaction between the nitrogens of MgTPP and AuNPs. The binding of organic molecules on metal nanoparticle surfaces via nitrogen atoms of the molecule has been observed by several authors. For example, using NMR technique, Kamat *et al.*[23,24] reported that the complex formation between benzylamine and AuNPs occurred via interaction of the non-bonding electrons on nitrogen of amino group of benzylamine with the surface of AuNPs. Kastonis *et al.*[25] also demonstrated the participation of lone pair of electrons on iminic nitrogen of porphyrin cycle in the attachment of meso-tetradodecylporphyrin molecules on Au(111). Thus, it will not be far-fetched to say that the binding of MgTPP with AuNPs (or the complex formation between MgTPP and AuNPs), in the present case, also occurs via the interaction of non-bonding electrons on nitrogens of MgTPP with the surface of the AuNPs. The

photoprotective role of AuNPs could thus be the result of the binding between MgTPP and AuNPs via nitrogens of MgTPP that prevents oxygen to attach to MgTPP.

In order to verify the interaction between MgTPP and AuNPs, the C 1s and N 1s XPS spectra of MgTPP (before and after irradiation), and the mixture of MgTPP and AuNPs were recorded. The Au(4f) XPS spectra of AuNPs alone and in its mixture with MgTPP were also recorded. The experimental atomic composition of different elements were determined from the XPS survey spectra analysis, and are shown in Table 1. The important feature of this Table is the increase in the oxygen content (1%) in irradiated MgTPP sample which is the result of the photooxidation of the molecule, as discussed below.

The deconvoluted C1s XPS spectra of both MgTPP (before irradiation) and its mixture with AuNPs (Figs. 7 a and b) show three peaks: the first at 284.71 eV corresponds to the aromatic carbon (-C=C-)[26-28] from MgTPP; the second at 285 eV is due to the aliphatic carbon (-C-C-) and -C-H of MgTPP and TOAB (see Fig. S1),[29,30] while the third, a low intensity, peak at 285.31 eV, appearing in the XPS of MgTPP, is attributed to the C-N and C=N bonds.[28] The corresponding peak due to C-N and C=N bonds in the mixture of MgTPP and AuNPs, however, appears at a bit higher binding energy (285.9 eV). A possible reason for this is that the nitrogen atom in MgTPP-AuNPs mixture is, as a result of the complex formation between the two, in a higher oxidized state as discussed below. This increases the electron-withdrawing character of nitrogen such that the adjacent carbon atom bonded to it becomes more electropositive.

The C1s spectrum of the irradiated MgTPP (Fig. 7 c) also shows three peaks, corresponding to (i) aliphatic C-C and C-H bonds at 285 eV, (ii) C-N bond at 285.39 eV, and (iii) a very weak signal at 287.19 eV attributable to carbonyl group, C=O.[29,30] Further, the peak at 287.19 eV is observed only in the irradiated sample of MgTPP as a result of the photodegradation of MgTPP after its irradiation in an aerobic atmosphere.

As far as the N 1s spectra are concerned, MgTPP by itself displays, in accordance with the literature, a main peak at 398.05 eV, arising from the four chemically equivalent pyrrolenine nitrogen atoms of the metalloporphyrin macrocycle,[15,31,32a] and a second less intense peak at 400.36 eV (Fig. 8a). Although, the exact origin of the second peak is less certain, it is most likely due to a protonated nitrogen, produced as a result of small degree of demetallation of MgTPP during its prolonged exposure to X-rays in the course of the experiment. This demetallation seems to be a general feature with magnesium porphyrins as has been reported by other authors also.[31,32]

Upon addition of AuNPs to MgTPP, the principal peak at 398.05 eV, corresponding to the four chemically equivalent pyrrolenine nitrogens in MgTPP, is found to be shifted about 4.4 eV towards high energy to 402.41 eV (Fig. 8b)). This shift suggests that the initial chemical environment of the four nitrogens of MgTPP has been lost, and that a new chemical environment around nitrogens in presence of AuNPs, giving rise to the N 1s signal at 402.41 eV, has been established. This change in N 1s pattern of MgTPP in presence of AuNPs can be easily understood in terms of the interaction between nitrogens of MgTPP and AuNPs if we recall that a complex with a high association constant (10^4 M^{-1}) is formed between MgTPP and AuNPs as soon as they are mixed together (Fig. 5).

The emergence of just a single peak in N 1s spectrum of the mixture of MgTPP with AuNPs (Fig. 8b) indicates that the four nitrogens of MgTPP in presence of AuNPs or in the complex are chemically equivalent. Further, the presence of this peak at higher energy (402.41 eV) suggests that the nitrogens are now in more positively charged or in higher oxidation state than they were in MgTPP alone.[33] In other words, the nitrogens, which were in trivalent state in MgTPP with a binding energy of 398.05 eV, have now, in presence of AuNPs or as a result of the complex formation with AuNPs, been converted into ammonium quaternary nitrogens (R_4N^+) which are known to possess a higher binding energy at 402 eV.[34-36] This, *i.e.*, the nitrogens acquiring a positive charge (+1), can come about only if the complex formation between MgTPP and AuNPs takes place via the implication of the non-bonding electrons on nitrogens of MgTPP since

nitrogens are already bound to the central metal, Mg. Further, as mentioned above, since all four nitrogens of MgTPP, in presence of AuNPs, are chemically equivalent, all these nitrogens, through their lone pair electrons, will participate in the process of complex formation with AuNPs, bearing in mind, of course, that the nitrogens are still bound to Mg. The complex is, thus, $MgTPP^{4+}$-AuNP; its schematic representation is shown in Scheme 1. The involvement of non-bonding electrons of nitrogen in complex formation between MgTPP and AuNPs is consistent with the observations of Kamat *et al.*[23,24] and Kastonis *et al.*[25], who, respectively, reported the binding of bezylamine and meso-tetradodecylporphyrin with AuNPs via interaction of the non-bonding electrons on nitrogen of the respective molecules.

One can thus see how the interaction between MgTPP and AuNPs involving the transfer of non-bonding electrons of nitrogens on MgTPP to AuNPs has led to the disappearance of the peak at 398 eV of MgTPP and to the appearance of the peak due to quaternary ammonium nitrogens at 402.41 eV in the XPS of MgTPP in its mixture with AuNPs (Fig. 8b). A small contribution to the signal at 402.41 eV from the quaternary nitrogens of free TOAB, ejected to make place for the attachment of MgTPP onto AuNPs, can not be ignored; TOAB attached to AuNP shows N 1s peak at 401.34 eV (Fig. S2).

The transfer of lone pair electrons from MgTPP to AuNPs is also evident from the changes observed in the Au(4f) peaks of AuNPs after the addition of MgTPP. The XPS spectrum of AuNPs alone (Fig. 9a) shows two peaks, namely, $4f_{7/2}$ and $4f_{5/2}$, at binding energies of 84.06 and 87.65 eV, respectively, corresponding to gold in zero oxidation state (Au^0).[37] In its mixture with MgTPP, however, these Au(4f) peaks are shifted to lower energies (Fig. 9b). This lowering of the Au(4f) binding energy suggests that the electron density around Au has increased[38,39] since it will facilitate the expulsion of the core electrons. This increase in electron density on Au occurs as a result of the transfer of electronic charge (lone pair of electrons) from nitrogens of MgTPP to AuNPs during their binding with each other, corroborating the observations made in N 1s spectra of

MgTPP in presence of AuNPs (Fig. 8b) where nitrogen has been shown to donate its electrons to AuNPs to form the $MgTPP^{4+}$-AuNP complex.

The N 1s XPS of degraded MgTPP after 5 hrs of illumination is presented in Fig. 8c. It shows two peaks of comparable intensity at 400.52 and 398.59 eV, although at similar energies as that seen for un-irradiated MgTPP (Fig. 8a). In spite of this resemblance, the origin of these peaks in the two cases is entirely different. In one case (un-irradiated sample), we are dealing with the structure of MgTPP molecule itself, whose absorption spectrum (Fig. 1a), in complete agreement with the literature, shows a strong Soret absorption band at 426 nm and other somewhat weaker Q bands at 523, 562 and 603 nm. In the case of irradiated or degraded MgTPP, we are dealing with rather new chemical products with altered molecular structure.[12,13] This is evident from the absorption spectrum of the photodegraded sample (Fig. 2, spectrum g) in which the main absorption of MgTPP at 426 nm has practically disappeared, and a much weaker band is visible at 420 nm. In addition, the fine structure of Q bands in the region of 500 to 650 nm is lost and an increase in the absorption at 467 and 793 nm is observed, confirming the formation of new chemical species as a result of the irradiation of MgTPP. Further, the intensity of the peak at 400.52 eV in irradiated sample, in contradistinction to the un-irradiated MgTPP, is almost comparable to that at 398.59 eV.

In light of this, the signal at 400.52 eV in illuminated sample of MgTPP, (Fig. 8c), has been assigned to the pyrrolenine nitrogen bound to oxygen, present as N-O-Mg in the photodegraded product. The presence of such a peak at 400.52 eV was also observed by Zhang *et al.*[15] in the XPS of photochemically degraded MgTPP, who ascribed it to be due to the formation of a N-O bond. The second peak at 398.59 eV in the XPS of the degraded sample is assigned to the nitrogens of the photodegraded product of MgTPP, a dematallized open chain structure. The photoreaction of metalloporphyrins with oxygen (singlet oxygen) during illumination is known to cause the ring-opening of the porphyrin cycle, finally resulting in the formation of a demetallized open-chain structure.[12,13,40]

Now to understand the mechanism underlying the protective role of AuNPs in the photodegradation of MgTPP, it should be noted that the photodegradation of porphyrins is brought about by the reactive oxygen species (ROS), and that during photochemical degradation of MgTPP, the formation of an adduct of MgTPP and oxygen, with oxygen bound to the nitrogen of MgTPP as N-O-Mg, takes place (our present study, Fig. 8c, and ref. 15). In other words, the binding of oxygen to the nitrogens of MgTPP is responsible for the photodegradation of MgTPP. Thus, the photoprotection imparted to MgTPP by AuNPs suggests that they have prevented oxygen (ROS) to bind with MgTPP at its nitrogen sites. One of the ways that AuNPs can do this is that they themselves react with MgTPP and occupy its nitrogen sites, and thereby deny oxygen the access to the nitrogens of MgTPP. The formation of a complex as seen in the absorption spectrum of MgTPP with the addition of AuNPs tells us that MgTPP is, indeed, bound to AuNPs, and that the binding between the two takes place via nitrogen atoms of MgTPP is confirmed by the XPS experiments. The role of AuNPs in photoprotection of MgTPP in aerobic conditions/medium thus lies in their ability to bind with the nitrogens of MgTPP before oxygen has a chance to attach itself to these nitrogens and cause photodamage.

One can thus see that both AuNPs and oxygen (ROS) vie for the same nitrogen sites of MgTPP, although one (AuNPs) to photoprotect it (MgTPP) while the other (oxygen) out to photodestroy it (MgTPP). Since AuNPs do render photoprotection to MgTPP, the question arises how AuNPs succeed in keeping oxygen at bay and win the race of binding with nitrogens? The answer to this is the manner in which oxygen and AuNPs react with MgTPP. AuNPs, as soon as they are mixed with MgTPP, readily bind to or react with MgTPP in its ground state, *i.e.*, even in dark prior to illumination, as is clear from the changes observed in the absorption spectrum of MgTPP (Fig. 5). Oxygen, on the other hand, reacts efficiently with MgTPP only during its illumination (Fig. 8c), because that is the time that MgTPP is photoexcited and generates triplet states, via intersystem crossing from its excited singlets. The MgTPP triplets promote ground state triplet molecular oxygen to produce ROS which then react with parent molecule, MgTPP, to cause its photooxidation and photodegradation. In other words, illumination is necessary for oxygen to interact with MgTPP.

In view of this, AuNPs possess an enormous edge over oxygen with regard to their interaction with MgTPP. To put it differently, AuNPs, when mixed with MgTPP, have got sufficient or all the time to react with MgTPP, without any interference from oxygen or other source, to occupy and saturate practically all the available nitrogen sites of MgTPP. Thus, when MgTPP is illuminated in presence of AuNPs, oxygen, to its great surprise and loss, finds that virtually all or quasi-totality of the nitrogen sites have already been occupied by AuNPs even before illumination. Consequently, the binding of oxygen (ROS) with nitrogens of MgTPP is strongly inhibited in presence of AuNPs. This results in a decreased formation of N-O species, which is reflected in the decreased amount of the photodegradation of MgTPP in presence of AuNPs.

Further, AuNPs not only deprive oxygen (ROS) of the access to nitrogens of MgTPP, but also help diminish the production of destructive ROS, and provide added photoprotection to MgTPP. This happens as a result of the decreased formation of the excited singlet states of MgTPP in presence of AuNPs as is seen from the quenching of MgTPP fluorescence with addition of AuNPs (Fig. 6). The decreased formation of MgTPP singlets produce smaller amounts of MgTPP triplets which, in turn, generate smaller quantities of ROS. The binding between AuNPs and MgTPP via its nitrogens is thus a key factor in the process of photoprotection. The greater the amount of MgTPP bound to AuNPs the greater is the degree of photoprotection rendered to MgTPP by AuNPs, as is seen in the inset of Fig. 3.

The beneficial role of AuNPs as photoprotector of MgTPP can also been seen in oxygen free solutions of MgTPP (Fig. 10A,B). Under anaerobic conditions, the photodegradation of MgTPP most probably proceeds directly from its excited singlet or/and triplet states, without the intermediacy of oxygen.[9b] Although, the exact mechanism for the photoprotection of MgTPP by AuNPs under anaerobic conditions can not be elucidated at the present time, the binding of AuNPs with MgTPP, which takes place as soon as the two are mixed together, might, once again, be the possible reason for the protection of MgTPP by AuNPs in anaerobic medium too. This binding causes the fluorescence quenching of MgTPP, *i.e.,* it results in the dissipation of the excited

states of MgTPP in presence of AuNPs. Since, the degradation of MgTPP under anaerobic conditions takes place via its excited states, the smaller quantities of these states in presence of AuNPs will lead to a diminished photodegradation of MgTPP.

Conclusions

We have demonstrated that AuNPs protect MgTPP efficiently in solution against photodegradation. With an appropriate concentration of AuNPs, virtually 100% photoprotection can be provided to MgTPP. The protecting ability of AuNPs is the result of their binding with MgTPP at its nitrogen sites, inhibiting, thus, the binding of reactive oxygen species (ROS) at these sites, known to cause photodegradation of MgTPP and many other porphyrins under aerobic conditions. This binding also decreases the formation of excited singlet states of MgTPP, which suppresses the generation of ROS and further improves the photostability of MgTPP. The same binding may also be responsible for the photoprotection provided to MgTPP by AuNPs under anaerobic conditions as well. The method of blocking the nitrogen sites of porphyrins thus offers us a new strategy and opens up new avenues to increase the photostability of various porphyrins used in a wide range of industrial (optoelectonic devices) and medical (photodynamic therapy) applications.

Acknowledgments

The authors thank Prof. Prashant V. Kamat of Radiation Laboratory, University of Notre Dame, for helpful discussions. The work described herein was supported by the Natural Sciences and Engineering Research Council of Canada.

Références

(1) K. Takahashi, T. Goda, T. Yamaguchi and T. Komura, *J. Phys. Chem. B.* 1999, **103**, 4868-4875.

(2) T. Hasobe, H. Imahori, P.V. Kamat, T.K. Ahn, S.K. Kim, D. Kim, A. Fujimoto, T. Hirakawa and S. Fukuzumi *J. Am. Chem. Soc.* 2005, **127**, 1216-1228.

(3) T. Hasobe, H. Imahori, P.V. Kamat and S.Fukuzumi, *J. Am. Chem. Soc.* 2003, **125**, 14962-14963.

(4) Y. Liu, X. Guo, N. Xiang, B. Zhao, H. Huang, H. Li, P. Shen and S. Tan, *J. Mater. Chem.* 2010, **20**, 1140-1146.

(5) H-P. Lu, C-L. Mai, C-Y. Tsia, S-J. Hsu, C-P. Hsieh, C-L. Chiu, C-Y. Yeh and EW-G. Diau, *Phys. Chem. Chem. Phys.* 2009, **11**, 10270-10274.

(6) R. Bonnett, *Chem. Soc. Rev.* 1995, **24**, 19-33.

(7) M.C. DeRosa, and R.J. Crutchley, *Coord. Chem. Rev.* 2002, **233**, 351-371.

(8) K. Davia, D. King, Y. Hong and S. Swavey, *Inorg. Chem. Commun.* 2008, **11**, 584-586.

(9) (a) M.G.P.M.S. Neves and J.A.S. Cavalerio, *J. Chem. Soc. Perkin Trans.* 1990,**1**, 1937-1943; (b) J.A.S. Cavalerio, H. Görner, P.S.S. Lacerda, J.G. MacDonald, G. Mark, M.G.P.M.S. Neves, R. Nohr, H.P. Schuchmann, C.V. Sonntag and A.C. Tomé, *J. Photochem. Photobiol. A.* 2001,**144**, 131-140.

(10) (a) J.D. Spikes, *Photochem. Photobiol.* 1991, **54**, 1079-1092; (b) J.D. Spikes, *Photochem. Photobiol.* 1992, **55**, 797-808.

(11) (a) G.S. Cox and D.G. Whitten, *J. Am. Chem. Soc.* 1982, **104**, 516-521; (b) M. Krieg and D.G. Whitten, *J. Photochem.* 1984, **25**, 235-252.

(12) T. Matsuura, K. Inoue, A.C. Ranade, and I. Saito, *Photochem. Photobiol.* 1980, **31**, 23-26.

(13) K. Smith, T. Brown, R. Troxlers, and J-J. Lai, *Photochem. and Photobiol.* 1982, **36**, 147-152.

(14) J.P. Zhang, P.Y. Zhang, Z. Zhang, G.H. Chen, F. Han and X.H. Wei, *Chinese Chem. Lett.* 2008, **19**, 1190-1192.

(15) J. Zhang, P. Zhang, Z. Zhang and X. Wei, *J. Phys. Chem. A.* 2009, **113**, 5367-5374.

(16) M. Jakob, H. Levanon, P.V. Kamat, *Nano Lett.* 2003, **3**, 353-358.

(17) M. Brust, M. Walker, D. Bethell, D.J Schiffrin, and R. Whyman, *J. Chem. Soc., Chem. Commun.* 1994, (**7**), 801-802.

(18) V. Subramanian, E.E. Wolf, and P.V. Kamat, *J. Am. Chem. Soc.* 2004, **126**, 4943-4950.

(19) H. Claes, *Biochem. Biophys. Res. Comm.* 1960, **3**, 585-590.

(20) T. Ung, M. Giersig, D. Dunstan and P. Mulvaney, *Langmuir* 1997, **13**,1773-1782.

(21) H.A. Benesi and J.H. Hildebrand, *J. Am. Chem. Soc.* 1949, **71**, 2703-2707.

(22) J. R Lakowicz. Principles of fluorescence spectroscopy; Springer, New York, **2006**, page 282.

(23) K.G. Thomas, J. Zajicek and P.V. Kamat, *Langmuir* 2002, **18**, 3722-3727.

(24) K.G. Thomas and P.V Kamat,. *Acc. Chem. Res.* 2003, **36**, 888-898.

(25) N. Katsonis, J. Vicario, T. Kudernac, J. Visser, M.M. Pollard and BL. Feringa, *J. Am. Chem. Soc.* 2006, **128**, 15537-15541.

(26) D. Pantea, H. Darmstadt, S. Kaliaguine and C. Roy, *Appl. Surf. Sci.* 2003, **217**, 181-193.

(27) S. Huh, J. Park, K. S. Kim, B. H. Hong, and S. B. Kim, *ACS Nano.* 2011, **5**, 3639-3644.

(28) F. Vitale, L. Fratoddi, C. Battocchio, E. Piscopiello, L. Tapfer, M. V. Russo, G. Polzonetti and C. Giannini, *Nano. Res. Lett.* 2011, **6**, 103.

(29) P.V. Galiy, A.V. Musyanovych, *Funct. Mater. Lett.* 2005, **12**, 467-475.

(30) N. T. T. Tran, T-H. Wang, C-Y. Lin, Y-C. Tsai, C-H. Lai and Y. Tai, *Bioconjugate Chem.* 2011, **22**, 1394-1401.

(31) S. Muralidharan and RG. Hayes, *J. Am. Chem. Soc.* 1980, **102**, 5106-5107.

(32) a) D.H. Karweik and N. Winograd, *Inorg. Chem.* 1976, **15**, 2336-2342; b) G. Polzonetti, C. Battocchio, A. Goldoni, R. Larciprete, V. Carravetta, R. Paolesse, and M.V. Russo, *Chem. Phys.* 2004, **297**, 307-314.

(33) J. Baltrusaitis, P.M. Jayaweera, V. H. Grassian, J. Baltrusaitis, P.M. Jayaweera and V.H. Grassian, *Phys. Chem. Chem. Phys.* 2009, **11**, 8295-8305.

(34) J.J. Jack, and D.M. Hercules, *Anal. Chem.* 1971, **43**,729-736.

(35) S. Virtanen, A. Soininen, V-M. Tiainen, D. Besic, M. Puk, T. Kinnari, J. Salo, R. Trebse, Aj. Trampuz, and Y. T. Konttinen, *SOT.* 2006, **29**, 290-295.

(36) A. Warshawsky, N. Kahana, V. Kampel, I. Rogachev, R.M. Kautzmann, JL. Cortina and C.H. Sampaio, *Macromol. Mater. Eng.* 2001, **286**, 285-295.

(37) G. Ertas, U. K. Demirok and S. Suzer, Appl. Surf. Sci. 2005, **249**, 12-15.

(38) P. Jiang, J-J. Zhou, R. L. Wang and S-S. Xie, *Nanotechnology* 2006, **17**, 3533-3538.

(39) M. Zhou, B. Wang, Z. Rozynek, Z. Xie, J. O. Fossum, X. Yu and S. Raaen, *Nanotechnology* 2009, **20**, 505606-505615.

(40) K.M. Smith, Porphyrins and Metalloporphyrins; Elsevier Scientific Publishing Company: Amsterdan-Oxford-New York, **1975**.

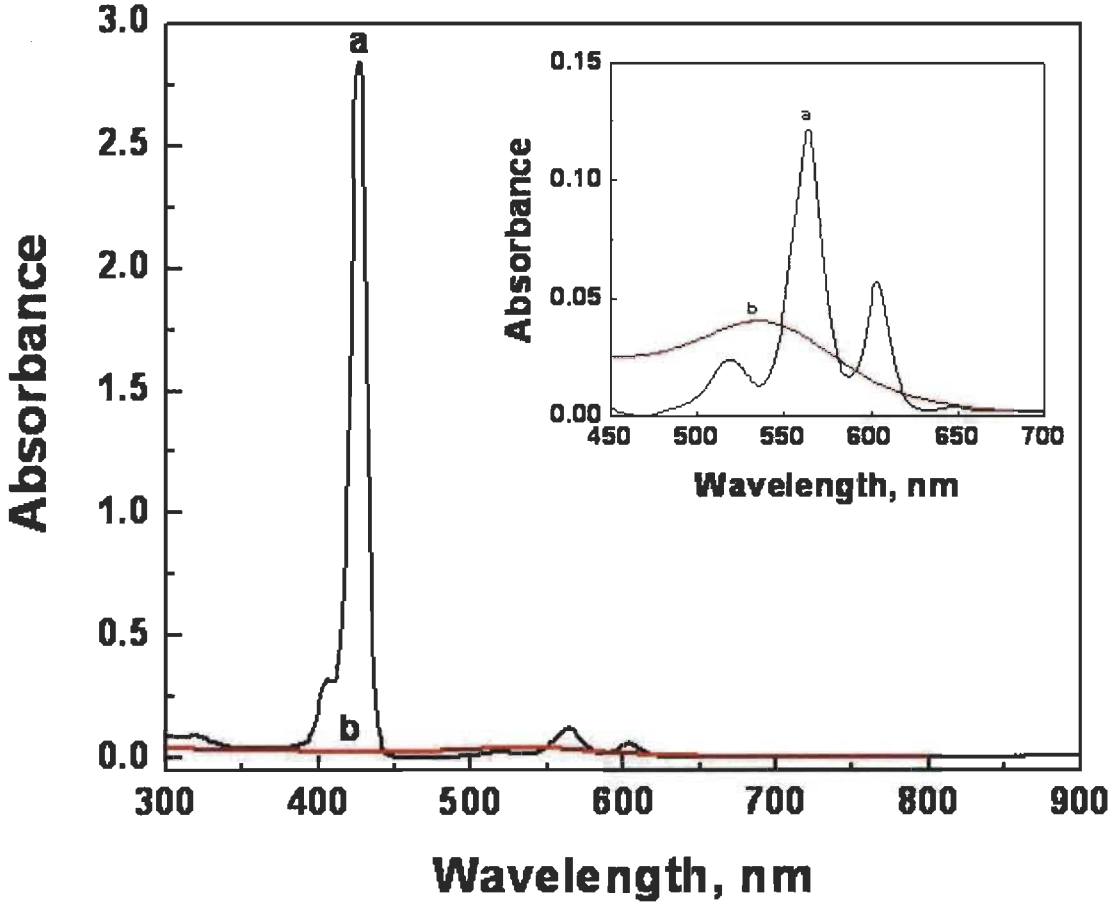

Fig. 1 Absorption spectra of (a) 5.3 μM MgTPP, and (b) 50 μM Au nanoparticles in toluene. The insert shows an expanded view of these spectra in the region of 450-700 nm.

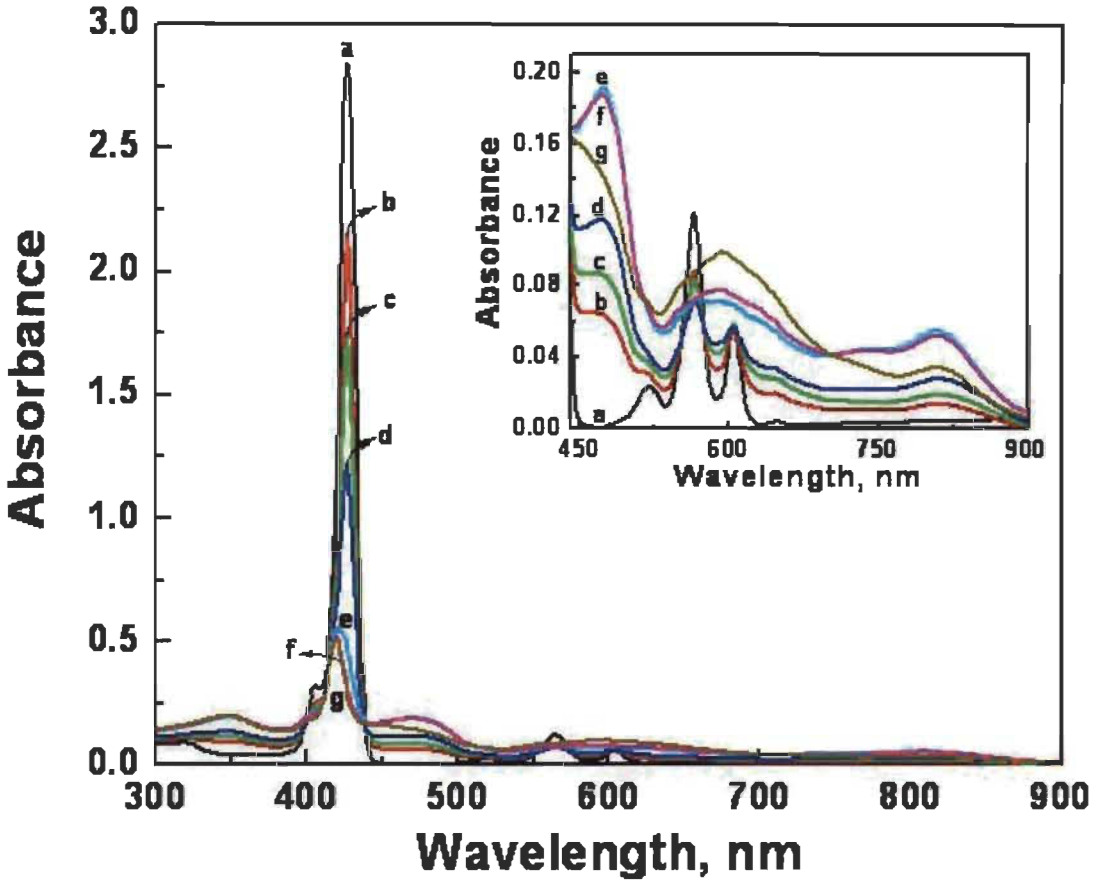

Fig. 2 Absorption spectra of MgTPP solution in toluene (5.3 μM) as a function of irradiation time (λ > 400 nm): (a) 0, (b) 20, (c) 30, (d) 45, (e) 120, (f) 180, and (g) 300 min. The insert shows an expanded view of these spectra in the region of 450-900 nm.

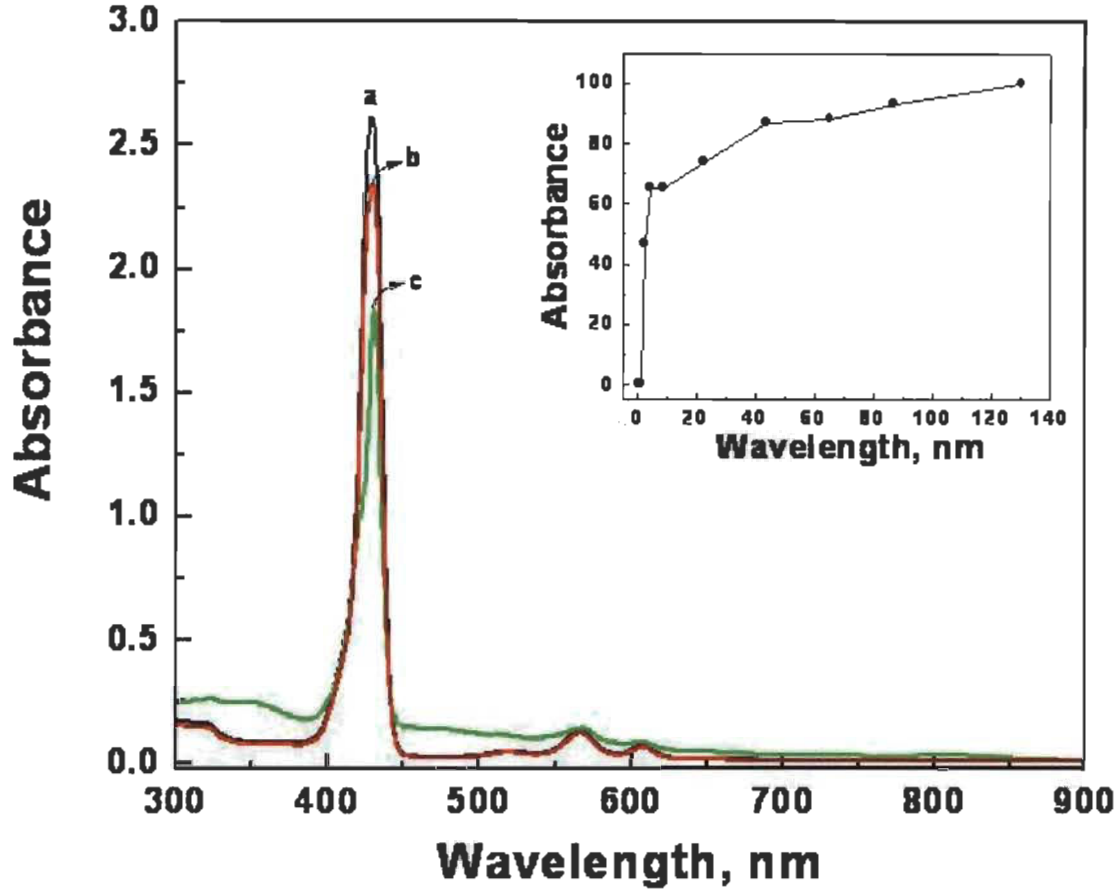

Fig. 3 Absorption spectra of MgTPP solution in toluene (5.3 μM) in presence of AuNPs (4.3 μM) at different time intervals of irradiation ($\lambda > 400$ nm): (a) 0, (b) 45, and (c) 300 min. The inset shows the effect of AuNPs concentration on the photoprotection of MgTPP; irradiation time is 5 hr. The % photoprotection of MgTPP was calculated from the variation of absorbance at 426 nm, using eq. 1 (see text).

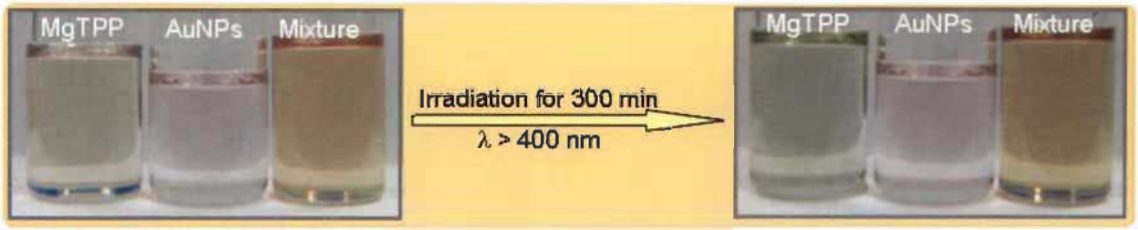

Fig. 4 Changes in the coloration of MgTPP (5.3 μM), AuNPs (43 μM), and their mixture in toluene after 300 min of irradiation ($\lambda > 400$ nm).

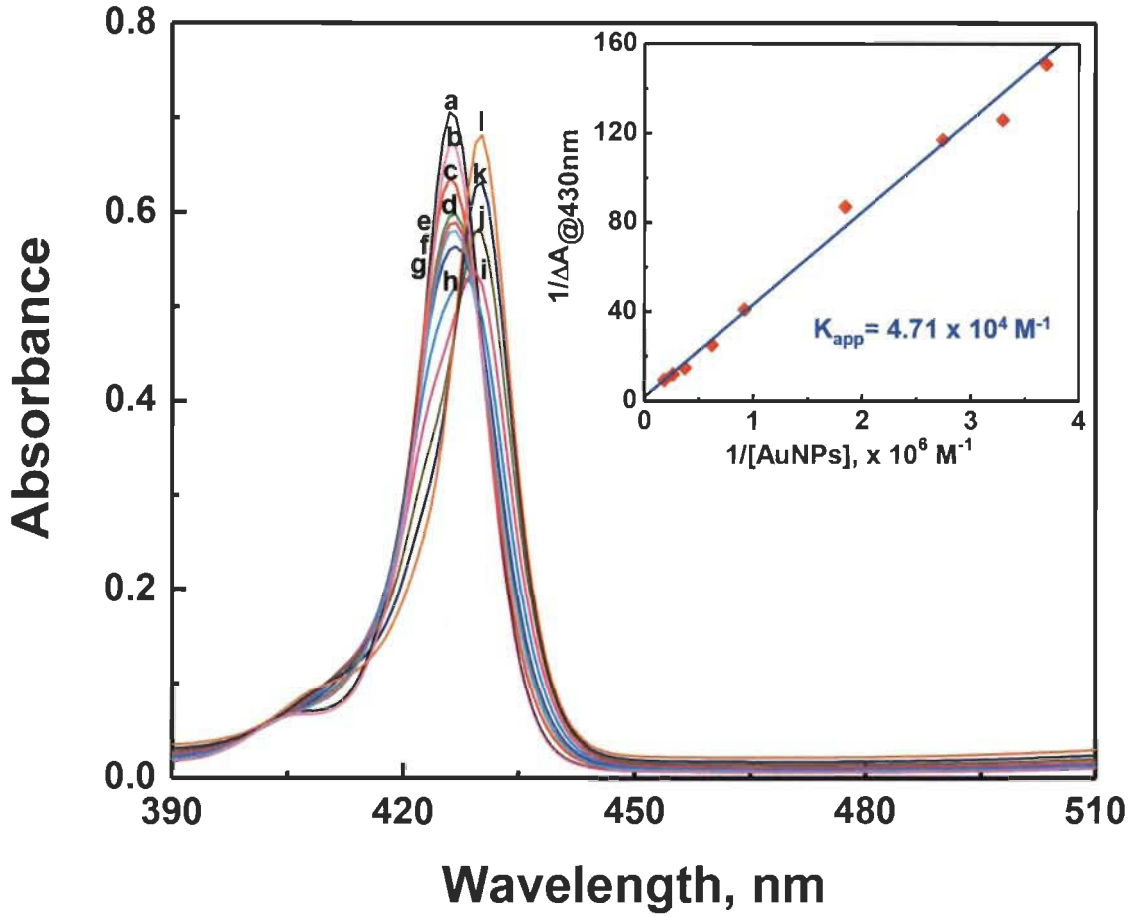

Fig. 5A Effect of AuNPs on the absorption spectra of MgTPP solution (1.3 μM) in toluene: (a) 0, (b) 0.13, (c) 0.19, (d) 0.27, (e) 0.30, (f) 0.36, (g) 0.54, (h) 1.08, (i) 1.62, (j) 2.70, (k) 3.78 and (l) 5.40 μM. The insert shows the plot of $1/\Delta A(430\ nm)$ vs 1/[AuNPs]. An apparent association constant (K_{app}) of $4.71 \times 10^4\ M^{-1}$ was obtained from the intercept-to-slope ratio of the plot.

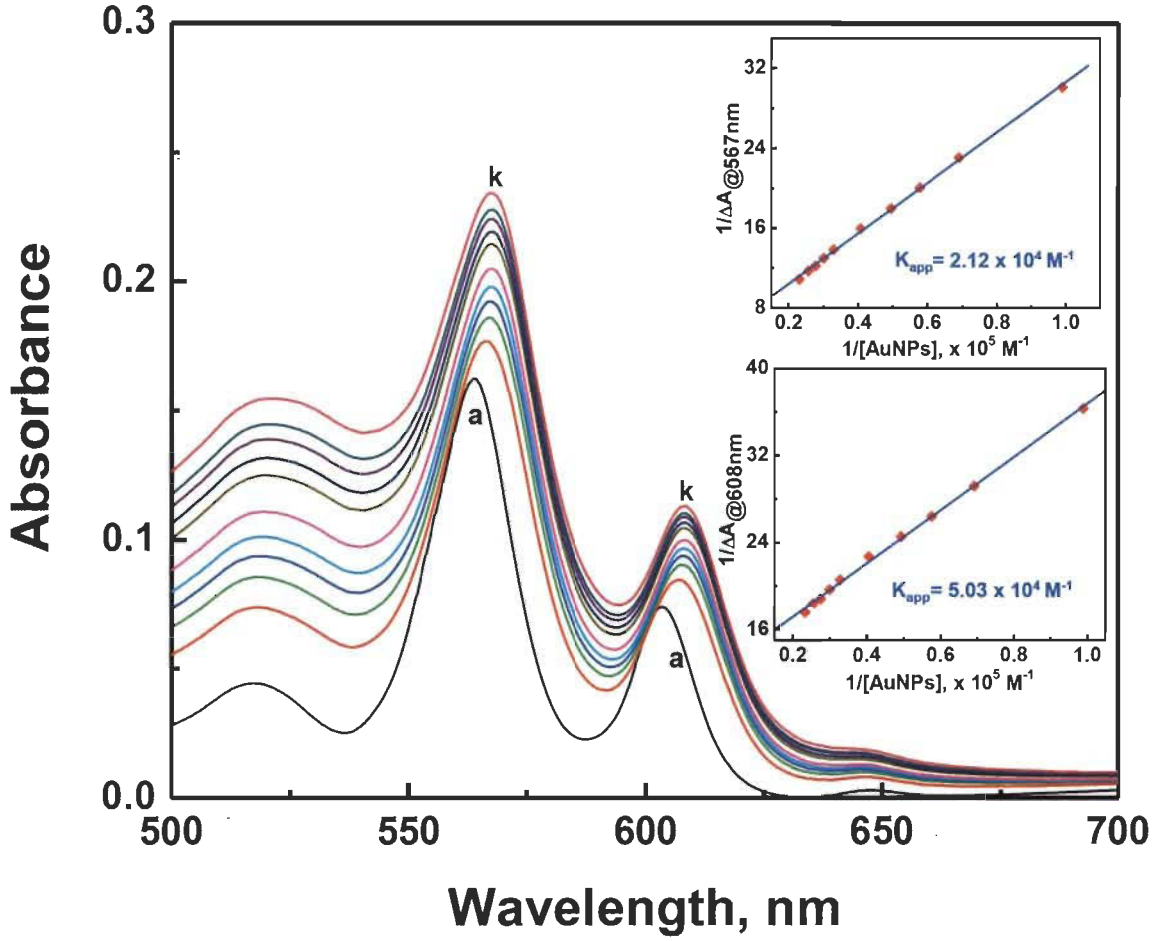

Fig. 5B Effect of AuNPs on the absorption spectra of MgTPP solution (10 μM) in toluene: (a) 0, (b) 10.11, (c) 14.44, (d) 17.33, (e) 20.22, (f) 24.55, (g) 30.33, (h) 33.22, (i) 36.11, (j) 39 and (k) 43.33 μM. The inserts show the plots of 1/ΔA(567 nm) and 1/ ΔA(608 nm) vs 1/[AuNPs].

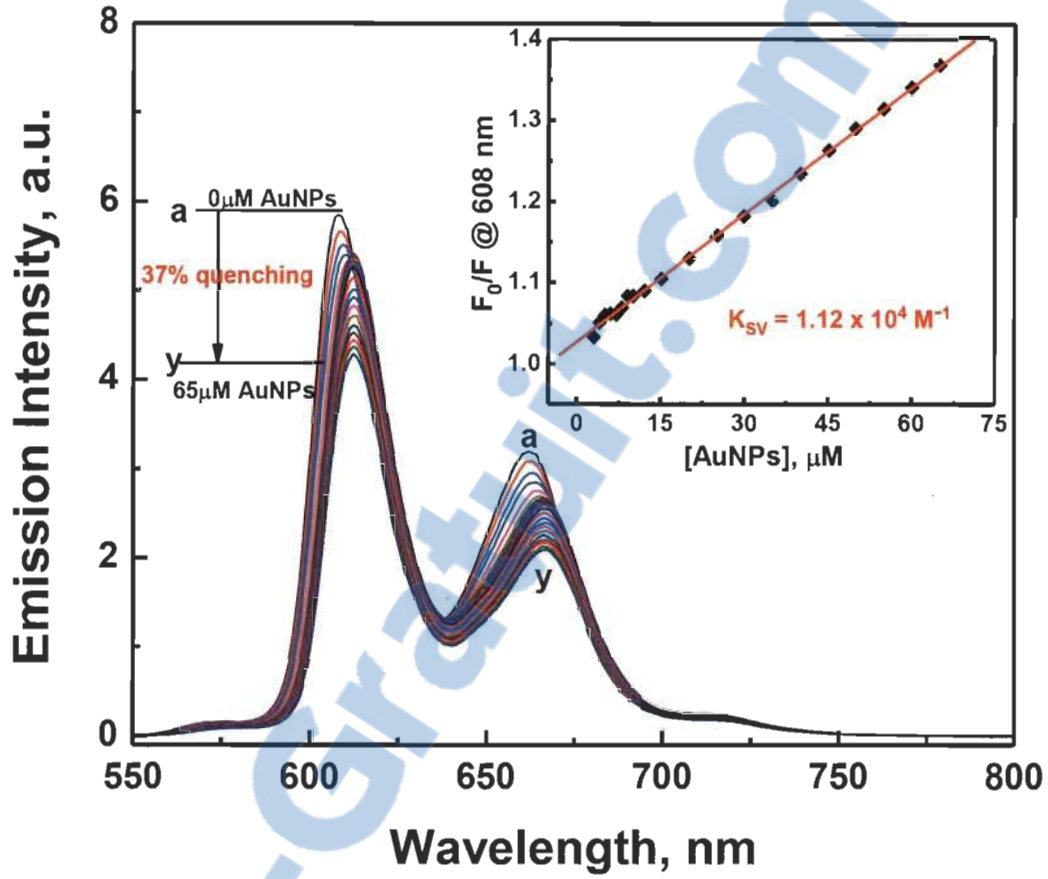

Fig. 6 Effect of AuNPs on the fluorescence emission spectra of MgTPP solution (2.5 μM) in toluene: (a) 0, (b) 0.25, (c) 0.5, (d) 1, (e) 2, (f) 3, (g) 4, (h) 5, (i) 6, (j) 7, (k) 8, (l) 9, (m) 10, (n) 12, (o) 15, (p) 20, (q) 25, (r) 30 , (s) 35, (t) 40, (u) 45, (v) 50, (w) 55, (x) 60 and (y) 65 μM. Excitation wavelength was 405 nm. The insert shows the Stern-Volmer plot (F_0/F vs [AuNPs], where: F_0 and F are the fluorescence intensities of MgTPP in absence and presence of AuNPs, respectively. The fluorescence was monitored at 608 nm.

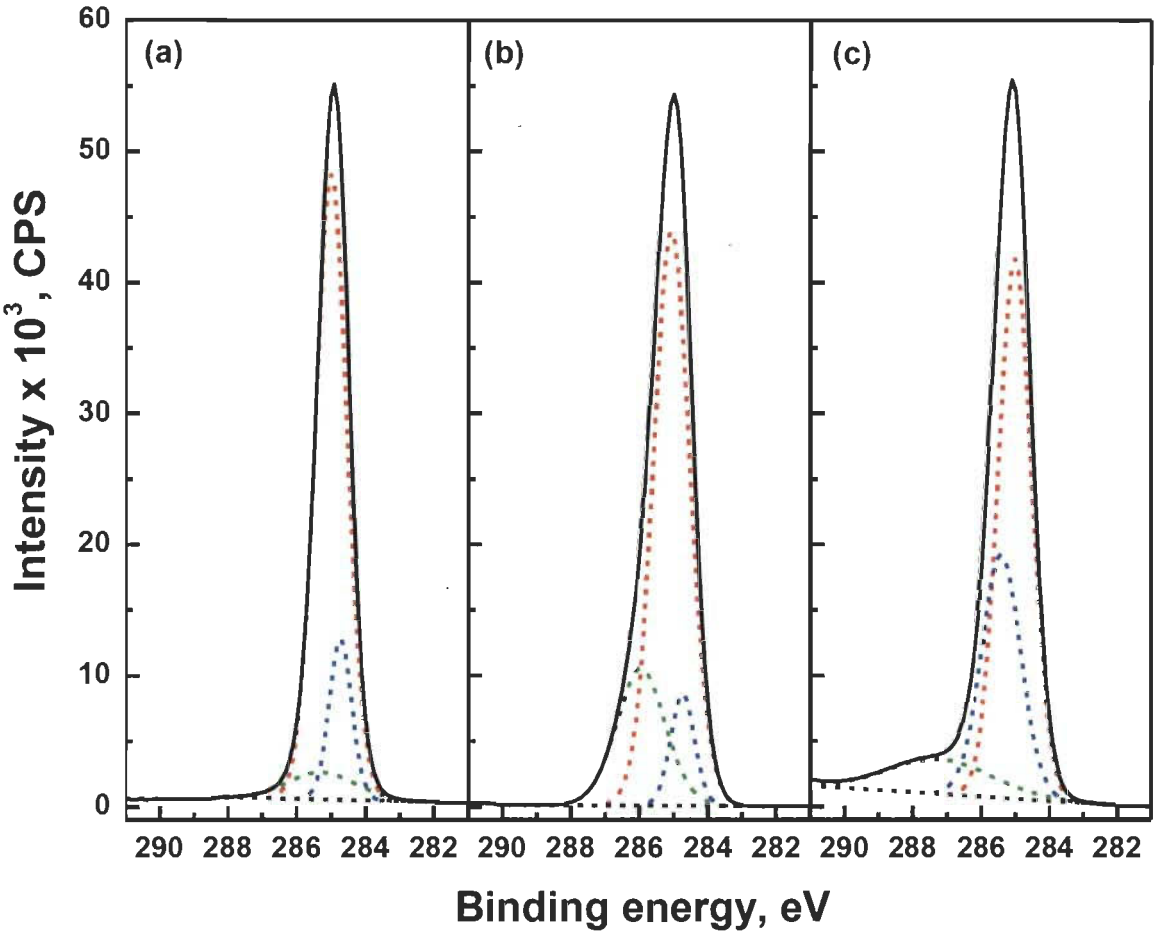

Fig. 7 C1s narrow scan XPS spectra for: (a) MgTPP, (b) the mixture of MgTPP and AuNPs, and (c) photodegraded MgTPP (irradiated for 300 min).

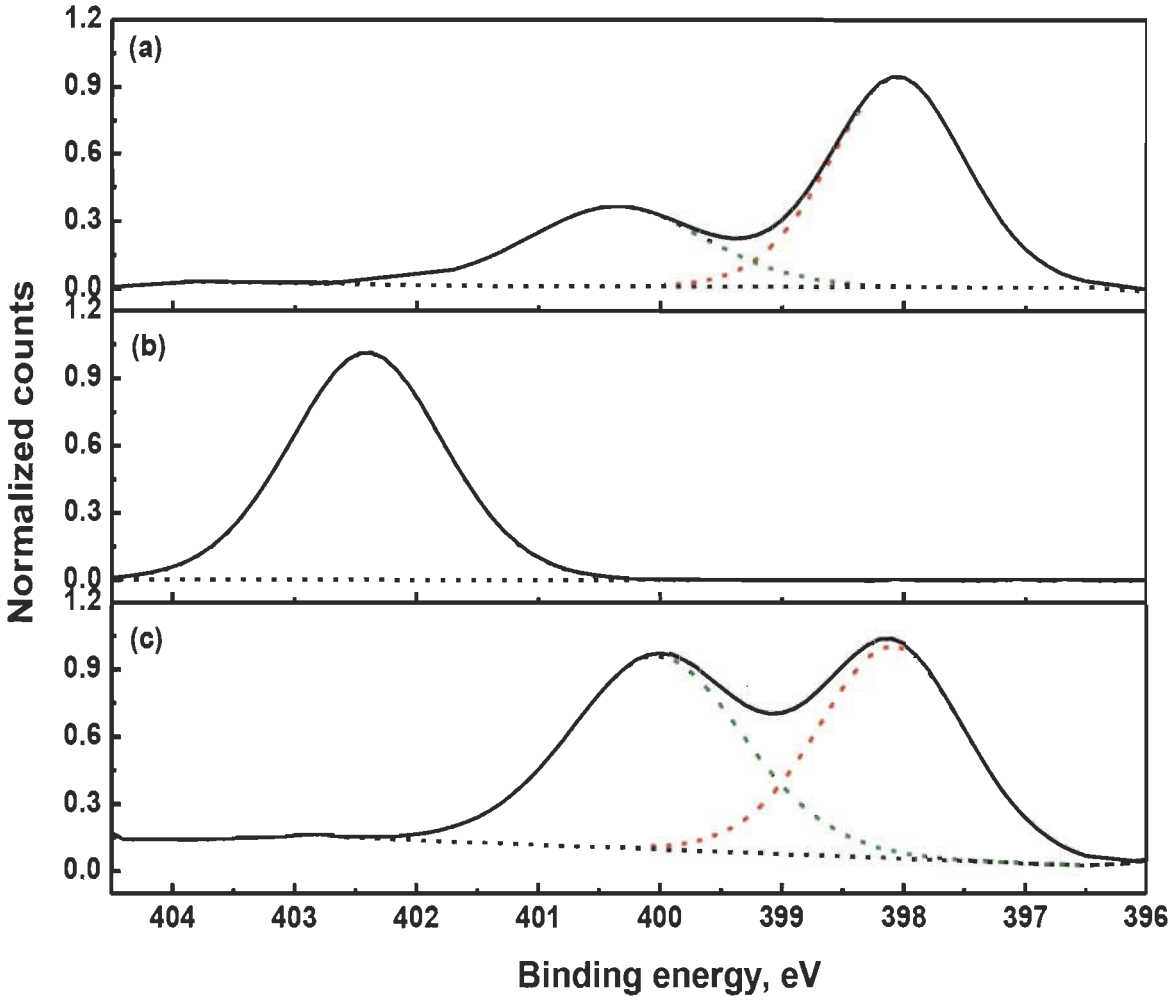

Fig. 8 N1s narrow scan XPS spectra for: (a) MgTPP, (b) the mixture of MgTPP and AuNPs, and (c) photodegraded MgTPP (irradiated for 300 min).

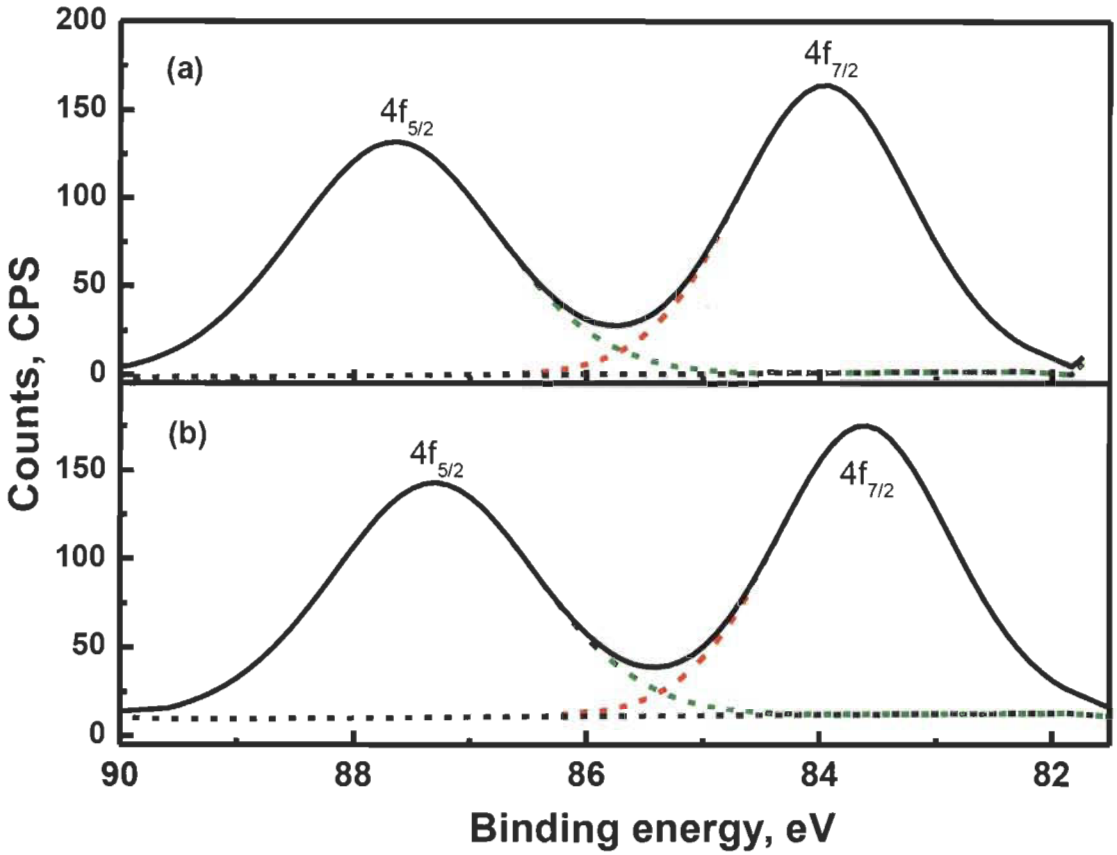

Fig. 9 Au(4f) narrow scan XPS spectra for: (a) AuNPs and (b) the mixture of AuNPs with MgTPP.

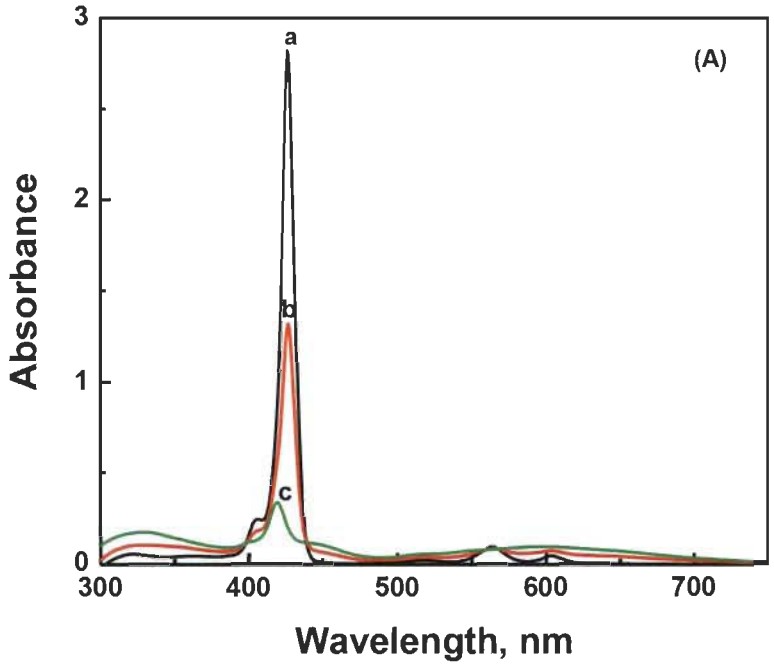

Fig. 10A Absorption spectra of MgTPP solution in toluene (5.3 μM) in an anaerobic atmosphere in absence AuNPs recorded at different time intervals of irradiation ($\lambda > 400$ nm): (a) 0, (b) 30, and (c) 300 min.

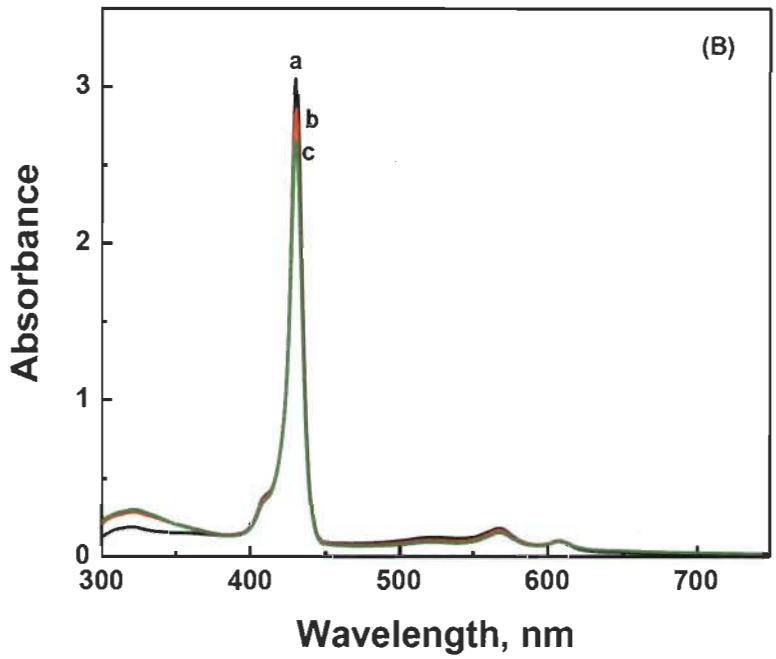

Fig. 10B Absorption spectra of MgTPP solution in toluene (5.3 μM) in an anaerobic atmosphere in presence of 22 μM AuNPs recorded at different time intervals of irradiation ($\lambda > 400$ nm): (a) 0, (b) 180, and (c) 300 min.

Table 1. Experimental atomic composition obtained by XPS analysis for MgTPP, photodegraded MgTPP and MgTPP-AuNPs mixture. Error in determination is ~ ± 1%.

Sample	Atomic content (%)*			
	C	O	N	Au(4f)
MgTPP	97.7	0.4**	1.9	0
Photodegraded MgTPP	97.3	1.0	1.7	0
MgTPP-AuNPs mixture	97.8	0.2**	1.7	0.3

* The atomic content of Mg is not presented in this Table because its binding energy was very difficult to record due to the poor signal to background counting ratio caused by the low core level cross section of the Mg 1s level. ** Adsorbed oxygen during the preparation of the samples.

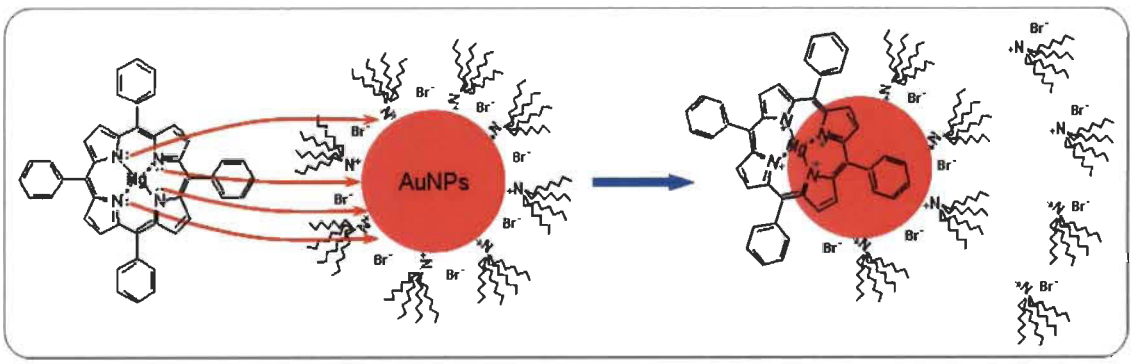

Scheme 1 Interaction between MgTPP and AuNPs via non-bonding electrons on nitrogens of MgTPP.

SUPPORTING INFORMATION

Beneficial Role of Gold Nanoparticles as Photoprotector of Magnesium tetraphenylporphyrin

Laurent Bekalé, Saïd Barazzouk, and Surat Hotchandani*

Groupe de Recherche en Biologie-Végétale, Université du Québec à Trois-Rivières, Trois-Rivières, Qc, G9A 5H7, Canada

* To whom correspondence should be addressed. e-mail: hotchand@uqtr.ca

High-resolution C1s and N1s XPS spectra for gold nanoparticles (AuNPs) are shown in Fig. S1 and S2, respectively. The C1s region of AuNPs comprises three distinct peaks. The peak appearing at 285 eV, is assigned to C-C and C-H from tetraoctylammonium bromide (TOAB), the stabilizing agent used in the preparation of AuNPs. The second peak at 286.07 eV is ascribed to C-N of quaternary amine from TOAB, while a smaller peak at higher binding energy (287.17 eV) is probably due to an impurity.

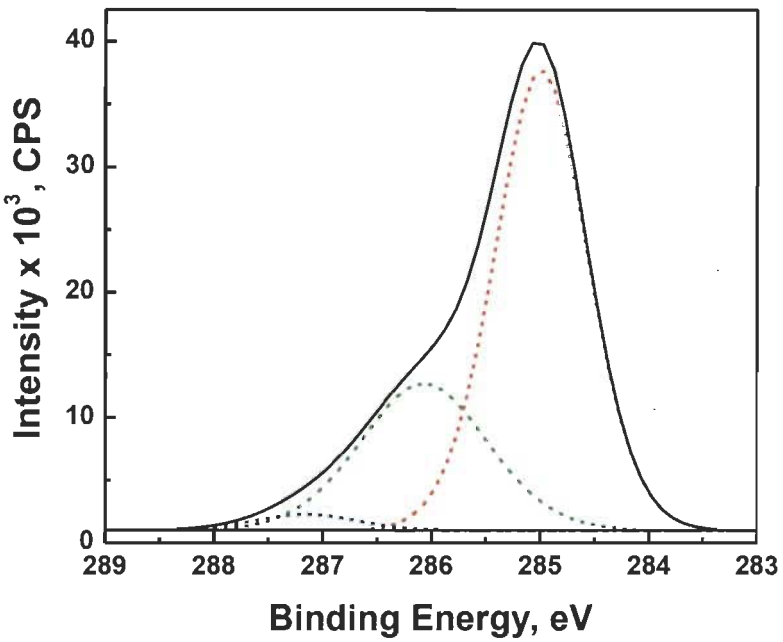

Fig. S1 C1s narrow scan XPS spectrum for AuNPs.

The N 1s spectrum of AuNPs (Fig. S2) presents two peaks with an intensity ratio of about 99:1, which appear at 401.34 (90.5%) and 402.96 eV (9.5%), respectively. Both peaks are characteristic of quaternary nitrogens, although, present in two different chemical environments. The first one at 401.34 eV is assigned to quaternary nitrogen (Oct_4N^+) of TOAB adsorbed on the surface of AuNPs[1]. The second peak, a weaker one, at high binding energy 402.96 eV, corresponds most probably to the small quantity of TOAB which is not in direct contact with gold surface of AuNPs, but rather through the intermediacy of bromide ions which are adsorbed on gold nanoparticles. This signal is

consistent with the work of Bureau *et al* who reported the presence of a similar peak for tetramethyl ammonium hydroxide $\{(CH_3)_4N^+, OH^-\}$ adsorbed on nickel surface[2].

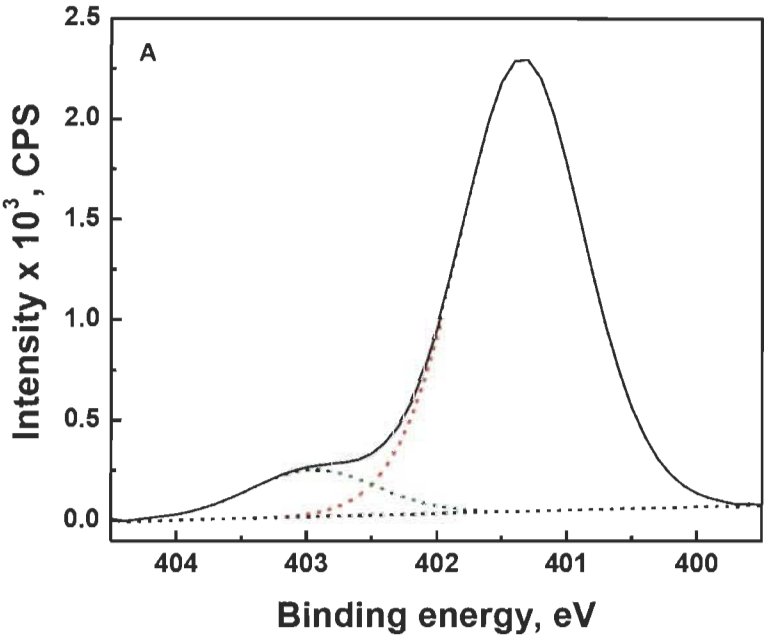

Fig. S2 N 1s narrow scan XPS spectrum for AuNPs.

Table S1. Fraction of the incident light absorbed by AuNPs of varying concentration in the mixture of MgTPP and AuNPs. The concentration of MgTPP in the mixture is constant at 5.3 μM, and the total light absorbed by this solution in the wavelength range (400-900 nm) is 494 i_0. The total incident light intensity is 5000 i_0.

Concentration of AuNPs (μM)	Amount of incident light absorbed by AuNPs	Total amount of incident light absorbed by the mixture (MgTPP + AuNPs)	The percentage of incident light absorbed by AuNPs in the mixture
2.17	39 i_0	494 i_0 +39 i_0 = 533 i_0	7.3
4.33	57 i_0	551 i_0	10.3
8.67	105 i_0	599 i_0	17.3
22	229 i_0	723 i_0	31.7
43.3	324 i_0	818 i_0	39.6
65	617 i_0	1111 i_0	55.6
130	1070 i_0	1573 i_0	68.6

References of supporting information

(1) J.R. Pels, F. Kapteijn, J.A. Moulijn, Q. Zhu, and K.M. Thomas, *Carbon*, 1995, **33**, 1641-1653.

(2) C. Bureau, and P.D. Chong, *Chem. Phys. Lett*, 1997, **264**, 186-19.

CHAPITRE III

ENHANCED PHOTOSTABILITY OF CHLOROPHYLL-*A* USING GOLD NANOPARTICLES AS AN EFFICIENT PHOTOPROTECTOR

Le contenu de ce chapitre a fait l'objet d'une publication en anglais dans la revue : *Journal of Materials Chemistry*, 2012, 22, 25316-25324.

3.1 Résumé de l'article

Une étude complète des propriétés photoprotectrices des nanoparticules d'or (AuNPs) a été effectuée dans ce second article scientifique afin d'établir que la méthode de photoprotection, précédemment présentée dans le premier article scientifique, pourrait également permettre d'accroître la stabilité des porphyrines de magnésium plus complexe que le tétraphénylporphyrine de magnésium (MgTPP), c'est-à-dire, les porphyrines possédant à la fois des doublets d'électrons libres sur les atomes d'azote du macrocycle et sur les groupes fonctionnels périphériques qui ne sont pas conjugués au macrocycle, comme c'est le cas avec les chlorophylles et les bactériochlorophylles. Nos résultats montrent que la photodégradation de la chlorophylle-*a* (Chl*a*) est ralentie en présence des AuNPs, et une augmentation pouvant atteindre un ordre de grandeur dans le temps de demi-vie de Chl*a* en présence d'AuNPs a été observée. Il a également été observé que dans des conditions *in vitro*, les AuNPs sont des agents photoprotecteurs bien plus efficaces que les molécules comme la β-carotène ou de quinones, qui sont connues pour être très efficaces dans des conditions *in vivo* (dans les plantes). Enfin, la capacité protectrice des AuNPs est le résultat de leur liaison avec les sites azotés du macrocycle porphyrique de la Chl*a*, et ce, avant la formation des espèces réactives de l'oxygène (ROS) par photosensibilisation. Ce mécanisme de photoprotection rend les AuNPs plus efficaces que les carotènes ou des quinones qui offrent une protection à la Chl*a* par neutralisation des ROSs après illumination. L'étude présentée dans cet article a été l'aboutissement du deuxième objectif opérationnel de cette thèse.

3.2 Deuxième article scientifique

Enhanced photostability of chlorophyll-*a* using gold nanoparticles as an efficient photoprotector

Saïd Barazzouk‡, Laurent Bekalé‡, and Surat Hotchandani*

Groupe de Recherche en Biologie-Végétale, Université du Québec à Trois-Rivières, Trois-Rivières, Qc, G9A 5H7, Canada

‡ contributed equally to this work

* To whom correspondence should be addressed. e-mail: hotchand@uqtr.ca

Abstract

Improving the photostability of chlorophylls is one of the main challenges to facilitate their industrial and biotechnological use. In this regard, we have employed gold nanoparticles (AuNPs) to photoprotect chlorophyll-*a* (Chl*a*). The results show that the photodegradation of Chl*a* is slowed down in presence of AuNPs, and an increase of as much as an order of magnitude in half-life time of Chl*a* in presence of AuNPs has been observed. It is further seen that under *in-vitro* conditions, AuNPs are much better photoprotective agents of Chl*a* than β-carotene or quinones, which are known to be very effective in natural living conditions (plants). The protecting ability of Chl*a* by AuNPs is the result of their efficient binding with Chl*a* at its nitrogen sites even in dark, thus, inhibiting the reaction of reactive oxygen species with Chl*a*, known to cause its degradation during illumination. The same property of AuNPs, *i.e.*, to bind with Chl*a* in dark, renders them better photoprotectant than carotene or quinones since these agents offer protection to Chl*a* during its illumination.

Introduction

The application of biomolecules in various fields of material science such as biomedical engineering,[1] optoelectronics,[2] *etc.*, is potentially one of the most important emerging new technologies. Recently, organic light-emitting diodes (OLEDs) have been fabricated using horse-heart cytochrome-c.[3] This biomolecule is also available in plants. Among the biomolecules, the chlorophylls are by far the most abundant on the earth. However, the application of chlorophylls in organic electronic devices such as OLEDs or organic photovoltaics (OPVs) has a major limitation and that is their high photodegradation. This is unfortunate since chlorophylls are the best photoreceptors in nature. Thus, if the photostability of chlorophylls could be significantly amended their technological application would be enormously improved since the long-term stability of the molecules is the prerequisite for their commercialization.

Recently, Ohtani *et al*[3] have successfully fabricated OLEDs from chlorophylls (*Chl*) extracted from spinach. They found that *Chl*-OLEDs that were rich in carotenoids emitted electroluminescent signals for much longer time (more than one minute) compared to less than five seconds for the *Chl*-OLEDs that were poor in carotenoids. The long operational time of carotenoids rich *Chl*-OLEDs was attributed to the antioxidant activities of carotenoids which prevented the destructive photooxidation of chlorophylls.

While it is interesting to note that the photostability of *Chl* has been improved to some extent by carotenoids, the results also show that carotenoids do not protect *in-vitro Chl* as effectively as they photoprotect *in-vivo Chl*, *i.e.*, in green plants. Further, electorluminescence lifetime of 1 minute for *Chl*-OLEDs rich in carotenoids does not bode well for their commercial success. It is thus highly imperative to search for an agent that can provide an efficient photoprotection to *Chl* under *in-vitro* conditions so that the utilization of *Chls* can be exploited in various optoelectronic devices.

In this context, we have recently shown[4] that the use of gold nanoparticules can help overcome the photodegradation of magnesium tetraphenylporphyrin (MgTPP), a

molecule structurally analogous to Chl*a*. In the present work, we demonstrate that gold nanoparticles (AuNPs) can also increase the photostability of Chl*a*. The UV-Visible, fluorescence and X-ray photoelectron spectroscopic studies have been carried out to assess the effect of AuNPs on the photostability of Chl*a*. The results show that the half-life time of Chl*a* (4.5 μM) has been extended from 10 to 100 minutes in presence of AuNPs (22 μM), indeed, quite a significant photoprotection. The protecting ability of Chl*a* by AuNPs is the result of their binding with Chl*a* at its nitrogen sites, inhibiting, thus, the binding of reactive oxygen species (ROS) at these sites, which are known to cause the photodegradation of Chl*a*. It is also seen that AuNPs are much more effective photoprotective agents of in-vitro Chl*a* than are the carotenoid molecule (*β*-carotene) and various quinones.

Materials and methods

Materials

Chl*a*, hydrogen tetrachloroaurate trihydrate, sulfuric acid (H_2SO_4), tetraoctylammonium bromide (TOAB), sodium borohydride ($NaBH_4$), sodium sulfate (Na_2SO_4), benzoquinone, 2,6-dichloro-p-benzoquinone (DCBQ), tetramethy-p-benzoquinone (Duroquinone), *β*-carotene and toluene, of the purest quality available, were purchased from Aldrich Chemical Co., and were used as received.

Synthesis of gold nanoparticles (AuNPs)

The procedure for preparing colloidal gold nanoparticles in an organic medium is a modified version[5] of that proposed by Brust *et al.*[6] Briefly, an aqueous solution of hydrogen tetrachloroaurate (III) hydrate [$(AuCl_4)^-$, 6 mL, 0.04 M)] was mixed with a solution of tetraoctylammonium bromide (TOAB) (0.05 M) in 14 mL toluene. The biphasic mixture was vigorously stirred for 30 min until all the $(AuCl_4)^-$ was transferred into the organic layer. An aqueous solution of sodium borohydride (6 mL, 0.4 M) was added, and the mixture was stirred for 3h. The organic layer was separated off, washed

twice with a dilute aqueous solution of H_2SO_4 and then washed five times with deionized water. Finally, the organic layer, constituting the colloidal gold nanoparticles, was dried overnight on Na_2SO_4 powder and then filtered. The final concentration of AuNPs, estimated on the basis of atomic Au concentration, was 13 mM[5].

Photodegradation measurements

The measurements were carried out in a 1-cm path length quartz cuvette. The illumination of Chl*a* solution (3 mL, 4.5 μM) in toluene was carried out using collimated light from a 150W xenon lamp that passed through a water filter to absorb heat. A red cut-off filter which allowed wavelengths greater than 640 nm was used. The light power reaching the sample was 40 $mW.cm^{-2}$. All operations with Chl*a* solutions were carried out in either subdued light or green light. The solutions were stored in dark in a refrigerator when not in use. All experiments were carried out in the presence of air.

The photodegradation experiments of Chl*a* in presence of various photoprotective agents, such as, AuNPs, β-carotene and quinones (all in 22 μM concentration), in order to assess their capacity to photoprotect Chl*a*, were also carried out under identical conditions as those for Chl*a* alone as described above.

Absorption and emission spectrometry

Absorption spectra were recorded with a Cary 5000 spectrophotometer. The fluorescence emission spectra were recorded with a FluoroLog-3 spectrofluorometer.

Transmission electron microscopy (TEM)

One drop (5-10 μL) of AuNPs was deposited onto glow-discharged carbon-coated electron microscopy grid. The excess liquid was absorbed by a piece of filter paper, and a drop of 2% uranyl acetate negative stain was added before drying. The liquid in excess

was wiped off, and the remaining film of stain was allowed to dry. The specimens were observed using a Philips EM 208S microscope operating at 80 kV.

X-ray photoemission spectroscopy (XPS)

XPS was performed on a Kratos Axis Ultra spectrometer (Kratos Analytical Ltd., UK), using a monochromatic Al Kα X-ray source (E = 1486.6 eV) with a power of 225 W, at a take-off angle of 90° relative to the sample surface. 250 μL of the sample (Chl*a*, 4.5 μM) or (AuNPs, 22 μM) or their mixture) was dropped onto an aluminum substrate and dried in a vacuum dessicator overnight to obtain a thin film. The dried samples were then transferred to the XPS sample holder. The measurements were made at room temperature under a high vacuum of 10^{-9} torr. The surface of the sample was ~ 20 mm^2, and the investigated area was typically 1 x 2 mm^2. Survey spectra for each sample over a binding energy range of 0 – 1300 eV were an average of three scans (at three different points) acquired at pass energy of 160 eV and resolution of 1 eV/step (lens in hybrid mode, which assures maximum sensitivity). High-resolution spectra of C 1s, N 1s, O 1s and Au(4f) for quantitative measurements of binding energy and atomic concentration were an average of five scans acquired at a pass energy of 40 eV and resolution of 0.1 eV/step. Because of the potential degradation of the surface during X-ray exposure, the spectra were collected in the same order (survey, C 1s, O 1s, N 1s, Au(4f)) such that the amount of exposure to X-rays was equivalent for all analyzed samples. The CasaXPS software was used for background subtraction (Shirley-type), peak integration, fitting and quantitative chemical analysis. The C 1s (C– C) peak at 285 eV was used to calibrate the binding energy scale. Binding energies values are given as ± 0.2 eV. Gaussian peak profiles were used for spectral deconvolution of C 1s, O 1s, N 1s and Au(4f) spectra. The magnesium metal binding energy was not recorded due to the poor signal to background counting ratio caused by the low core level cross section of Mg 1s level.

Percentage photostability

The percentage photostability provided to Chl*a* by AuNPs was calculated using the formula as described by Claes :[7]

$$\frac{E_3 - E_2}{E_1 - E_2} \times 100 \qquad (1)$$

where E_1, E_2, and E_3 are, respectively, the concentration (or absorbance) of Chl*a* before irradiation, after irradiation without AuNPs, and after irradiation in the presence of AuNPs.

Results

Photodegradation of chlorophyll-a (Chla)

Figure 1A presents the absorption spectra of Chl*a* (4.5 μM) and gold nanoparticles (50 μM) in toluene. The principal absorption peaks of Chl*a* (spectrum a) in the red at 665 nm, Q band, and at 433 nm in the blue, Soret band, are in agreement with those reported in the literature,[8] and that Chl*a* is present in monomeric form.[9] The 530 nm absorption band (spectrum b) is characteristic of the surface plasmon band of gold nanoparticles (8 nm),[10] as is verified by the TEM micrograph of the AuNPs which revealed an average particle diameter of 8 nm (Fig. 1B).

The absorption spectra of Chl*a* solution in toluene as a function of the time of illumination with red light ($\lambda > 640$ nm) are displayed in Fig. 2. The choice of toluene as solvent is due to the fact that gold nanoparticles to be used have been prepared in toluene. As seen from the figure, there is a progressive decrease of Chl*a* absorbance as illumination time increases. In 2 minutes, about 25% decrease in the absorbance of major absorption bands in the red (665 nm) and blue (433 nm) regions was observed. On continued exposure, the absorbance at 665 nm decreased 60% in 10 minutes and by

80% in 30 minutes. An increase in absorbance at wavelengths above 690 nm and between 460 and 580 nm was observed. These results are in good agreement with those reported by Jones and Mackay[8] Merzlyak *et al.*[11] and Tregub *et al.*[12] who studied the photodegradation of Chl*a* in micelles, methanol and various other organic solvents, respectively.

Noteworthy, however, in the present experiments is the appearance of a band in near-infra red region at 870 nm arising from the photooxidized product of Chl*a* whose intensity increases as illumination time increases. The photodegradation of Chl*a* in aerobic conditions, as in many metalloporphyrins, is caused by the reactive oxygen species (ROS) which are produced during the illumination of Chl*a*.[13-17]

Photoprotective action of gold nanoparticles

In order to investigate the role of AuNPs as photoprotector of Chl*a*, the illumination of Chl*a* solution (4.5 μM) in the presence of AuNPs was carried out under identical conditions using a red cut-off filter providing excitation wavelengths greater than 640 nm. Since, the absorption maximum of AuNPs in toluene is at 530 nm (Fig. 1), there was no interference from the direct absorption of the incident light ($\lambda >$ 640 nm) by AuNPs.

The addition of AuNPs, as is clear from Fig. 3, does seem to provide protection to Chl*a* against photodegradation. After 30 minutes of illumination, Chl*a* degraded only 16% in the presence of AuNPs (22 μM) compared to the 80% photodegradation (at 665 nm) in the absence of AuNPs (Fig. 2). In other words, a photoprotection of 84% has been provided to Chl*a* by 22 μM AuNPs. In addition, the photooxidation product absorbing at 870 nm totally disappeared. Further, it is found that the degradation of Chl*a* is dependent upon the Au nanoparticles concentration (inset of Fig. 3). That is, the higher the concentration of AuNPs, the greater is the photoprotection provided to Chl*a* against irradiation. Higher concentrations of AuNPs beyond 88 μM, however, provided

no additional protection. The percentage photoprotection was calculated using eq. (1), described in the Experimental section.

However, to get a meaningful insight into the photostability imparted to Chl*a* by AuNPs, the photodegradation kinetics of Chl*a* was studied, and is presented in Fig. 4, and described in ESI section. As seen from the inset of the figure, the photodegradation of Chl*a* follows a pseudo-first order kinetics with half-life times of 10 and 100 minutes in absence and in presence of AuNPs, respectively, indicating a tremendous improvement in the photostability of Chl*a* in presence of AuNPs. The reaction rate constants and half-lives are presented in Table 1. The beneficial role of AuNPs in the increased photostability of Chl*a* is also possibly, in part, responsible for the improved photoelectrochemical performance of a Chl*a*-AuNPs based solar cell compared to that of Chl*a* cell as reported earlier.[5]

To exclude the possibility that the tetraoctylammonium bromide (TOAB), a surfactant used in the preparation of AuNPs, had any photoprotective role, a solution of TOAB (0.05 M) in toluene was added to Chl*a* solution. The Chl*a* was not photoprotected, confirming that it is the AuNPs, rather than TOAB, that provide the photoprotection to Chl*a*. Furthermore, AuNPs themselves subjected to irradiation for same time period (5-60 min) under identical conditions did not show any photochemical changes. The photoprotection provided to Chl*a* by AuNPs is due to the binding between AuNPs and Chl*a* that prevents ROS from interacting with Chl*a*, similar to that reported recently by Bekalé *et al.*[4] in case of magnesium tetraphenylporphyrin (MgTPP).

The binding of Chl*a* with AuNPs is manifested by the changes occurring in the absorption spectrum of Chl*a* as AuNPs are added (Fig. 5). A decrease in the absorption of Chl*a* at ~ 432 nm and an appearance of a new band at ~ 437 nm, as the concentration of AuNPs increases, indicates the formation of Chl*a*-AuNPs complex. A decrease in the absorption at 665 nm is also visible. The changes in the absorption (ΔA) at 437 nm were used to determine the association constant between Chl*a* and AuNPs employing Benesi-Hildebrand method. [18] An apparent association constant, K_{app}, of 5.70×10^5 M^{-1} for

Chl*a*-AuNPs complex was obtained from the intercept-to-slope ratio of the double reciprocal plot of $1/\Delta A$ vs 1/[AuNPs] (inset, Fig. 5). The high value of K_{app} suggests a strong binding between AuNPs and Chl*a*. The association constant has also been obtained from the fluorescence quenching experiments of Chl*a* in the presence of AuNPs. Figure 6 presents the fluorescence spectra of Chl*a* in toluene in the presence of varying concentration of AuNPs. The fluorescence emission of Chl*a* exhibits a maximum at 675 nm, which is characteristic of emission from monomeric Chl*a* in nonpolar solvent. Upon addition of gold nanoparticles, one observes a progressive quenching of the fluorescence of Chl*a* with increasing amounts of AuNPs. This quenching occurs as a result of the formation of a weakly or non-fluorescent ground state complex between fluorophore (Chl*a*) and quencher (AuNPs).

Thus, following the approach described by Lakowicz,[19] the dependence of fluorescence intensity on quencher concentration can be obtained by considering the association or complex formation constant, K_S, between the fluorophore and quencher, *i.e.*, K_S = [F-Q]/[F][Q], where [F-Q] is the concentration of the complex, and [F] and [Q] are, respectively, the concentrations of uncomplexed fluorophore and quencher. Proceeding further as demonstrated in reference 19, one finally obtains the relation between fluorescence intensity and concentration of the quencher as follows:

$$I_0/I = 1 + K_S\,[Q] \qquad (2)$$

where I_0 and I are the fluorescence intensities of Chl*a* in absence and in presence of the quencher, AuNPs, respectively.

The ratios of the fluorescence intensity (I_0/I), measured at 675 nm, without and with AuNPs, were plotted against AuNPs concentration (inset of Fig. 6). From the slope of the linear plot, a value of $\sim 10^4$ M^{-1} for the association constant, K_S, was obtained. This value, although smaller than that obtained from absorption measurements (inset, Fig. 5), is, nevertheless, high. A high value of the association constant suggests a strong

interaction between Chl*a* and AuNPs, which, it should be pointed out, also helps the heterogenous charge transfer at Chl*a*-AuNP interface, as has been reported earlier.[5]

Since AuNPs possess an affinity for nitrogen atoms, the complex formation between Chl*a* and AuNPs is the result of the binding of AuNPs with the nitrogens of Chl*a*, as described below in XPS studies, and is at the heart of the photoprotection provided to Chl*a* by AuNPs.

X-ray photoelectron spectroscopy (XPS) studies

In order to better understand the mechanism by which AuNPs interact with Chl*a* and provide it the photoprotection, XPS study of Chl*a*, AuNPs, and their mixture in a concentration ration of 1:5, has been carried out. The low resolution (survey) spectra of these three samples are shown in Fig. S-1 (ESI). All samples show the spectroscopic signature of carbon at around 285, nitrogen at ~ 400, and oxygen at ~ 532 eV. In samples containing AuNPs, one can also notice the presence of Au(4f) signal, corresponding to the $f_{5/2}$ and $f_{7/2}$ components, at binding energies of ~352 and 334 eV, respectively. The magnesium metal binding energy was not recorded due to the poor signal to background counting ratio caused by the low core level cross section of the Mg 1s level. To obtain more XPS information, the high-resolution scans of the XPS spectra of C1s, O1s and N1s levels with their respective deconvolutions were obtained, and are as follows.

Figure S-2 shows high-resolution spectra of the C 1s regions for Chl*a* and Chl*a*-AuNPs mixture. The most significant contribution to these spectra comes from the peak at 285 eV, which corresponds to the aliphatic carbon (C-C) and C-H of Chl*a* and TOAB (the underline refer to the atom in question).[20,21] The signal pertaining to the aromatic carbons (-C=C-) of Chl*a* at 284.7 eV is rather hidden in the envelope of C-1 peak, and is thus not visible. The contribution of the carbons bound to nitrogen (C-N, C=N) and those bound to oxygen by single bond (-C-O), peak C-2, appears at 286.1-286.5 eV.[20,21] The weak peak, C-3, at 288.9-289.1 eV is attributed to the carbonyl of the ketone

(>C=O) and ester (-O-C=O) groups in Chl*a* (Scheme 1).[21,22] The fact that the position of this peak remains unaltered even after the addition of AuNPs is an important indication that the interaction between Chl*a* and AuNPs does not involve the nonbonding electrons of carbonyl oxygen of ketone and ester groups (*i.e.*, >C=O and -O-C=O) of Chl*a*. This observation is also supported by the O 1s spectra (*vide infra*).

The high-resolution scans of the XPS spectra of O1s levels of Chl*a* and Chl*a*-AuNPs with their decomposition into three components are shown in Fig. S-3. The O-1 peak at ~ 533.1-533.4 eV is attributed to the ether-type oxygen in ester group (-O-C=O)[23] of Chl*a* (Scheme 1). The most intense peak, O-2, at 532.3-532.5 eV has been assigned to the carbonyl oxygen from ketone (>C=O) and ester groups (-O-C=O) of Chl*a*.[23] It is important to point out, once again, that this peak has virtually remained unchanged after the addition of AuNPs (Fig. S-3, Chl*a*-AuNPs), confirming, as mentioned above in Fig. S-2, that the interaction between Chl*a* and AuNPs does not implicate the carbonyl groups of Chl*a*. Finally, the O-3 peak at lower binding energy ~ 530.2- 531 eV, has been attributed to the molecular adsorbed oxygen, O_2.

The deconvolution of N1s levels of Chl*a*, AuNPs and Chl*a*-AuNPs are displayed in Fig. 7. The main peak, N-1, at binding energy of 398.1-398.9 eV in Chl*a* (Fig. 7) is characteristic of the pyrrolenine nitrogen atoms of the porphyrin macrocycle of Chl*a* (Scheme 1), and is in good agreement with the reported data for Chl*a* and many other metalloporphyrins.[24-26] A second peak (N-2), a shoulder, in the XPS of Chl*a* alone can also be seen at ~ 400 eV. Although, the exact origin of this peak is less certain, it is most likely due to the protonated nitrogen, produced as a result of a small degree of demetallation of Chl*a* during its exposure to X-rays in the course of the experiment. This demetallation seems to be a general feature with magnesium porphyrins as has been reported by many other authors.[25-27]

The N 1s spectrum of AuNPs shown in Fig. 7 presents two peaks (N-3 and N-4), with an intensity ratio of about 90:10, which appear at 401.34 and 402.96 eV, respectively. Both peaks are characteristic of quaternary nitrogens, although, present in

two different chemical environments. The first one, N-3, at 401.34 eV is assigned to quaternary nitrogen (Oct_4N^+) of TOAB adsorbed on the surface of AuNPs.[28] The second peak N-4, a weaker one, at high binding energy of 402.96 eV, corresponds most probably to the small quantity of TOAB which is not in direct contact with the surface of AuNPs, but rather through the intermediacy of bromide ions which are adsorbed on gold nanoparticles. This signal is consistent with the work of Bureau *et al.* who reported the presence of a similar peak for tetramethyl ammonium hydroxide {$(CH_3)_4N^+$, OH^-) adsorbed on nickel surface.[29]

The N 1s spectrum of Chl*a* shows a drastic change after addition of AuNPs (Fig. 7, Chl*a*-AuNPs). Indeed, the presence of AuNPs causes the disappearance of a large fraction of the principal peak, N-1, corresponding to the pyrolenine nitrogens in Chl*a* at 398.1-398.9 eV, with the simultaneous appearance of a new and intense peak, N-5, at 402.4 eV. In other words, the pyrolinene nitrogens of Chl*a*, present initially in a chemical state represented by a binding energy of 398.1-398.9 eV, find themselves, after interaction with AuNPs, in a new chemical state in which the expulsion of the core electrons has been made rather more difficult, thereby needing comparatively a higher energy, *i.e.*, 402.4 eV. The requirement of a higher energy suggests that the electron density around nitrogens of Chl*a*, represented by N-5 peak, has decreased or that the nitrogens are relatively in a more positively charged state than they were in Chl*a* alone, represented by N-1 peak. In other words, the nitrogens in Chl*a*, with a binding energy of 398.1 eV, have, now, in presence of AuNPs, been converted into positively-charged tetravalent ammonium quaternary nitrogens ($R_4N^{\delta+}$) which are known to possess a higher binding energy at 402 eV.[30-32] This, *i.e.*, the nitrogens acquiring a positive charge, occurs as a result of the interaction between Chl*a* and AuNPs *via* the transfer of non-bonding electrons on nitrogens of Chl*a*, leading to the formation of the complex Chl*a*-AuNPs as is depicted in Scheme 2.

One can, therefore, say that the complex formed between Chl*a* and AuNPs, with a high association constant of $\sim 10^5$ M^{-1} (Fig. 5), is the result of their binding with each other via non-bonding electrons on Chl*a* nitrogens. This is consistent with our recent

work on MgTPP and AuNPs,[4] and is also consistent with the observations of Kamat *et al.*[33,34] and Kastonis *et al.*[35], who, respectively, reported the binding of benzylamine and meso-tetradodecylporphyrin with AuNPs via interaction of the non-bonding electrons on nitrogen of the respective molecules.

The comparison of the Au (4f) core-level spectrum of AuNPs with that for the mixture of AuNPs with Chl*a* also confirms that the nitrogens of Chl*a* have donated electrons to AuNPs during the formation of the Chl*a*-AuNP complex. The Au (4f) core-level spectrum of AuNPs (Fig. 8) shows two peaks, namely, $4f_{7/2}$ and $4f_{5/2}$, at binding energies of 84.1 and 87.6 eV, respectively, corresponding to gold in zero oxidation state (Au^0).[36] In its mixture with Chl*a*, however, these Au(4f) peaks are shifted to lower energies (83.4 and 87.2 eV). This lowering of the Au(4f) binding energy suggests that the electron density around Au has increased[37,38] since it will facilitate the expulsion of the core electrons. This increase in electron density on Au occurs as a result of the transfer of electronic charge (lone pair of electrons) from nitrogens of Chl*a* to AuNPs during their binding with each other, corroborating the observations made in N 1s spectra of Chl*a*-AuNPs (Fig. 7) where nitrogen has been shown to donate its electrons to AuNPs to form the Chl*a*-AuNPs complex.

Comparison of the photoprotective ability of AuNPs with other Chla photoprotectors

In order to further assess the advantageous role of gold nanoparticles in photoprotection of Chl*a*, photodegradation experiments of Chl*a* (4.5 μM) in presence of other potential Chl*a* photoprotectants, such as, carotenoid (all-trans β-carotene) and quinones (dichlorobenzoquinone, duroquinone, *etc.)*, all in 22 μM solutions in toluene, were also carried out under identical conditions using a red cut-off filter providing excitation wavelengths greater than 640 nm where the individual absorption of quinones and β–carotene was negligible. These molecules are known to provide photoprotection to Chl*a* and, thus, to plants[7,39-42] via several means: (i) They can function as "triplet valves" by reacting with excited Chl*a* triplet, and thus prevent Chl*a* triplet from promoting oxygen to its singlet excited state to produce ROS, (ii) They can consume the

singlet oxygen that is formed, thereby diminishing its quantities, and, thus, its harmful effects, and (iii) They can directly quench the excited Chl*a* singlets, which decreases the intersystem crossing yield of singlet Chl*a* to triplet Chl*a*, leading to a decreased ROS production. The photoprotection of Chl*a* and, thus, of plants by carotenoids, quinones, *etc.*, occurs via their reaction with the excited states of Chl*a* during its illumination.

The present results (Fig. 9) show that Au nanoparticles are a much more effective (80%) photoprotectant of Chl*a* in solution than β-carotene or quinones which provide photoprotection of only 28 and 9%, respectively. These results confirm the beneficial role of gold nanoparticles as an effective photoprotective agent for Chl*a* *in vitro* conditions, which is the consequence of the binding of AuNPs with Chl*a* at its nitrogen sites prior to the illumination, as discussed below and recently demonstrated in case of MgTPP,[4] in contrast to the photoprotective action of carotenoids and other antioxidants which provide photoprotection to Chl by their interaction with the excited states of Chl during illumination.

Discussion

The irreversible photodegradation of chlorophyll (Chl), as in many metalloporphyrins, is known to be mainly a photooxidative process, brought about by various reactive oxygen species (ROS), namely, singlet oxygen, superoxide ion, *etc.*[39,42-52] Light absorption by Chl*a* results in the formation of its excited singlets (^{1}Chl*a**). If not readily used photochemically, they get converted into triplet excited states (^{3}Chl*a**). Chlorophyll triplet states are long-lived energetic species which can easily react with the triplet ground state of oxygen ($^3O_2$) to produce strongly photooxidative ROS. These ROS attack the nitrogens of the porphyrin macrocycle of Chl*a* and cause its photodegradation.[24,53] Therefore, if these nitrogen sites can be shielded from the attack of ROS by some harmless agent, Chl*a* will be well protected. In the present case of Chl*a* admixed with AuNPs, the AuNPs are just doing that. By binding with the nitrogens of Chl*a*, as seen in XPS studies (Fig. 7), AuNPs are

essentially providing an impregnable golden armor to Chl*a* against the deadly attack of ROS which are produced during its illumination.

What is unique with AuNPs as photoprotector of Chl*a*, is that they readily bind with the nitrogens of Chl*a* as soon as they are mixed together, even in dark prior to the illumination. This is clear from the changes observed in the absorption spectrum of Chl*a* as AuNPs are added (Fig. 5). Consequently, the ROS, which are generated during the illumination of Chl*a*, find, to their utter dismay, that only very few free nitrogen sites are available to bind with and cause damage, since most of them have already been occupied by AuNPs in dark long before the ROS were even produced as a result of the illumination. The binding of the ROS with nitrogens of Chl*a* is, thus, strongly inhibited in presence of AuNPs, which is reflected in the decreased amount of the photodegradation or in the increased degree of photoprotection of Chl*a* in presence of AuNPs (Figs. 3 and 4).

The same trait, *i.e.,* the ability of AuNPs to bind to Chl*a* in its ground state in dark prior to the illumination also gives them an added advantage over other conventional protective agents, such as, carotenoids and quinones. These compounds, as mentioned earlier, provide photoprotection to Chl*a* by functioning as (i) triplet valves, (ii) scavengers of ROS, and (iii) quenchers of Chl*a* excited singlet states to help dissipate excess energy on Chl*a* excited singlets. The photoprotection of Chl*a* by carotenoids, quinones, *etc.*, thus, occurs via their interaction with the excited states of Chl*a* rather than its ground state as is the case with AuNPs. As noted above, oxygen too reacts with the excited states of Chl*a*, and produces ROS that cause the photodegradation of Chl*a*. In a nutshell, the carotenoids react with Chl*a* excited states so that lesser and lesser amounts of ROS be produced, while paradoxically oxygen also reacts with the excited states of Chl*a* but to produce larger and larger quantities of ROS. Said otherwise, both carotenoids and oxygen react with the same excited states of Chl*a*, although one (carotenoids) to protect it (Chl*a*) while the other (ROS) to destroy it. It is thus evident that carotenoids or other antioxidants must compete with oxygen for Chl*a* excited states to fully assert their role of photoprotectors.

In view of this, AuNPs possess an enormous edge over carotenoids, quinones, *etc.*, vis-à-vis their *modus operandi*. In fact, the very ability of AuNPs to bind with Chl*a* in its ground state in dark gives them a super advantage over these conventional protective agents. Carotenoids and other antioxidants do not *per se* bind with Chl*a* to protect its vulnerable nitrogen sites from the harmful attack of ROS. They simply act when it is already too late, *i.e.*, when Chl*a* is in excited state (^{1}Chl*a**). In contrast, AuNPs, by the virtue of their simply being in contact with Chl*a*, even prior to the illumination and with no competition from other source, react with Chl*a* to capture and block the nitrogen sites of Chl*a*, leaving, thereby, a very little room for ROS to get attached to the nitrogens and cause photodegradation of Chl*a*. This makes AuNPs quite efficient and better photoprotectors of Chl*a* in solution than many other well-known photoprotectors (carotenoids, *etc.*) as can be seen from Fig. 9, in that AuNPs provide a huge photoprotection of ~80% to Chl*a*, β-carotene provides a photoprotection of only 28%, while quinones a meagre protection of 9%.

Conclusions

The present work clearly shows that AuNPs, in micromolar concentration, can protect Chl*a* efficiently in solution against photodegradation, better than what *β*-carotene and quinones can do. The protecting ability of AuNPs is the result of their binding with Chl*a* at its nitrogen sites, inhibiting, thus, the binding of reactive oxygen species at these sites, known to cause the photodegradation of Chl*a* and many other porphyrins. It is also shown that an increase of as much as an order of magnitude in half-life of Chl*a* in presence of AuNPs can be achieved. Thus, the use of gold nanoparticles as efficient photoprotector of Chl*a* offers us new possibilities to increase the photostability of various porphyrins used in a wide range of industrial (optoelectonic devices such as OLEDs and photovoltaics) and medical (photodynamic therapy) applications.

Acknowledgments

S.B and L.B contributed equally to this work. The authors thank Prof. Prashant V. Kamat of Radiation Laboratory, University of Notre Dame, for many helpful discussions. The work described herein was supported by the Natural Sciences and Engineering Research Council of Canada (NSERC).

Références

(1) R. S. Phadke, *Appl. Biochem. Biotechnol.* 2001, **96**, 279-286.

(2) H. Tajima, K. Shimatani, T. Komino, S. Ikeda, M. Matsuda, Y. Anodo and H. Akiyama, *Colloid Surf. A: Physicochem. Eng. Asp.,* 2006, **284-285**, 61-65.

(3) N. Ohtani, N. Kitagawa, T. Matsuda, *JJAP* 2011, **50**, 01BC08-1-01BC08-3.

(4) L. Bekalé, S. Barazzouk and S. Hotchandani, *J. Mater. Chem.* 2012, **22**, 2943-2951.

(5) S. Barazzouk, P.V. Kamat and S. Hotchandani, *J. Phys. Chem. B* 2005, **109**, 716-723.

(6) M. Brust, M. Walker, D. Bethell, D.J Schiffrin and R. Whyman, *J. Chem. Soc., Chem. Commun.* 1994, **7**, 801-802.

(7) H. Claes, *Biochem. Biophys. Res. Comm.* 1960, **3**, 585-590.

(8) C. E. Jones and R. A. Mackay, *J. Phys. Chem.* 1978, **82**, 63-65.

(9) A. J. Hoff and J. Amesz, In *Chlorophylls*; Scheer, H., Ed.; CRC Press: Boca Raton, FL, 1995; p 726.

(10) V. Subramanian, E. E, Wolf, P. V. Kamat, *J. Am. Chem. Soc.* 2004, **126**, 4943-4950.

(11) M.N. Merzlyak, S.I. Pogosyan, L. Lekhimean, T.V. Zhigolova, I.F. Khozina, Z. Cohen and S.S. Khushchev, *Rus. J. Plant Physiol.* 1996, **43**, 160-168.

(12) S. Tregub, S. Schoch, G. Erago and H. Scheer, *J. Photochem. Photobiol. À* 1996, **98**, 51-58.

(13) C. H. Foyer, In *Photosynthesis*; John Wiley & Sons, New York. 1984; p. 3-13.

(14) A. Dreuw, G. R. Fleming and M.H. Gordon, *Biochem. Soc. Trans* 2005, **33**, 858-862.

(15) F. Fungo, L. Otero, E. Durantini, W. J. Thompson, J. J. Silber, T. A. Moore, A. L. Moore, D. Gust and L. Sereno *Phys. Chem. Chem. Phys.* 2003, **5**, 469-475.

(16) W. W. Adams III, C.R. Zarter and B. Demmig-Adams, *BioSience* 2004, **54**, 41-49.

(17) T. Golan, P. Müller-Moulé and K. K. Niyogi, *Plant, Cell and Environment* 2006, **29**, 879-887.

(18) H.A. Benesi and J.H. Hildebrand, *J. Am. Chem. Soc.* 1949, **71**, 2703-2707.

(19) Lakowicz, J. R. *Principles of fluorescence spectroscopy*; Plenum Press: New York, 1993, chapter 8, pp. 282.

(20) N.H. Tran, M.A. Wilson, A.S. Milev, J.R. Bartlett, R.N. Lamb, D. Martin and G.S.K. Kannangara, *Advances in Colloid and Interface Science* 2009, **145**, 23-41.

(21) N. T. T. Tran, T-H. Wang, C-Y. Lin, Y-C. Tsai, C-H. Lai and Y. Tai, *Bioconjugate Chem.* 2011, **22**, 1394-1401.

(22) P.V. Galiy, A.V. Musyanovych, *Funct. Mater. Lett.* 2005, **12**, 467-475.

(23) S. Agraharam, D.W. Hess, P.A. Kohl and S.A.B. Allen, *J. Electrochem. Soc.* 2000, **147,** 2665-2670.

(24) J. Zhang, P. Zhang, Z. Zhang and X. Wei, *J. Phys. Chem. A.* 2009, **113**, 5367-5374.

(25) S. Muralidharan and RG. Hayes, *J. Am. Chem. Soc.* 1980, **102**, 5106-5107.

(26) D.H. Karweik and N. Winograd, *Inorg. Chem.* 1976, **15**, 2336-2342.

(27) G. Polzonetti, C. Battocchio, A. Goldoni, R. Larciprete, V. Carravetta, R. Paolesse, and M.V. Russo, *Chem. Phys.* 2004, **297**, 307-314.

(28) J.R. Pels, F. Kapteijn, J.A. Moulijn, Q. Zhu, and K.M. Thomas, *Carbon*, 1995, **33**, 1641-1653.

(29) C. Bureau, and P.D. Chong, *Chem. Phys. Lett*, 1997, **264**, 186-192.

(30) J.J. Jack, and D.M. Hercules, *Anal. Chem.* 1971, **43**,729-736.

(31) S. Virtanen, A. Soininen, V-M. Tiainen, D. Besic, M. Puk, T. Kinnari, J. Salo, R. Trebse, AJ. Trampuz and Y. T. Konttinen, *SOT*. 2006, **29**, 290-295.

(32) A. Warshawsky, N. Kahana, V. Kampel, I. Rogachev, R.M. Kautzmann, JL. Cortina and C.H. Sampaio, *Macromol. Mater. Eng*. 2001, **286**, 285-295.

(33) K.G. Thomas, J. Zajicek and P.V. Kamat, *Langmuir*. 2002, **18**, 3722-3727.

(34) K.G. Thomas and P.V Kamat, *Acc. Chem. Res.* 2003, **36**, 888-898.

(35) N. Katsonis, J. Vicario, T. Kudernac, J. Visser, M.M. Pollard and BL. Feringa, *J Am. Chem. Soc.* 2006, **128**, 15537-15541.

(36) G. Ertas, U. K. Demirok and S. Suzer, Appl. Surf. Sci. 2005, **249**, 12-15.

(37) P. Jiang, J-J. Zhou, R. L. Wang and S-S. Xie, *Nanotechnology* 2006, **17**, 3533-3538.

(38) M. Zhou, B. Wang, Z. Rozynek, Z. Xie, J. O. Fossum, X. Yu and S. Raaen, *Nanotechnology* 2009, **20**, 505606-505615.

(39) Foote, C.S.; Chang, Y.C.; Denny, R.W. *J. Am. Chem. Soc.* 1970, **92**, 5216-5218.

(40) (a) Miller, N.; Carpentier, R. *Photochem. Photobiol.* 1991, **54**, 465-472. (b) Bukhov, N.G.; Sridharan, G.; Egorova, E.A.; Carpentier, R. *Biochem. Biophys. Acta* **2003**, *1604*, 115-123. (c) Rajagopal, S.; Egorova, E.A.; Bukhov, N.G.; Carpentier, R. *Biochem. Biophys. Acta* 2003, **1606**, 147-152.

(41) Siefermann-Harms D. *Biochem. Biophys. Acta* 1985, **811**, 325-355.

(42) Truscott, T.G. *J. Photochem. Photobiol. B: Biol.* 1990, **6**, 359-371.

(43) Apel, K.; Hirt, H. *Ann. Rev. Plant Biol.* 2004, **55**, 373-399.

(44) Joly, D.; Carpentier, R. *Biochem.* 2007, **46**, 5534-5541.

(45) Beddard, G.S.; Davidson, R.S.; Trethewey, K.R. *Nature* 1977, **267**, 373-374.

(46) Havaux, M.; Kloppstech, K. *Planta* 2001, **213**, 953-966.

(47) Amarie, S.; Standfuss, J.; Barros, T.; Kühlbrandt, W.; Dreuw, A.; Wachtveitl, J. *J. Phys. Chem. B* 2007, **111**, 3481-3487.

(48) Dreuw, A.; Fleming, G.R.; Gordon, M.H. *Phys. Chem. Chem. Phys.* 2003, **5**, 3247-3256.

(49) Demmig-Adams, B.; Adams III, W.W. *Science* 2002, **298**, 2149-2153.

(50) Kadlecek, P.; Rank, B.; Ticha, I. *J. Plant Physiol.* 2003, **160**, 1017-1024.

(51) Ledford, H.K.; Niyogi, K.K. *Plant Cell Environ.* 2005, **28**, 1037-1045.

(52) Guo, W.H.; Tu, C.Y.; Hu, C.H. *J. Phys. Chem. B* 2008, **112**, 12158-12167.

(53) J. P. Zhang, P. Y. Zhang, Z. Zhang, G. H. Chen, F. Han and X. H. Wei, Chin. Chem. Lett., 2008, **19**, 1190-1192.

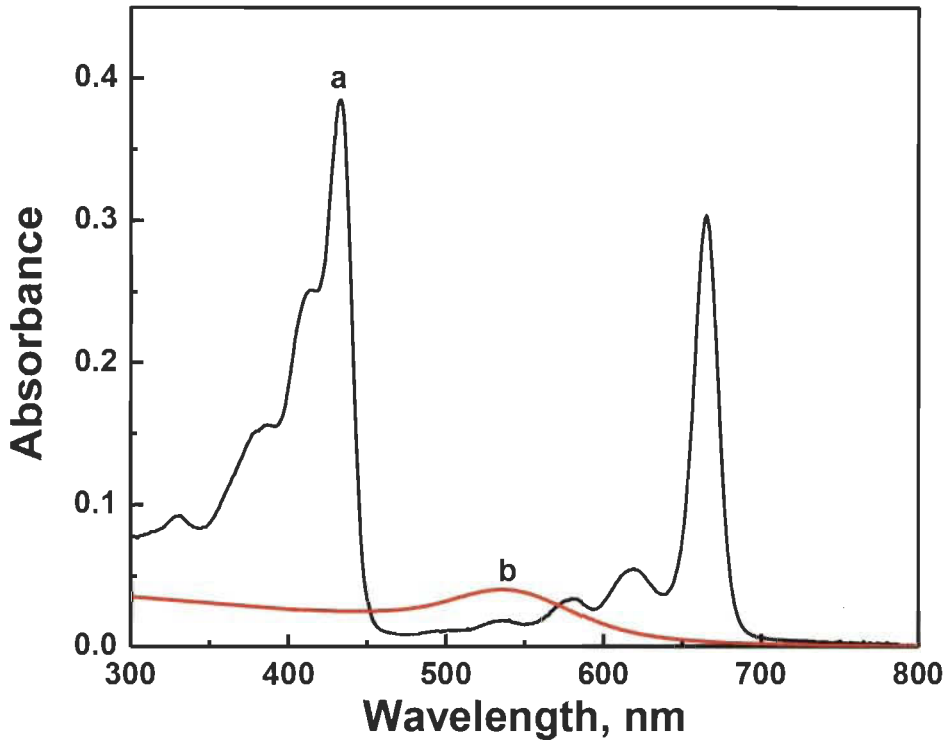

Fig. 1A Absorption spectra of (a) 4.5 μM Chl*a* and (b) 50 μM AuNPs (8nm) in toluene.

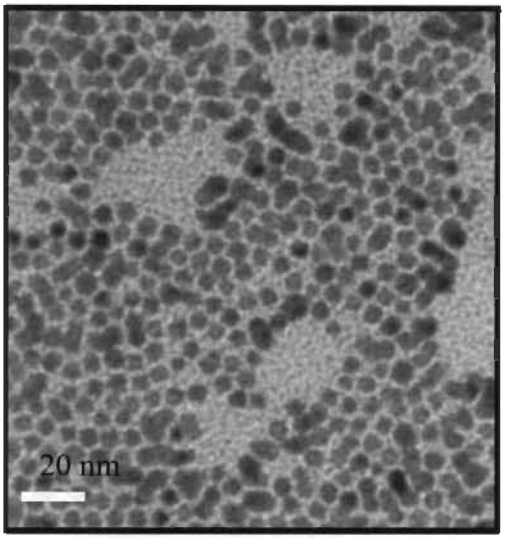

Fig. 1B TEM image of gold nanoparticles showing a mean diameter of 8nm.

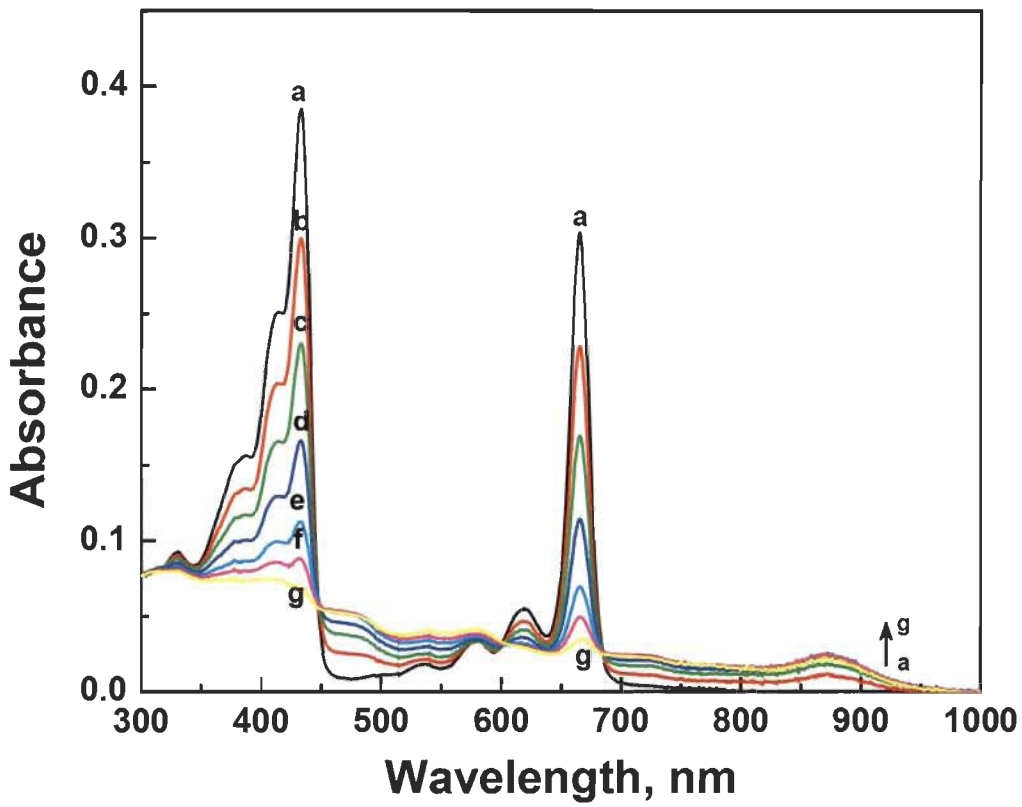

Fig. 2 Absorption spectra of Chl*a* solution in toluene (4.5 μM) as a function of irradiation time with red light (λ > 640 nm): (a) 0, (b) 2, (c) 5, (d) 10, (e) 20, (f) 30 and (g) 60 min.

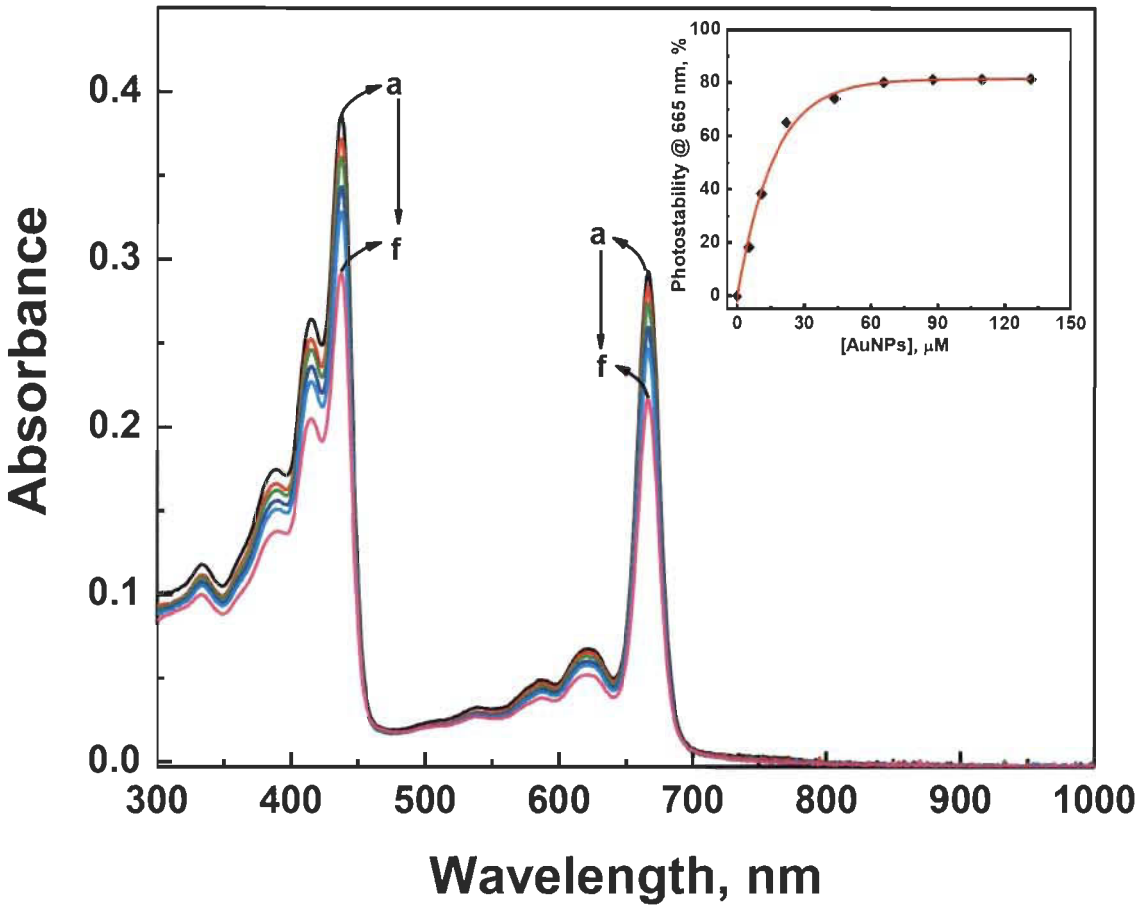

Fig. 3 Absorption spectra of Chl*a* solution in toluene (4.5 μM) in the presence of 22 μM of AuNPs (8 nm particle size) as a function of irradiation time with red light (λ > 640 nm): (a) 0, (b) 5, (c) 10, (d) 20, (e) 30 and (f) 60 min. The inset shows the effect of AuNPs concentration on the photoprotection of Chl*a* at 665 nm; red-light irradiation period is 30 minutes. The % photoprotection of Chl*a* was calculated from the variation of absorbance at 665 nm, using eq. 1.

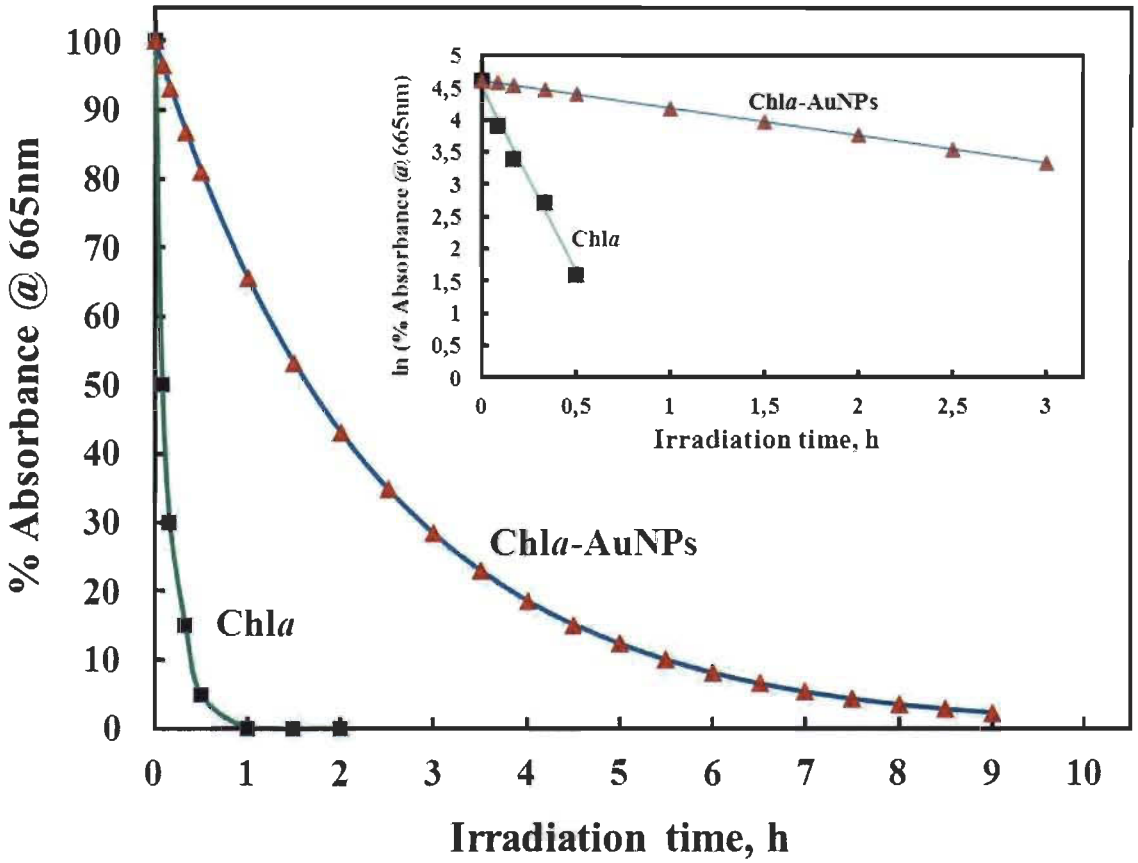

Fig. 4 Photostability of Chl*a* solution in toluene (4.5 μM) in absence (a) and presence (b) of 22 μM of AuNPs as a function of irradiation time with red light (λ > 640 nm). The insert shows the first order photodegradation kinetics of Chl*a* absence and presence of AuNPs (see eq. (4) in SI).

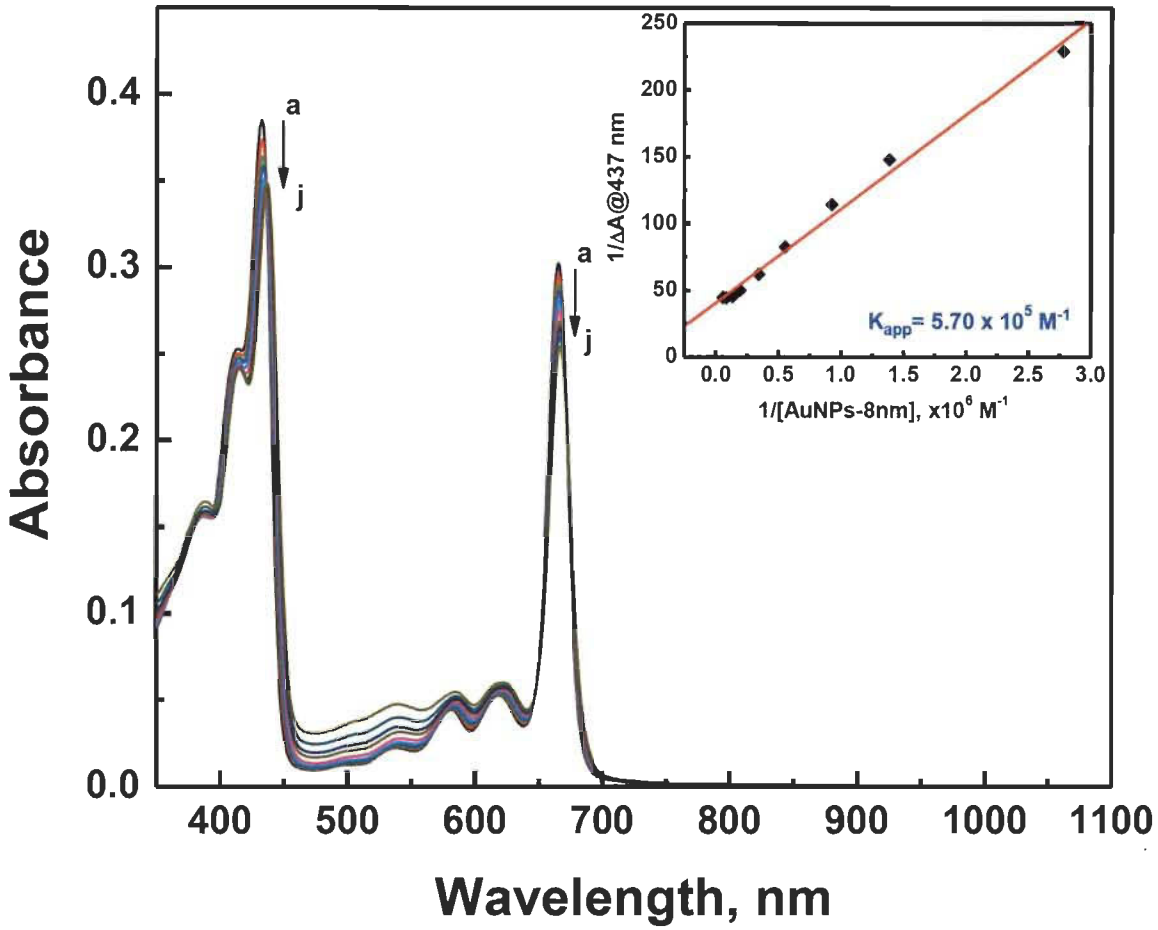

Fig. 5. Effect of AuNPs on the absorption spectra of Chl*a* solution (4.5 μM) in toluene: (a) 0, (b) 0.36, (c) 0.72, (d) 1.08, (e) 1.80, (f) 2.89, (g) 5.05, (h) 7.22, (i) 11.55 and (j) 18.05 μM. The insert shows the plot of 1/ΔA(437 nm) vs 1/[AuNPs]. An apparent association constant (K_{app}) of 5.70 x 10^5 M^{-1} was obtained from the intercept-to-slope ratio of the plot.

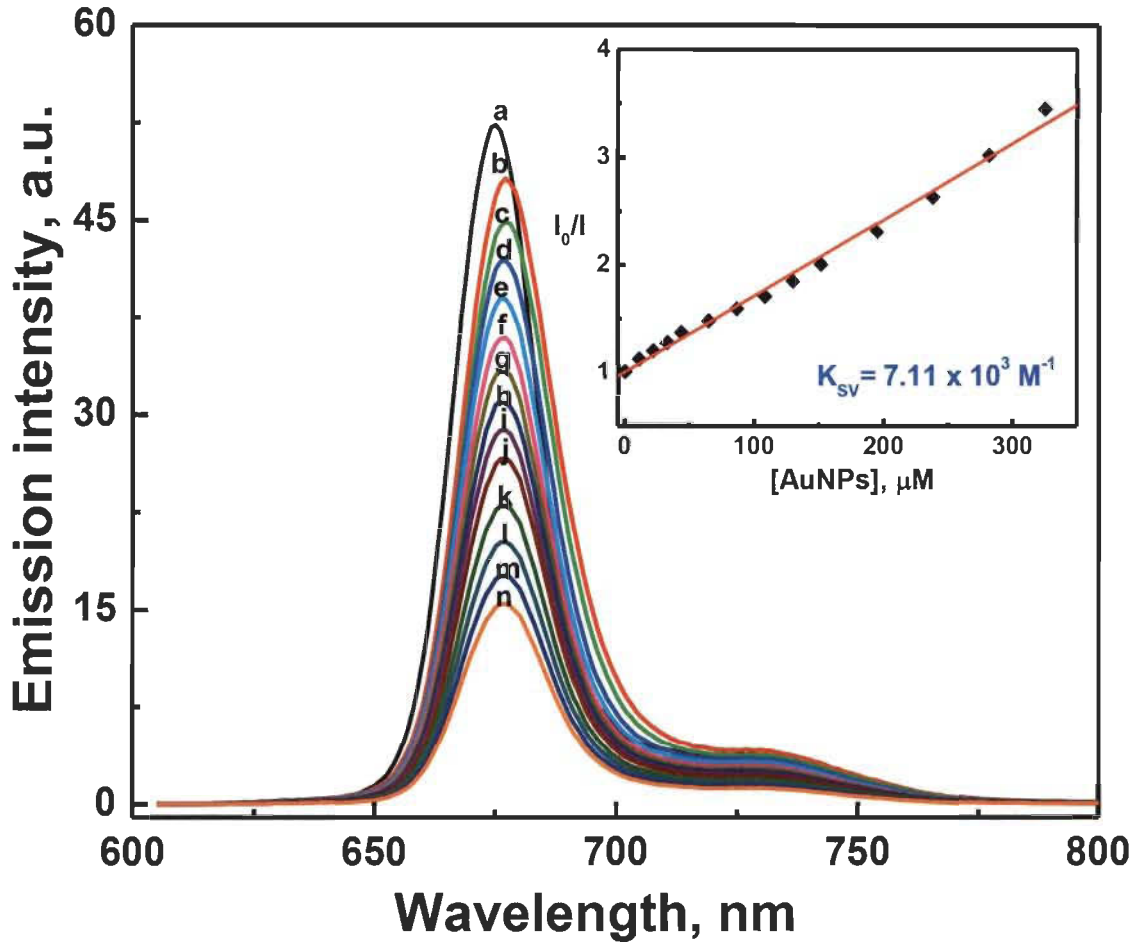

Fig. 6. Emission spectra of 4.5 μM Chl*a* in toluene recorded in the presence of different concentrations of AuNPs: (a) 0, (b) 10.83, (c) 21.67, (d) 32.50, (e) 43.34, (f) 65.01, (g) 86.68, (h) 108.35, (i) 130.02, (j) 151.69, (k) 195.03, (l) 238.37, (m) 281.71 and (n) 325.05 μM. Excitation wavelength was 433 nm. The insert shows Stern-Volmer plot of the quenching of Chl*a* by AuNPs. The fluorescence intensity was monitored at 675 nm.

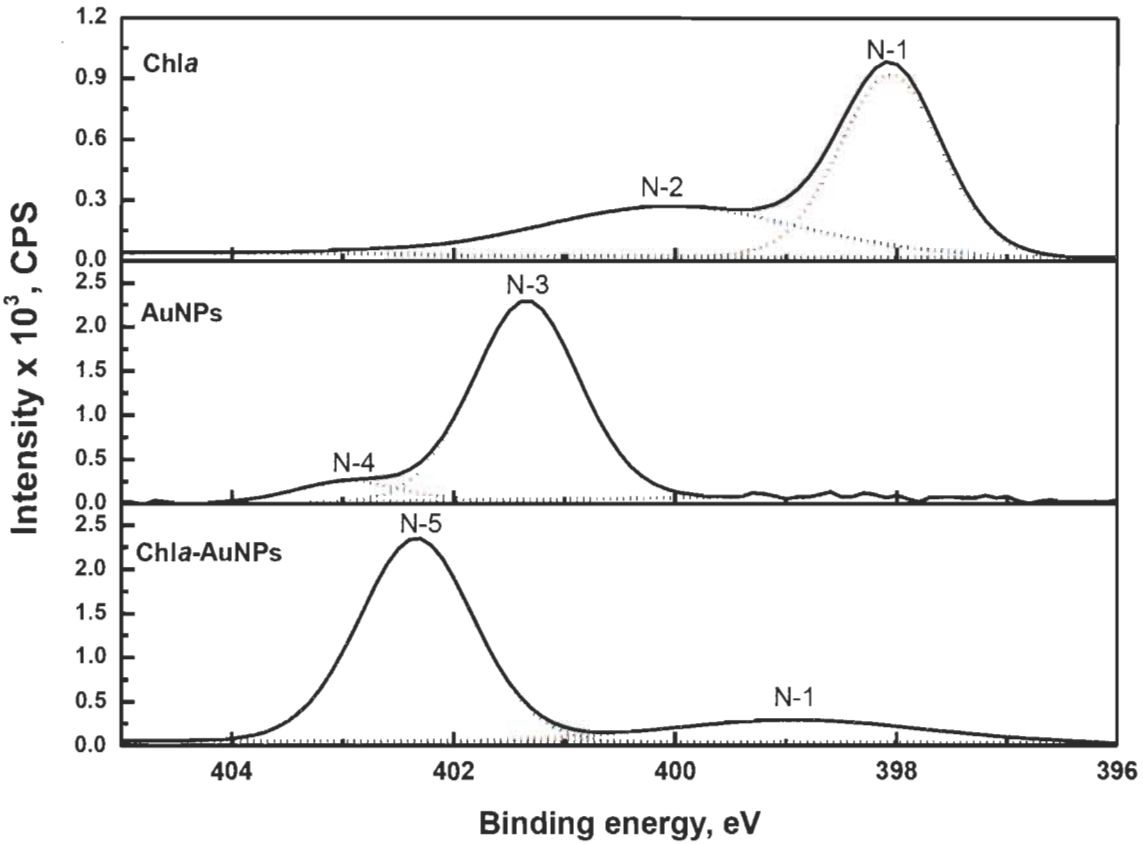

Fig. 7. N 1s narrow scan XPS spectra for Chl*a*, AuNPs and Chl*a*-AuNPs.

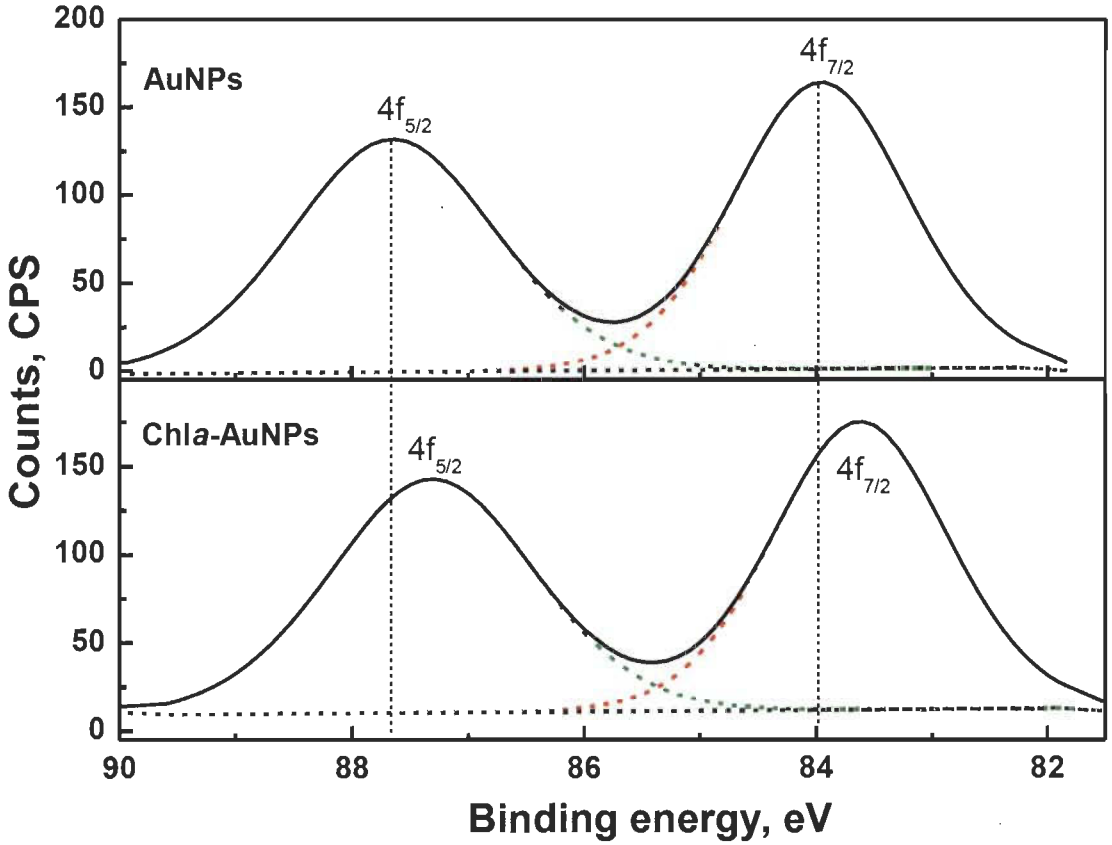

Fig. 8 Au(4f) narrow scan XPS spectra for AuNPs and Chl*a*-AuNPs.

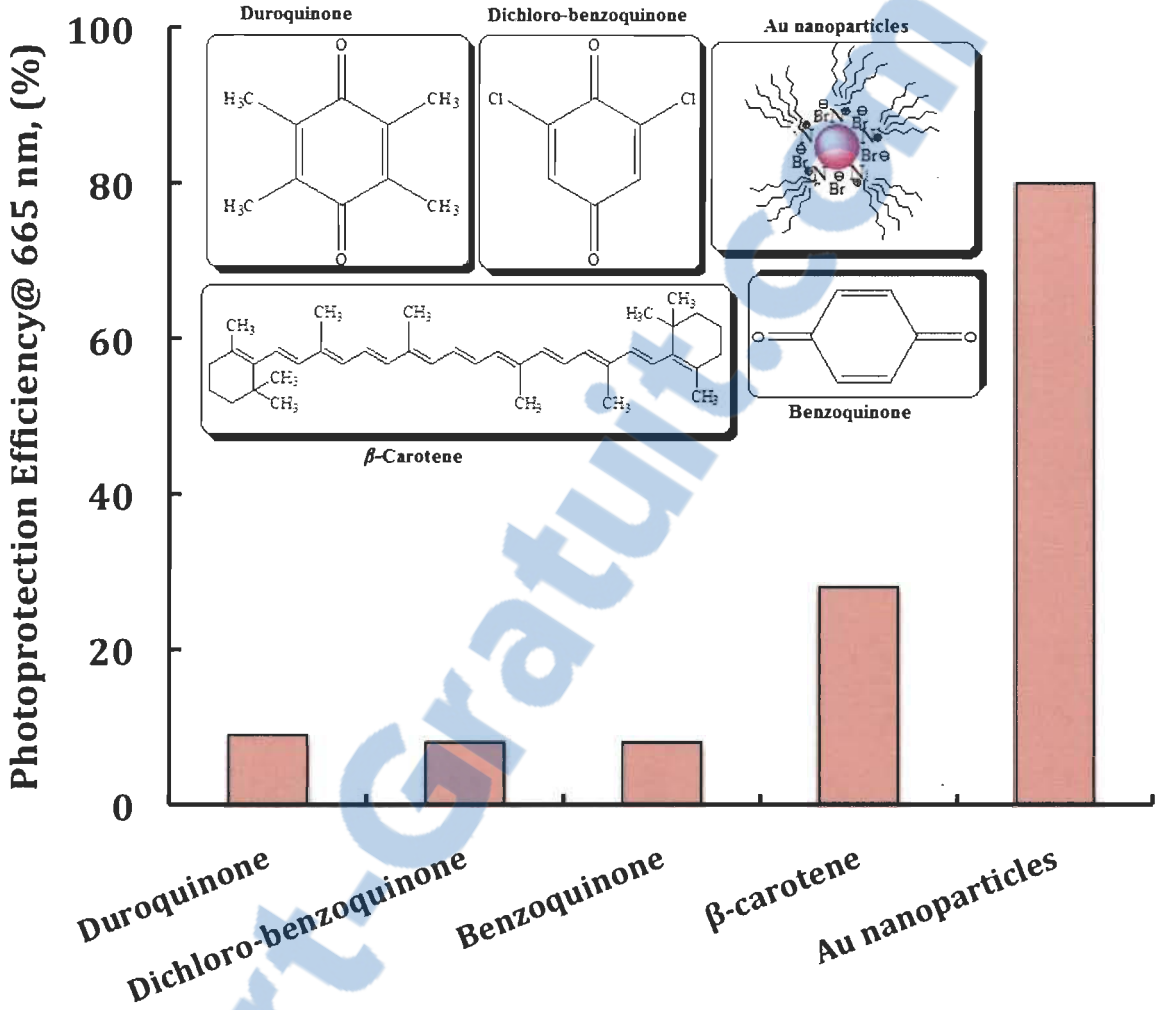

Fig. 9 Photoprotection efficiency provided to Chl*a* (4.5μM) by various additives (22 μM) in toluene. The molar ratio of Chl*a* to additive is ~ 1:5. The molecular structures of corresponding additives are also shown

Table 1 Pseudo first order reaction data for Chl*a* and Chl*a*-AuNPs

Samples	Correlation coefficient (R^2)	Rate constant (min^{-1})	Half-life time (min)
Chl*a*	0.97	0.075	10
Chl*a*-AuNPs	0.99	0.007	100

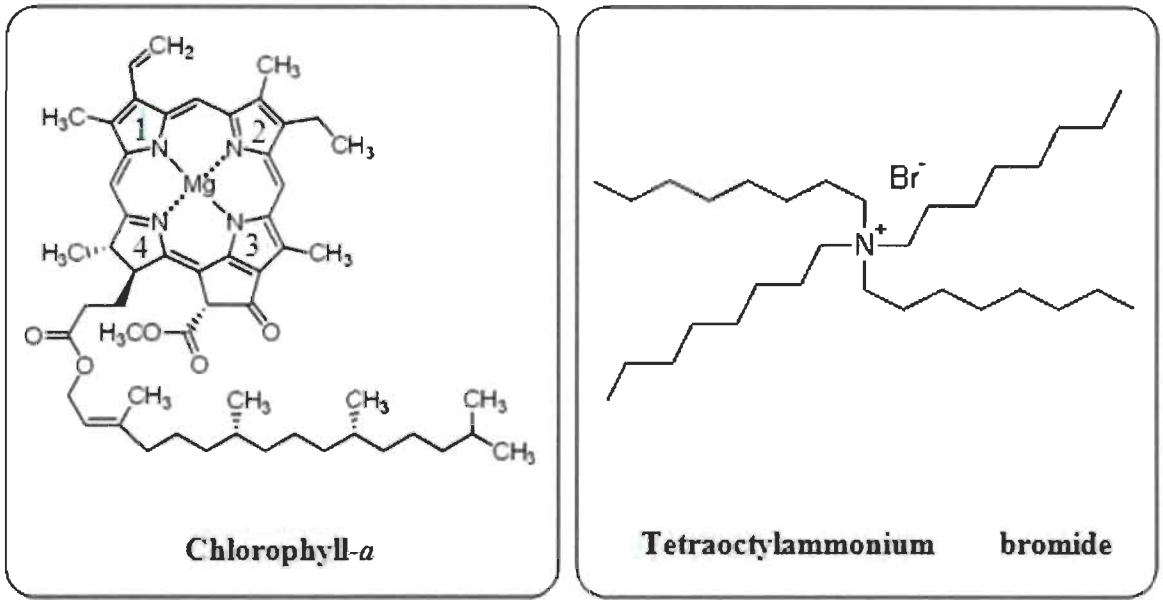

Scheme 1 Structure of chlorophyll-*a* (Chl*a*) and Tetraoctylammonium bromide (TOAB)

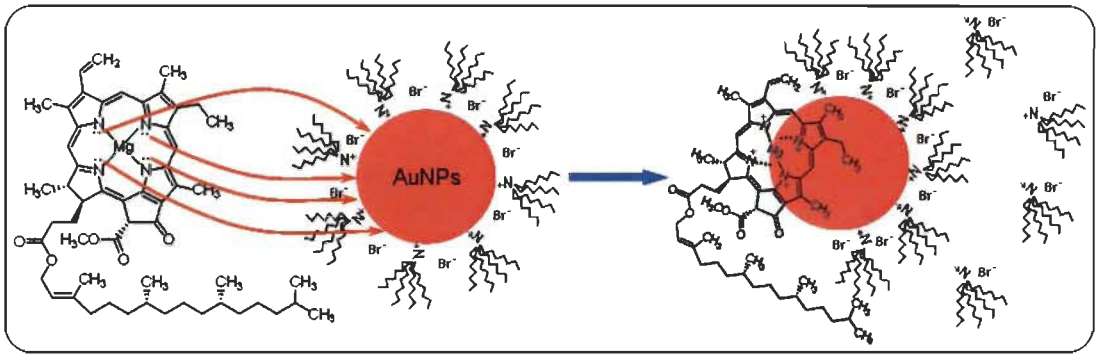

Scheme 2 Mechanism of ligand-exchange reaction between Chl*a* and AuNPs.

SUPPORTING INFORMATION

Enhanced photostability of chlorophyll-*a* using gold nanoparticles as an efficient photoprotector

Saïd Barazzouk‡, Laurent Bekalé‡, and Surat Hotchandani*

Groupe de Recherche en Biologie-Végétale, Université du Québec à Trois-Rivières, Trois-Rivières, Qc, G9A 5H7, Canada

‡ contributed equally to this work

* To whom correspondence should be addressed. e-mail: hotchand@uqtr.ca

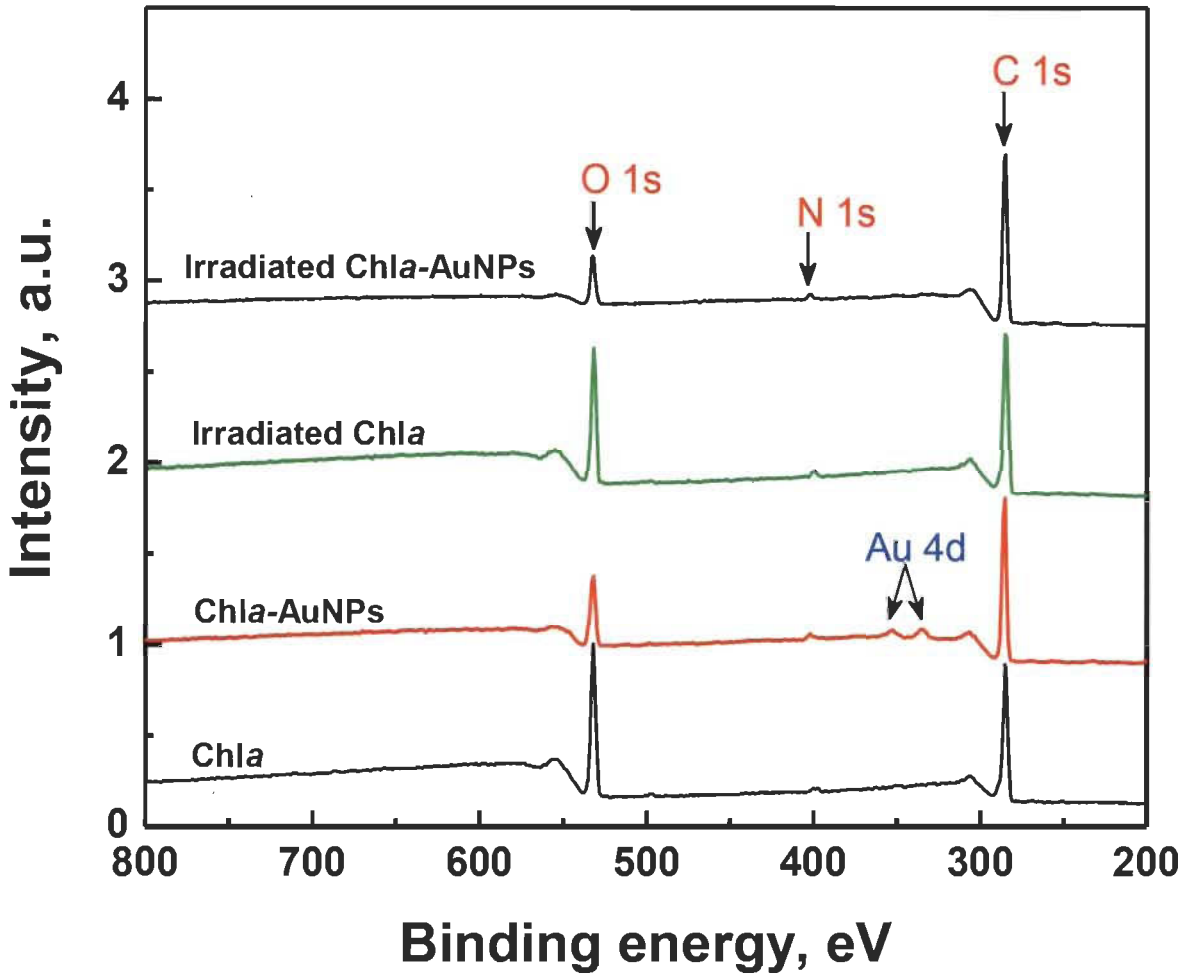

Fig. S-1 XPS survey spectra of Chl*a*, Chl*a*-AuNPs, irradiated Chl*a* and irradiated Chl*a*-AuNPs.

High-resolution C1s and N1s XPS spectra for gold nanoparticles (AuNPs) are shown in Fig. S-2 and S-3, respectively. The C1s region of AuNPs comprises three distinct peaks. The peak appearing at 285 eV, is assigned to C-C and C-H from tetraoctylammonium bromide (TOAB), the stabilizing agent used in the preparation of AuNPs. The second peak at 286.07 eV is ascribed to C-N of quaternary amine from TOAB, while a smaller peak at higher binding energy (287.17 eV) is probably due to an impurity.

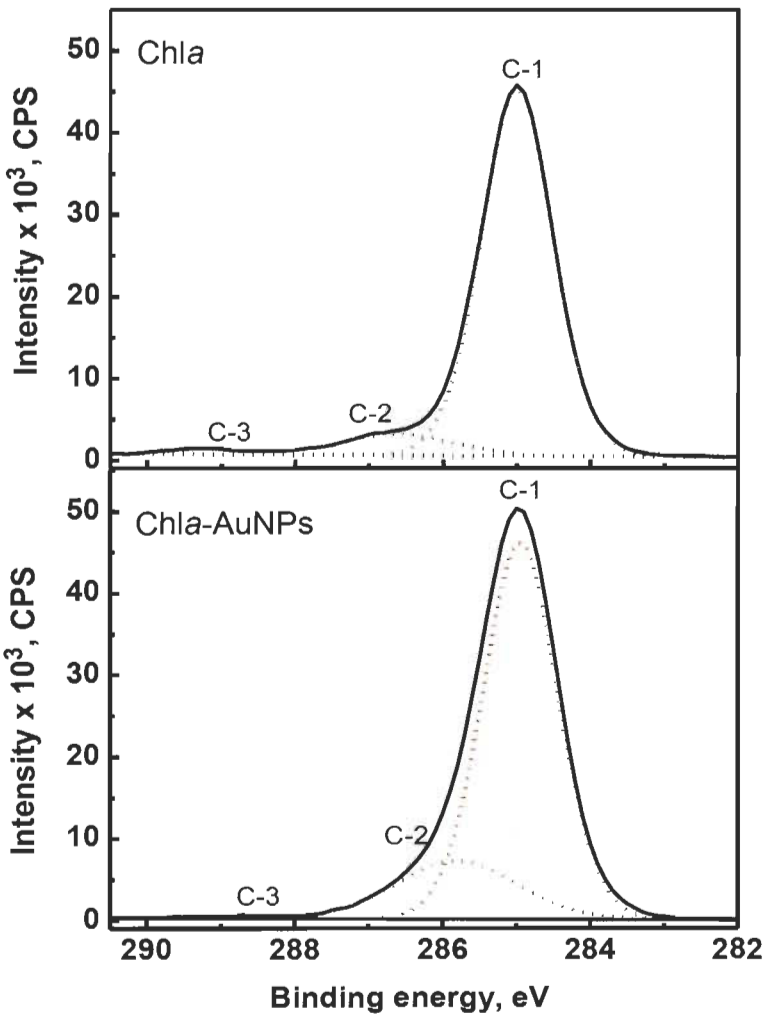

Fig. S-2 C 1s narrow scan XPS spectra for Chl*a* and Chl*a*-AuNPs.

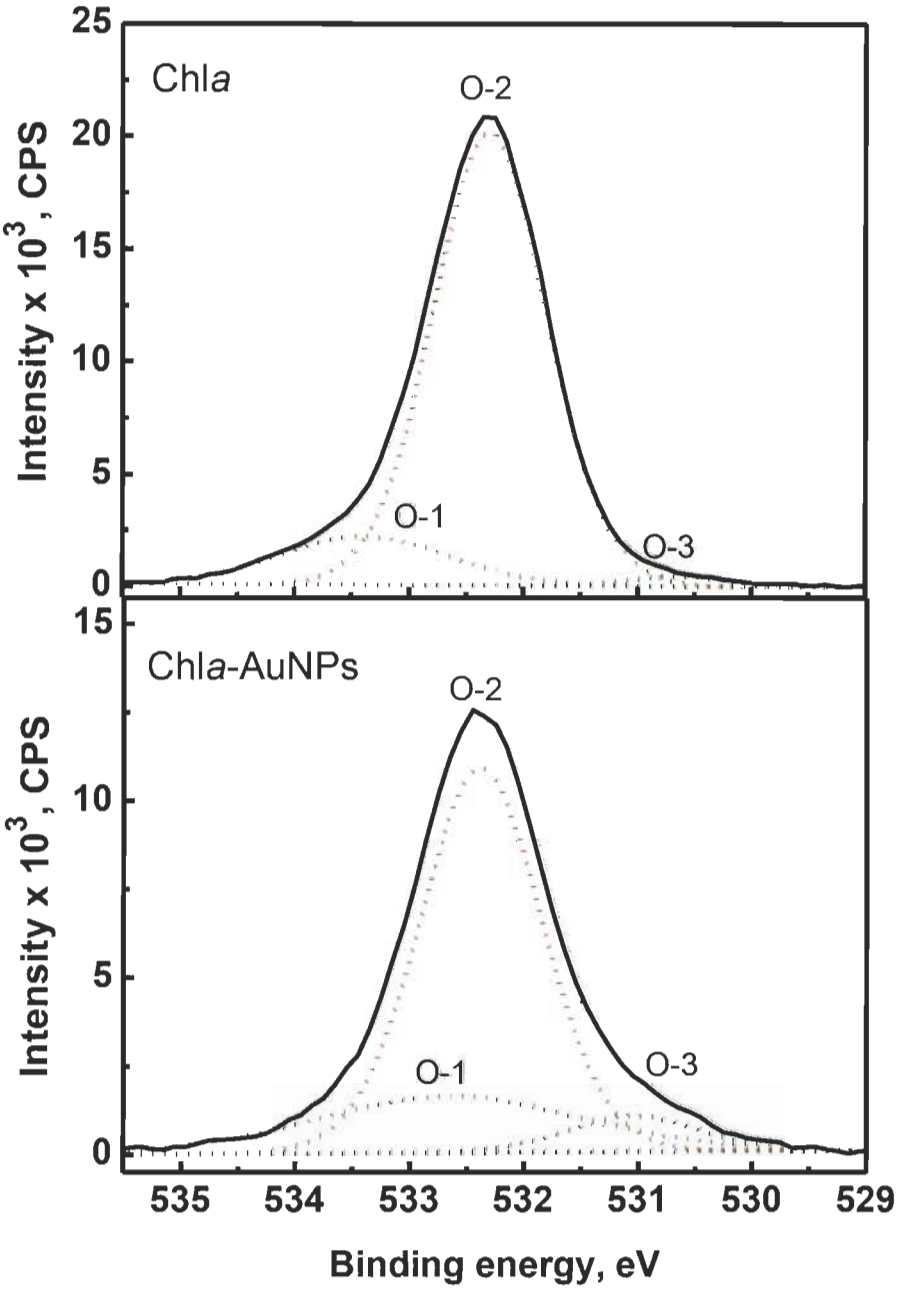

Fig. S-3 O 1s narrow scan XPS spectra for Chl*a* and Chl*a*-AuNPs.

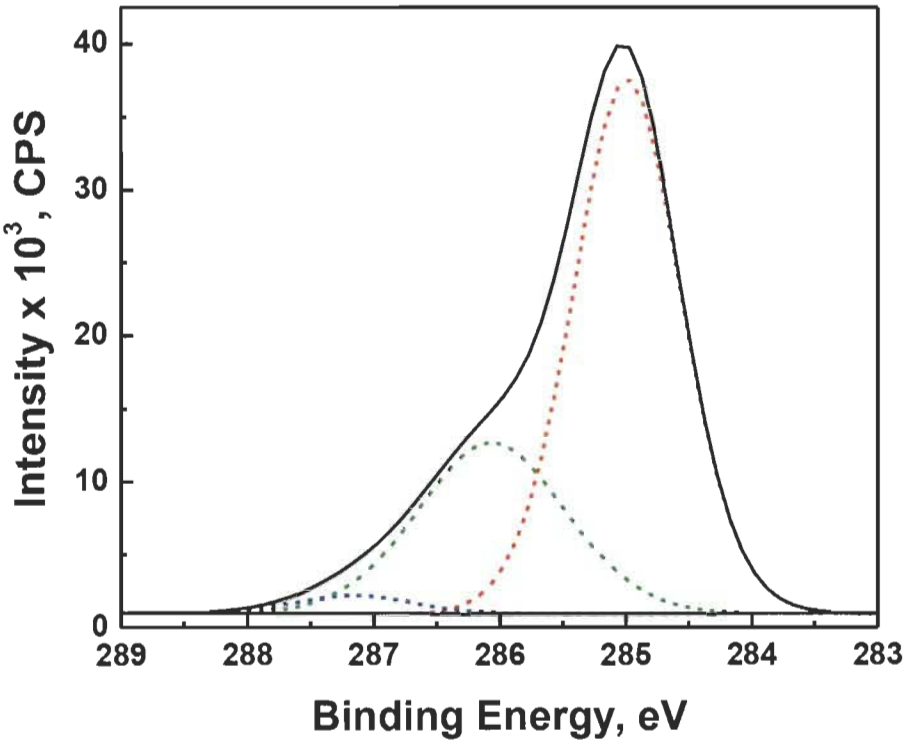

Fig. S-4 C1s narrow scan XPS spectrum for AuNPs.

Kinetics of Photochemical reaction

The photodegradation of Chl*a* in presence of O_2 can be described by following equation

$$Chla + O_2 \xrightarrow{h\nu} Chla(O_2) \qquad (1)$$

The photodegradation rate of Chl*a* was monitored by recording the absorbance at 665 nm as a function of irradiation time, and is:

$$-\frac{d[Chla]}{dt} = k[Chla]^*[O_2] \qquad (2)$$

Where [Chl*a*] denotes the concentration of Chl*a*, $[O_2]$ denotes the concentration of O_2, t is the reaction time, and k is the rate constant. As the $[O_2]$ remains constant as the reaction proceeds, the reaction can be considered pseudo-first-order because it depends on the concentration of [Chl*a*] only.

Thus, eq. (2) can be written as follows:

$$-\frac{d[Chla]}{dt} = k'[Chla] \qquad (3)$$

where $k' = k[O_2]$

Solving eq. (3), one obtains eq. (4)

$$\ln([Chla]_t) = -k't + \ln([Chla]_0) \qquad (4)$$

Where $[Chla]_0$ is the initial concentration of Chl*a* and $[Chla]_t$ is the concentration of Chl*a* at any time t. A plot of $\ln([Chla]_t)$ *vs* t should yield a straight line with a slope of k'; a typical plot is shown in the inset of Fig. 4.

CHAPITRE IV

NANOSILVER COULD USHER IN NEXT-GENERATION PHOTOPROTECTIVE AGENTS FOR NATURAL PORPHYRINS

Le contenu de ce chapitre a fait l'objet d'une publication en anglais dans la revue : *Particle & Particle Systems Characterization*, 2014, 31, 843-850.

4.1 Résumé de l'article

Une étude sur les propriétés photoprotectrices des nanoparticules d'agent (AgNPs) a été effectuée dans ce troisième article scientifique afin de démontrer que la méthode de photoprotection, précédemment présentée dans les deux premiers articles scientifiques pourrait être utilisée pour améliorer simultanément la stabilité, l'émission de fluorescence et la capacité de génération d'oxygène singulet des porphyrines de magnésium. Les résultats présentés dans cet article montrent clairement que l'emploi des AgNPs (en concentration très faible) est une méthode simple, efficace, rapide et rentable pour améliorer simultanément la photostabilité, l'émission de fluorescence et l'efficacité de production de l'oxygène singulet par photosensibilisation de la chlorophylle-*a* (Chl*a*). De plus, il est également rapporté que les AgNPs dans des conditions *in vitro*, les AgNPs sont des agents photoprotecteurs bien plus efficaces que les caroténoïdes. La capacité protectrice des AgNPs est le résultat de leur liaison avec les sites azotés du macrocycle porphyrique de la Chl*a*, et ce, avant la formation des espèces réactives de l'oxygène (ROS) par photosensibilisation. L'utilisation des AgNPs offre de nouvelles voies pour améliorer les propriétés photochimiques et photophysiques des porphyrines. Par conséquent, nous prévoyons que le présent article peut ouvrir la voie pour le développement d'une nouvelle génération d'agents photoprotecteurs qui pourrait également jouer un rôle prometteur dans l'imagerie médicale et la thérapie photodynamique. L'étude présentée dans cet article a été l'aboutissement du troisième et dernier objectif opérationnel de cette thèse.

4.2 Troisième article scientifique

Nanosilver Could Usher in Next-Generation Photoprotective Agents for Magnesium Porphyrins

Laurent Bekalé*, Saïd Barazzouk* and Surat Hotchandani*

Département de chimie, biochimie et physique, Université du Québec à Trois-Rivières, C. P. 500, Trois-Rivières (Québec), G9A 5H7, Canada

* To whom correspondence should be addressed. e-mail: bekale@uqtr.ca; hotchand@uqtr.ca; Said.Barazzouk@uqtr.ca

Abstract

A novel strategy, based on silver nanoparticles (AgNPs), has been developed for simultaneously improving: 1) photostability, 2) fluorescence emission, and 3) singlet oxygen generation ability of natural porphyrin (i.e., chlorophyll (Chl) molecules). The benefit of AgNPs as photoprotector of Chl is that they spontaneously bind with the nitrogen atoms of Chl as soon as they are mixed together, even in the dark prior to the illumination, inhibiting thus the binding of reactive oxygen species (ROS) at nitrogen sites, known to cause the photodegradation of porphyrins.

Keywords: Nano-Silver, Chlorophyll, Photoprotection, Metal-enhanced fluorescence, Metal-enhanced singlet oxygen generation.

Nanoscale materials have received considerable attention because their structure and properties differ significantly from those of the atoms and molecules, as well as those of the bulk materials.[1] For this reason, many researchers continue to explore their amazing properties of these nanomaterials to address specific needs and problems in a number of sectors such as microelectronics, materials, environment, energy, healthcare, etc.[2] Therefore, it is of great interest to investigate how these nano-objects can improve the photostability of porphyrins such as chlorophylls.

Chlorophyll (Chl), in recent years, has attracted great interest for the biotechnological applications. Ohtani et al., have recently reported that Chl extracted from spinach is a promising material for the fabrication of the organic light-emitting diodes (OLEDs).[3] Moreover, Shao et al., have found that Chl could be used as potent photosensitizer (photosensitizing agent) in hybrid phototransistors.[4] Further, Fan et al. have recently discovered that Chl extracted from the leaves of Chimonanthus salicifolius could have great potential for cancer imaging.[5] Finally, Gilmar et al. have recently demonstrated the potential of Chls as possible countermeasure against mosquito larvae.[6] However, despite the growing efforts to use Chls as active ingredient in a wide range of modern biotechnological applications, the *in vitro* Chl has a crucial disadvantage, which is its high photoinstability under aerobic conditions. In other words, the photo-instability of Chls is one of the primary concerns that hinders their utilization in the majority of the biotechnological areas. Therefore, if the photostability of Chl could be significantly amended, their technological application would be enormously improved.

So far, many approaches to enhance the photostability of *in vitro* chlorophyll have been explored. Itoh et al. have reported that chlorophyll-*a* (Chl*a*), adsorbed on silicate layers of smectite, showed photostable properties.[7] They have also prepared a chlorophyll-mesoporous silica conjugate, and suggested that the interaction between Chl and the supporting silica materials in nanoscale space could increase the photostability of Chl.[8] In our research team, we decided to approach the problem using noble metal nanoparticles. We recently employed gold nanoparticles to photoprotect Chl*a* by

suppressing the binding of reactive oxygen species (ROS, namely, singlet oxygen, superoxide ion and hydrogen peroxide) at nitrogen sites of porphyrin macrocycle of Chl*a*. [9] Although these materials have been proven to enhance the photostability of *in vitro* Chl, they have some other limitations in that they have been found to quench the fluorescence of Chl and also limit its capability to generate singlet oxygen ($^1O_2$). As such, the above mentioned Chl photoprotective agents do not meet the requirements when we aim to improve the photostability of *in vitro* Chls, especially with an objective to take advantage of their near-infrared fluorescent properties for imaging, and their strong singlet oxygen generation abilities for photodynamic therapy. Therefore, it is critically important to develop functional materials that could enhance the photostability of Chls without compromising their fluorescence emission and their ability to generate $^1O_2$ so that they can be successfully exploited in various areas of materials science and biotechnology.

We have selected silver nanoparticles (AgNPs) to assess the possibility of simultaneously improving these photophysical properties of Chl molecules. There are three reasons that strongly motivated our choice of AgNPs. First, AgNPs are attractive owing to their excellent metal-enhanced fluorescence properties (MEF), i.e., increasing the fluorescence emission of fluorophores close to metallic nanoparticles.[10] Second, AgNPs are also attractive due to their excellent metal-enhanced singlet oxygen generation properties (ME$^1O_2$), i.e., increasing the singlet oxygen generation efficiency of the photosensitizers close to metallic nanoparticles.[11] Finally, AgNPs find use in many fields; the major applications include their use in textile engineering, electronics and optics,[12-16] and, most importantly, in the medical field as bactericidal [17] and therapeutic agent.[18]

In this communication, we report an unprecedented observation that AgNPs are the potential additives to simultaneously increase the photostability, fluorescence emission, as well as singlet oxygen generation capability of *in vitro* Chl*a*. The UV-visible, fluorescence and X-ray photoelectron spectroscopic (XPS) studies have been carried out to assess the effect of AgNPs on Chl*a*. The results show that the

half-life of Chl*a* (4.5 μM) has been extended from 49 to 770 minutes in the presence of ultralow concentration of AgNPs (0.36 nM). Additionally, it is seen that AgNPs are much more effective photoprotective agents of *in vitro* Chl*a* than are the carotenoid molecules (i.e., β-carotene and lycopene). The protecting ability of Chl*a* against photodegradation by AgNPs is the result of their binding with Chl*a* at its nitrogen sites, thus inhibiting the binding of reactive oxygen species (ROS) at these sites, which are known to cause the photodegradation of Chl*a*. In addition to their significant photoprotective performance, we have also observed that AgNPs improve MEF and ME^1O_2 properties of Chl*a* by 1.2 and 2 times, respectively.

The procedure for preparing silver nanoparticles (AgNPs) in an organic medium is a modified version of that proposed by Korgel et al.[19] **Figure 1A** shows the UV-visible absorption spectra of the silver colloids. A localized plasmon resonance peak at around 430 nm was observed for AgNPs, which is in good agreement with that of roughly spherical AgNPs.[20] The formation of AgNPs was confirmed by the observation of Ag 3d peaks in XPS (**Figure 1B**). The XPS peaks corresponding to Ag 3d (5/3) and Ag 3d (2/3) appeared at binding energies of about 368.3 and 374.3 eV, respectively, in good agreement with bulk silver metallic values.[21] Transmission electron microscopy (TEM) confirmed the existence of spherical Ag nanoparticles (as illustrated in **Figure 1C**). Furthermore, from the analysis of TEM images of 100 nanoparticles, an average diameter of 5.3 ± 0.76 nm was determined for AgNPs (**Figure 1D**). **Figure 2A** presents typical changes in the absorption spectra of Chl*a* solution in toluene as a function of irradiation time with red light ($\lambda > 640$ nm). The principal absorption peaks of Chl*a* (see initial spectrum at 0 min of irradiation) in the red at 665 nm (Q band) and at 433 nm in the blue (Soret band) are in good agreement with those reported in the literature,[22] and that Chl*a* is present in monomeric form. Photodegradation is characterized by the decrease in the intensity of both Soret and Q bands on exposure of Chl*a* to red light. As seen from **Figure 2A**, there is a quick and progressive decrease of Chl*a* absorbance as the irradiation time increases. In 5 minutes, about 10% decrease in the absorbance of Q-band in the red (665 nm) was observed. On continued exposure, the absorbance at 665 nm decreased 36% in 20 minutes and by 73% in 90 minutes. These

results of Chl*a* are in good agreement with those reported by Jones and Mackay,[23] Merzlyak et al.,[24] and Tregub et al.,[25] who studied the photodegradation of Chl*a* in micelles, methanol and various other organic solvents, respectively. In order to evaluate the effect of AgNPs as a potential photoprotective additive to reduce the photodegradation of Chl*a*, the irradiation of Chl*a* solution (4.5 μM) in the presence of AgNPs was carried out under identical conditions as for Chl*a* alone (irradiation with red light, $\lambda > 640$ nm). As is clear from **Figure 2B**, the addition of AgNPs seems to provide a remarkable protection to Chl*a* against photodegradation. Indeed, after 90 minutes of irradiation, Chl*a* bleached only 10 % in the presence of AgNPs (0.36 nM) compared to the 73% photodegradation in absence of AgNPs (see **Figure 2A**). In other words, a huge photoprotection of ~ 90% has been provided to Chl*a* by AgNPs (0.36 nM). The decrease in photodegradation of Chl*a* in the presence of AgNPs can also be seen visually (**Figure S1** in the Supporting Information). While the color of Chl*a* solution changes from light green to clear after irradiation, the color of Chl*a* admixed with AgNPs remains virtually the same after irradiation, thus indicating clearly the photoprotective action of AgNPs. It is worthy to point out that even after a very long time of irradiation, i.e., 540 min. a photoprotection of higher than 70% has been provided to Chl*a* by AgNPs (0.36 nM). This is the first experimental demonstration that highlights the beneficial effect of AgNPs in increasing enormously the photochemical stability of Chl*a*.

To get a meaningful insight into the photostability imparted to Chl*a* by AgNPs, the photodegradation kinetics of Chl*a* was studied, and is presented in **Figure 3**, and described in the supporting information section. The photodegradation kinetics of Chl*a* in the absence and presence of AgNPs follows pseudo-first order kinetics. It is found that AgNPs induced a dramatic decrease of the photodegradation rate constant of Chl*a*, i.e., from 1.4×10^{-2} to 9×10^{-4} min^{-1}, resulting into an enormous increase in the half-life from 49 minutes for free Chl*a* to 770 minutes for Chl*a* mixed with AgNPs and indicating an enormous improvement (i.e., 15714% increase) in the photostability of Chl*a* brought about by AgNPs (**Table 1**).

Our findings also reveal that the photoprotection of Chl*a* is dependent upon the AgNPs concentration (inset **Figure 3**). That is, the higher the concentration of AgNPs, the greater is the photoprotection provided to Chl*a* against irradiation. However, AgNPs concentration greater than 0.36 nM did not provide any additional protection. The percentage photoprotection was calculated using eq. (1), described in Experimental section. To exclude the possibility that the 1-nonanthiol (NT), a surfactant used in the preparation of AgNPs, had any photoprotective role, a solution of NT (50 mM) in toluene was added to Chl*a* solution. Chl*a* was not photoprotected, confirming that it is the AgNPs, rather than NT, that provide the photoprotection to Chl*a*. Furthermore, AgNPs themselves subjected to the irradiation for the same time period (540 min) under identical conditions did not show any photochemical changes.

In order to substantiate the advantage of using AgNPs compared to other chlorophyll protoprotective agents, such as carotenoids, which have been found to protect green plants,[26] similar photodegradation experiments of Chl*a* with red light irradiation ($\lambda > 640$ nm) were carried out in presence of different carotenoids, i.e., β-carotene and lycopene. It is found that lycopene (22 μM) provides a photoprotection of only 28% whereas β-carotene (22 μM) no more than 22 % as shown in **Figure 4**, which are about 3 .and 4 times inferior to the photoprotection imparted by the ultralow concentration of AgNPs (0.36 nM).

Once the role of AgNPs as efficient photoprotector was established, we then embarked upon the study of the influence of AgNPs on the fluorescence emission of Chl*a*. The fluorescence spectra of Chl*a* (4.5 μM), AgNPs (0.36 nM), and their mixture are presented in **Figure 5**. The samples were excited at 625 nm, right into the red absorption region of Chl*a*, where AgNPs have no absorption. An enhancement of Chl*a* fluorescence in presence of AgNPs is clearly noticeable. Dividing the fluorescence intensity of Chl*a* in presence of AgNPs by that in absence of AgNPs yields an enhancement factor of 1.2. An increase in fluorescence of similar smaller magnitude (1.18 times) has also been reported by other authors.[27b]

It should, however, be mentioned that the observed enhancement of fluorescene of Chl*a* in the present study is not due to an additional fluorescence emitted by AgNPs because they do not exhibit any fluorescence in the fluorescence region of Chl*a* (**Figure 5**). The fluorescence enhancement observed in the current work could be understood as the result of the modification of local electromagnetic field in the vicinity of Chl*a* caused by the localized surface plasmon resonance at the surface of silver nanoparticles. The plasmonic field of metallic nanoparticle increases the radiative rate of the fluorophore, leading to an enhancement of the quantum yield of its fluorescence. This explanation has also been put forward by other researchers with regard to the fluorescence enhancement of chlorophylls in light-harvesting complexes placed near a silver metal layer.[27, 28] Further, the fluorescence enhancement factor does not depend upon the concentration of the AgNPs as shown in the inset of **Figure 5**.

It is worth mentioning that the photostability of fluorescing species is thought to be closely linked to MEF phenomenon. [10c] This is due to the fact that MEF occurs as a result of the augementation of radiative rate constant of the fluorophore leading to shorter excited state lifetimes. Accordingly, if the fluorophore spends less time in the excited state, there is a smaller probability for the reactions between excited fluorophore and molecular O_2 to occur, thereby producing lower amounts of singlet oxygen (known to cause the photodegradation of the fluorophore) and increasing the photostability. That is, MEF enchances the photostability of fluorophores as a result of the lower production of the singlet oxygen ($^1O_2$). However, it is interesting and extremely important to point out that the enhanced photoprotection provided to Chl*a* by adding of AgNPs is not due to MEF phenomenon just described, because in our case, the presence of AgNPs actually increases the ability of Chl*a* to generate more $^1O_2$ which would cause more photodegration and thus decrease the photostability of Chl*a*. The photoprotection provided to Chl*a* by AgNPs, as mentioned in Introduction, is rather due to the binding of AgNPs at the nitrogen sites of Chl*a* that prevents the attachment of $^1O_2$ at the same nitrogen sites which causes the photodegradation. The effect of AgNPs on the $^1O_2$ generation and its photoprotective action of Chl*a* are further discussed below.

To prove that the presence of AgNPs in Chl*a* solution promotes the production of $^1O_2$, the aerobic irradiation of Chl*a* solution (4.5 μM) in the absence and presence of AgNPs (0.36 nM) was performed employing 9,10-dimethyl-anthracene (DMA) as an $^1O_2$ chemical sensor in toluene. This sensor is a highly fluorescent probe with emission comprising of three bands in the 400-500 nm wavelength region, and reacts efficiently with $^1O_2$ to form the non-fluorescent DMA 9,10-endoperoxide in many organic solvents.[29] The Metal-enhanced generation of $^1O_2$ (ME^1O_2) by Chl*a* in absence and presence of AgNPs was measured by following the decrease in the fluorescence emission of DMA upon its photosensitized conversion into the corresponding non-fluorescent 9,10-endoperoxide (**Scheme 1**, in the Supporting Information). **Figure 6** displays a typical time dependence of the photoinduced decrease in the fluorescence emission of DMA with increasing irradiation time in presence of Chl*a* (4.5 μM) and in presence of the mixture of Chl*a* (4.5 μM) + AgNPs (0.36 nM). From the figure, a 2-fold enhancement (i.e., from 5 x 10^{-4} s^{-1} to 9 x 10^{-4} s^{-1}) in the photo-oxidation rate of DMA sensitized by Chl*a* in presence of AgNPs (i.e., Chl*a*@AgNPs) can be clearly seen compared to the photo-oxidation rate of DMA sensitized by Chl*a* alone under same irradiation conditions. Since, the decrease in DMA fluorescence is due to its photo-oxidation by $^1O_2$, producing nonfluorescent endoperoxide, the results suggest that the yield of $^1O_2$, generated by Chl*a*, is enhanced by a factor of two in the presence of silver nanoparticles. To confirm that the high efficiency of $^1O_2$ generation observed in the mixture of Chl*a* + AgNPs is, indeed, due to an increase in the photosensitized oxidation of DMA brought about only by Chl*a* and not by AgNPs, the photo-production of $^1O_2$ by AgNPs in the absence of Chl*a* was verified. DMA, subjected to the irradiation in the presence of AgNPs under identical conditions, did not show any decrease in the fluorescence of DMA (data not shown), indicating that AgNPs alone are not able to produce $^1O_2$ at all.

As $^1O_2$ is known to play an indispensable role in the photodynamic therapy (PDT), a medical technique that uses a combination of light and photosensitizing drugs to produce cytotoxic $^1O_2$ to induce selective damage to the tumor cells, we envision that AgNPs will play very promising dual roles in PDT: (1) as a photoprotector to increase

the photostability of the photosensitizers by increasing their half lives (Fig. 3 and Table 1) so that they can generate $^1O_2$ for longer periods of time, and (2) as a booster of the cytotoxic $^1O_2$ production *via* metal–photosensitizer interactions.

At first sight, one may be intrigued by the simultaneous enhancement of both the fluorescence emission and the yield of $^1O_2$, since the enhancement in fluorescence, due to the shortened singlet lifetime of the fluorophore, requires that the yield of $^1O_2$ should decrease. Both these enhancements can, however, be reconciled if we take the metal-fluorophore (AgNPs and Chl*a*) interactions into account that lead to a modification of the local electromagnetic field in the vicinity of Chl*a* moieties. This same electromagnetic field can also modify the spin-orbit coupling (a quantum mechanical process that is responsible for intersystem crossing) in the fluorophore[30] leading to the increase in its triplet formation and thus the yield of $^1O_2$. Such contrasting behavior, i.e., the enhancement of both the fluorescence emission and the yield of $^1O_2$, has also been recently reported by de Melo et al. in case of silver-pectin nanoparticles.[31]

Finally, to understand the origin of the photoprotective effect of AgNPs, the interactions between AgNPs and Chl*a* were studied by UV-vis and X-ray photoemission spectroscopy (XPS) techniques. With the addition of only a small quantity of AgNPs (0.36 nM) to Chl*a* solution, a change in the absorption spectrum of Chl*a* was observed (**Figure S2**). A bathochromic shift (~ 4 nm) of Soret band and a decrease in the intensity of Q-band at 665 nm can clearly be seen as the concentration of AgNPs increases. These changes in the UV-vis absorption spectrum of Chl*a*, induced by AgNPs, indicate the formation of a complex between Chl*a* and AgNPs (AgNPs@Chl*a*) through the pyrrolenine nitrogen atoms of the porphyrin macrocycle of Chl*a* as shown later.

The changes in the absorption (ΔA) at 665 nm were used to determine the association constant between Chl*a* and AgNPs employing Benesi-Hilderbrand method.[32] An average apparent association constant, K_{app}, for Chl*a*@AgNPs complex, obtained from the intercept-to-slope ratio of the double reciprocal plot of $1/\Delta A$ vs 1/[AgNPs], is 2.6×10^8 M^{-1} (inset of **Figure S2B**).The high value of K_{app} observed

suggests a strong binding between Chl*a* and AgNPs. Furthermore, based on the fact that nitrogen atoms possess strong affinity towards Ag nanoparticle surface compared to oxygen atoms, it is reasonable to assume that the Chl*a*@AgNPs complex is formed *via* pyrrolenine nitrogen atoms of the porphyrin macrocycle of Chl*a* rather than the oxygen atoms of the carbonyl group (see structure of Chl*a*). Several authors have also observed the preferential interaction of the AgNPs surface towards the nitrogen atoms compared to oxygen atoms. For example, by comparing the interaction of AgNPs with three free-base porphyrins, i.e., tetra(4-aminophenyl) porphyrin, tetrakis(1-methyl-4-pyridionio)-porphyrin tetra(*p*-toluenesulfonate) and tetrakis(4-carboxyphenyl)-porphyrin, Murphy et al.[33] reported that amine shows a stronger interaction with AgNPs surface relative to the carboxyl groups.

To further support that the complex formation between AgNPs and Chl*a* occurs via nitrogen atoms of Chl*a*, XPS spectra were recorded. The great advantage of the XPS is its capability of detecting the chemical bonds which are involved in the complex formation. The XPS spectrum of N 1s region of Chl*a* (**Figure S3A**) shows two peaks. The main peak at 398.2 eV corresponds to the pyrrolenine nitrogen atoms of the porphyrin macrocycle of Chl*a*. The second less intense peak observed at 400 eV, is most likely due to the protonated nitrogen, produced as a result of a small degree of demetallation of Chl*a* during its exposure to X-rays in the course of the experiment. These observed peaks are in fair agreement with the reported XPS data for Chl*a* and other magnesium porphyrins.[9, 34, 35] After adding AgNPs to Chl*a* solution (Chl*a*@AgNPs), the principal peak at 398.2 eV disappears while a new peak appears at 402.2 eV (**Figure S3B**), suggesting that a new chemical environment has been established. In other words, the tertiary nitrogens in Chl*a*, with a binding energy of 398.2 eV have now, in the presence of AgNPs, been converted into positively charged tetravalent ammonium quaternary nitrogens ($R_4N^{\delta+}$) which are known to possess a higher binding energy at 402 eV.[9, 34, 35] This result confirms that the Chl*a*@AgNPs complex is formed *via* the implication of the lone pair electrons on the pyrrolenine nitrogen atoms of chlorophyll.

To exclude the possibility that the oxygen atoms in carbonyl groups of chlorophyll molecules are implicated in the formation of the complex Chl*a*@AgNPs, the O 1s XPS spectrum of Chl*a* was recorded in absence and presence of AgNPs. No significant change in the position of O 1s peak of Chl*a* was observed upon the addition of AgNPs (**Figure S4**), confirming that oxygen atoms of Chl*a* are not implicated in the Chl*a*@AgNPs complex formation. Thus, the XPS results conclusively show that the complex formation occurs via the binding of the nitrogen atoms of Chla to AgNP. This complex Chl*a*@AgNP consists of 32 molecules of Chl*a* bound to one Ag nanoparticle as described in Supporting Information; the schematic representation of the complex is depicted in Scheme 1.

Since the synthesized 1-nonanthiol-stabilized Ag nanoparticles are coated with a monolayer of surfactant (1-nonanthiol), the formation of complex Chl*a*@AgNP implies ligand exchange between 1-nonanthiol and Chl*a* on AgNP's surface. The fixation of Chl*a* to AgNP's surface therefore necessitates that 1-nonanthiol move out and make room for Chl*a*. Said otherwise, ligand exchange takes place between the incoming ligand Chl*a* and 1-nonanthiol. This is rendered possible in view of the fact that the nitrogen atoms of Chl*a* preferentially coordinate to silver atoms to form strong coordination bonds, while the sulphur atoms of 1-nonanthiol show only weak interactions with silver atoms. Consequently, 1-nonanthiol, initially attached to AgNPs, is easily replaced by Chl*a* to yield AgNPs@Chl*a* complex. Previous studies also bear the same conclusion. For example, using a flexible tetradentate ligands, 1,3-bis(2-pyridylthiol)propane, Xie et al.[36] reported that silver atoms have strong affinity towards the nitrogen atoms compared to sulfur atoms. Nath et al.[37] also demonstrated the replacement of the thiol moiety from dodecanethiol (DDT) encapsulated Ag organosol (Ag-DDT) upon the addition of dodecylamine (DDA) to form the DDA encapsulated Ag organosol (Ag-DDA).

In light of these results, one can say that the benefit of AgNPs as a photoprotector of Chl*a* is that they readily bind with the nitrogens of Chl*a* as soon as they are mixed with Chl*a*. Consequently, $^1O_2$, which is generated during the illumination of Chl*a*, finds,

to its great disappointment, that only very few free nitrogen sites are available to bind with and cause damage, since most of them have already been occupied by AgNPs in dark long before $^1O_2$ was even produced as a result of the illumination.

This very ability of AgNPs to bind with Chl*a* in its ground state in dark prior to the illumination also gives them an added advantage over other conventional protective agents, such as carotenoids. These molecules provide photoprotection to Chl*a* by suppressing the formation of $^1O_2$ by functioning as (i) triplet valves, i.e., they react with the excited triplets of Chl*a*, and thus prevent Chl*a* triplets from transferring their energy to oxygen to produce $^1O_2$, (ii) as scavengers of $^1O_2$, thereby diminishing its quantities, and, thus, its harmful effects, and (iii) as quenchers of the excited Chl*a* singlets; this decreases the intersystem crossing yield of singlet Chl*a* to triplet Chl*a*, leading to a decreased triplet yield of Chl*a* and, hence, to a decreased $^1O_2$ production.

The photoprotection of Chl*a* by carotenoids, thus, occurs *via* their interaction with the excited states of Chl*a* which suppresses the production of $^1O_2$. In other words, the carotenoids react with the excited states of Chl*a* so that lesser and lesser amounts of $^1O_2$ are produced, while, paradoxically, oxygen also reacts with the excited states of Chl*a* but produces larger and larger quantities of $^1O_2$. Thus, both the carotenoids and oxygen react with the same excited states of Chl*a*, although one (carotenoids) to protect it (Chl*a*) while the other ($^1O_2$) out to destroy it. It is thus evident that carotenoids must compete with oxygen for the excited states of Chl*a* to excercise their role as photoprotectors. In contrast, the photoprotection of Chl*a* by AgNPs occurs as a result of the binding of AgNPs with Chl*a* at its nitrogen sites as soon as they are mixed together even prior to the illumination. Consequently, AgNPs do not have to compete with any other source, and thus impart a higher photoprotection to Chl*a* than do the carotenoids (Fig. 4).

In conclusion, the present work clearly shows that the employment of AgNPs (in ultra low concentration) is a simple, efficacious, fast, and cost-effective method for simultaneously improving the photostability, fluorescence emission and singlet oxygen generation capacity of *in vitro* Chl*a*. It is also noted that AgNPs can protect Chl*a* in

solution against photodegradation better than what carotenoids can do. The protective ability of Chl*a* by AgNPs is the result of their binding with Chl*a* at its nitrogen sites, thus inhibiting the binding of $^1O_2$ at these sites, known to cause the photodegradation of Chl*a* and other porphyrins. The use of AgNPs offers new routes to ameliorate the photochemical and photophysical properties (photostability, fluorescence emission and singlet oxygen generation capacity) of chlorophylls. We, therefore, envisage that the present work may pave the way for the development of a new generation of photoprotective agents which could also play a promising role in imaging and photodynamic therapy.

Experimental Section

All chemicals were purchased from Aldrich Chemical Co., and were used as received. All aqueous solutions were prepared with deionized water.

Synthesis of Silver Nanoparticles (AgNPs): The procedure for preparing colloidal silver nanoparticles (AgNPs) in an organic medium is a modified version of that proposed by Korgel et al.[19] Briefly, an aqueous solution of sodium nitrate ($NaNO_3$) (30 mL, 5 M) was mixed with a solution of tetraoctylammonium bromide (TOAB) (50 mM) in 50 mL toluene. The biphasic mixture was vigorously stirred for 1 h. An aqueous solution of silver nitrate (7.5 mL, 30 mM) was added to the organic phase, and the mixture was stirred for 45 min. The organic layer was separated off, and 189 μL of nonanthiol was added to it to cap the silver; the mixture was further stirred for 15 min. An aqueous solution of sodium borohydride (6.25 mL, 416 mM) was then added dropwise over 35 min period while stirring vigorously. The stirring was continued for additional 15 h. The organic layer was extracted and washed 3 times with dilute ethanol to remove unbounded thiols. Finally, the organic layer, constituting the colloidal silver nanoparticles, was dried overnight on Na_2SO_4 powder and then filtered. The final concentration of AgNPs, estimated on the basis of atomic concentration, was 9 mM. The particle core diameter was estimated by using IMAGEJ® software analysis of the TEM

micrographs. The TEM micrographs of these AgNPs revealed an average particle diameter of 5.3 ± 0.76 nm.

Photodegradation Measurements: The measurements were carried out in a 1-cm path length quartz cuvette. The illumination of Chl*a* solution (3 mL, 4.5 μM) in toluene was carried out using collimated light from a 150W xenon lamp that passed through a water filter to absorb heat. A red cut-off filter that allowed wavelengths greater than 640 nm was used. The light power reaching the sample was 40 mW cm^{-2}. All operations with Chl*a* solutions were carried out in either subdued light or green light. The solutions were stored in dark in a refrigerator when not in use. All experiments were carried out in the presence of air.

Absorption and Emission Spectrometry: Absorption spectra were recorded with a Cary 5000 spectrophotometer. The emission spectra were recorded with a FluoroLog-3 spectrofluorometer.

Transmission Electron Microscopy: TEM image of the AgNPs was taken with a Philips EM 208S microscope on carbon-coated grids and operating at 80 kV.

Singlet Oxygen Sensor: The 9,10-dimethyl-anthracene (DMA) was used to evaluate the ability of Chl*a* and Chl*a*@AgNPs to produce singlet oxygen ($^1O_2$). In a typical experiment, 3 mL toluene solution of Chl*a* (4.5 μM) containing 0.5 μM of DMA, and 3 mL toluene solution of Chl*a* (4.5 μM) containing 0.5 μM DMA and 0.36 nM AgNPs were placed in a 1-cm path length quartz cuvette and illuminated with collimated light from a 150 W xenon lamp that passed through a water filter to absorb heat. A red cut-off filter which allowed wavelengths greater than 640 nm was used. The illumination was carried out under gentle magnetic stirring for different periods of time (0, 5, 10, 15, 20 s and 1, 3, 5, 7, 9, 11, 13, 15, 17 and 20 min).The DMA fluorescence emission was recorded between 380-550 nm with excitation at λ_{ex} 360 nm. The first-order rate constant of the photoprocess (photooxidation of DMA) was obtained from the plot of $\ln F_0/F$ as a function of the illumination time t; F_0 and F represent the fluorescence

intensity of DMA at time 0 and time t, respectively. The slope of the linear plot thus obtained allowed us to calculate the rate constant (k) of the photoprocess.

X-Ray Photoemission spectroscopy: XPS was performed on a Kratos Axis Ultra spectrometer (Kratos Analytical Ltd., UK), using a monochromatic Al Kα X-ray source (E= 1486.6 eV) with a power of 225 W, at a take-off angle of 90° relative to the sample surface. 400 μL of the sample was dropped on an aluminum substrate and dried in vacuum dessicator overnight to obtain a thin film. The dried sample was then transferred to the XPS sample holder. The measurements were made under a high vacuum of 10^{-9} torr, at room temperature. The surface of the sample was ~ 20 mm^2, and the investigated area was typically 1 x 2 mm^2. High-resolution spectra of Ag 3d, N 1s and O 1s were an average of five scans acquired at a pass energy of 40 eV and resolution of 0.1 eV/step, for quantitative measurements of binding energy. The CasaXPS software was used for background subtraction (Shirley-type), peak integration, fitting and quantitative chemical analysis. The C 1s (C– C) peak at 285 eV was used to calibrate the binding energy scale. Binding energies values are given at ± 0.2 eV. Gaussian peak profiles were used for spectral deconvolution of Ag 3d, O 1s and N 1s spectra.

Percentage Photostability: The percentage photostability was calculated using the formula as described by Claes:[38]

$$\frac{E_3 - E_2}{E_1 - E_2} \times 100 \qquad (1)$$

where E_1, E_2, and E_3 are, respectively, the concentration (or absorbance) of Chl*a* before irradiation, after irradiation without AgNPs, and after irradiation in the presence of AgNPs.

Supporting Information

Supporting Information is available online from the Wiley Online Library or from the author.

Acknowledgements

The work described herein was supported by the Natural Sciences and Engineering Research Council of Canada (NSERC).

References

[1] a) X. Xue, F. Wang, X. Liu, *J. Mater. Chem.* **2011**, 21, 13107; b) M. M. Khin, A. S. Nair, V. J. Babu, R. Murugan, S. Ramakrishna, *Energy Environ. Sci.* **2012**, 5, 8075. b) X. Chen, C. Li, M. Grätzel, R. Kostecki, S. S. Mao, *Chem. Soc. Rev.* **2012**, 41, 7909. d) E. Roduner, *Chem. Soc. Rev.* **2006**, 35, 583.

[2] R. A. McIntyre, *Science progress*, **2012**, 95, 1.

[3] N. Ohtani, N. Kitagawa, T. Matsuda, *JJAP*. **2011,** 50, 01BC08-1-01BC08-3.

[4] S. Y. Chen, Y. Y. Lu, F. Y. Shih, P. H. Ho, Y. F. Chen, C. W. Chen, Y. T. Chen, W. H. Wang, *Carbon*. **2013**, 63, 23.

[5] L. Fan, Q. Wu, M. Chu, *International Journal of Nanomedicine*. **2012**, 7, 3071.

[6] G. S. Erzinger, S. Wohllebe, F. Vollrath, S. C. Souza, P. Richter, M. Lebert, D. P. Häder, *Parasitol. Res*. **2011**, 109, 781.

[7] a) Y. Kodera, H. Kageyama, H. Sekine, Y. Inada, *Biotechnol. Lett.* **1992**, 14, 119; b) A. Ishii, T. Itoh, H. Kageyama, T. Mizoguchi, Y. Kodera, A. Matsushima, K. Torii, Y. Inada, *Dyes Pigments*. **1995**, 28, 77; c) T. Itoh, A. Ishii, Y. Kodera, A. Matsushima, M. Hiroto, H. Nishimura, T. Tsuzuki, T. Kamachi, I. Okura and Y. Inada, *Bioconjugate Chem*. **1998**, 9, 409.

[8] T. Itoh , K. Yano, Y. Inada ,Y. Fukushima, *J. Am. Chem. Soc.* **2002**, 124, 13437.

[9] S. Barazzouk, L. Bekalé, S. Hotchandani, *J. Mater. Chem*. **2012**, **22**, 25316.

[10] a) P. P. Pompa, L. Martiradonna, A. D Torre, F. D Sala, L. Manna, M. De Vittorio, F. Calabi, R. Cingolani, R. Rinaldi, *Nature nanotechnology*. **2006**, 1, 126; b) C. D. Geddes, J. R. Lakowicz, *Journal of Fluorescence*. **2002**, 12, 121. c) J. R. Lakowicz, Analytical Biochemistry. **2011**, 298, 1.

[11] Y. Zhang, K. Aslan, M. J. R. Previte, C. D. Geddes, *J Fluoresc.* **2007**, 17, 345.

[12] P. Zhang, C. Shao, Z. Zhang, M. Zhang, J. Mu, Z. Guo, Y. Liu, *Nanoscale*, **2011**, 3, 3357.

[13] D. A. McFarland, R. P. Van Duyne, *Nano Letters*, **2003**, 3, 1057.

[14] H. Zhu, M. Du, M. Zhang, P. Wang, S. Bao, L.Wang, Y. Fu, J. Yao, *Biosens Bioelectron*. **2013**, 49, 210.

[15] A. H. Alshehri, M. Jakubowska, A. Młożniak, M. Horaczek , D. Rudka, C. Free, J. D. Carey, *ACS Appl. Mater. Interfaces*, **2012**, 4, 7007.

[16] K. Liu, S. Qu, X. Zhang, F. Tan, Z. Wang, *Nanoscale Research Letters*, **2013**, 8, 88.

[17] J. Jain, S. Arora, J.M. Rajwade, P. Omray, S. Khandelwal, K.M. Paknikar, *Mol Pharm*, **2009**, 6, 1388.

[18] K. K. Wong, S. O. Cheung, L. M. Huang, J. Niu, C. Tao, C. M. Ho, C. M. Che, P. K. Tam, *ChemMedChem*, **2009**, 4, 1129.

[19] B. A. Korgel, S. Fullam, S. Connolly, D. Fitzmaurice, *J. Phys. Chem. B*. **1998**, 102, 8379.

[20] V. Amendola, O. M. Bakr, F. Stellacci, *Plasmonics*. **2010**, 5, 85.

[21] Y. Lai, H. Zhang, K. Xie, D. Gong, Y. Tang, L. Sun, C. Lin, Z. Chen, *New Journal of Chemistry*. 2010, 34, 1335.

[22] J. Zvezdanovic, D. Markovic, *J. Serb. Chem. Soc*. **2008**, 73, 271.

[23] C. E. Jones, R. A. Mackay, *J. Phys. Chem.* **1978**, 82, 63.

[24] M. N. Merzlyak, S. I. Pogosyan, L. Lekhimean, T. V. Zhigolova, I. F. Khozina, Z. Cohen, S. S. Khushchev, *Rus. J. Plant Physiol*. **1996**, 43, 160

[25] S. Tregub, S. Schoch, G. Erago, H. Scheer, *J. Photochem. Photobiol., A*. **1996**, 98, 51.

[26] a) G. E. Bartley, P. A. Scolnik, *The Plant Cell*. 1995, 7, 1027; b) M. A. Montenegro, M. A. Nazareno, E. N. Durantini, C. D. Borsarelli, *Photochemistry and Photobiology*. **2002**, 75, 353.

[27] a) S. Mackowski, S. Wolrmke, A. J. Maier, T. H. P. Brotosudarmo, H. Harutyunyan, A. Hartschuh, A. O. Govorov, H. Scheer, C. Braluchle, *Nano Lett.* **2008**, 8, 558. b) I. D. Anatoliy, D. G. Chris, *Appl. Phys. Lett.* **2012**, 100, 093115. c) A. Kadir, R. L. Joseph, D. G. Chris, Anal Bioanal Chem, **2005**, 382, 926.

[28] a) D. Kowalska, B. Krajnik, M. Olejnik, M. Twardowska, N. Czechowski, E. Hofmann, S. Mackowski, *The Scientific World Journal*, **2013**, 2013, Article ID 670412. b) A. Kadir, G. Ignacy, M. Joanna, M. Evgenia, L. R. Joseph, D. G. Chris, Current opinion in Biotechnology, **2005**, 16, 55.

[29] a) E. Albiter, S. Alfaro, M. A. Valenzuela, *International Journal of Photoenergy*. **2012**, 2012, 1. Article ID 987606; b) A. Gomes, E. Fernandes, J. L.F.C. Lima, *J. Biochem. Biophys. Methods*, **2005**, 65, 45.

[30] a) N. L. Pacioni, M. Gonzalez-Bejar, E. Alarcon, K. L. McGilvray, J. C. Scaiano, *J. Am. Chem. Soc*, **2010**, 132, 6298; b) A. E. Cohen, *J. Phys. Chem. A*, **2009**, 113, 11084.

[31] L. S. A. de Melo, A. S. L. Gomes, S. Saska, K. Nigoghossian, Y. Messaddeq, S. J. L. Ribeiro, R. E. de Araujo, *J Fluoresc*, **2012**, 22, 1633.

[32] H. A. Benesi, J. H. Hildebrand, *J. Am. Chem. Soc*. **1949**, 71, 2703.

[33] S. Murphy, L. Huang, P. V. Kamat, *J. Phys. Chem. C*. **2011**, 115, 22761.

[34] L. Bekalé, S. Barazzouk, S. Hotchandani, *J. Mater. Chem*. **2012**, 22, 2943.

[35] a) J. J. Jack, D. M. Hercules, *Anal. Chem*. **1971**, 43, 729; b) S. Virtanen, A. Soininen, V. M. Tiainen, D. Besic, M. Puk, T. Kinnari, J. Salo, R. Trebse, A. J. Trampuz, Y. T. Konttinen, *Suomen Ortopedia ja Traumatologica*. **2006**, 29, 290.

[36] Y.-B. Xie, C. Zhang, J.-R. Li, X.-H. Bu, *Dalton Trans.*, **2004**, 562.

[37] S. Nath, S. K. Ghosh, S. Kundu, S. Praharaj, S. Panigrahi, T. Pal, *Journal of Nanoparticle Research*. **2006**, 8, 111.

[38] H. Claes, *Biochem. Biophys. Res. Commun*. **1960**, 3, 585.

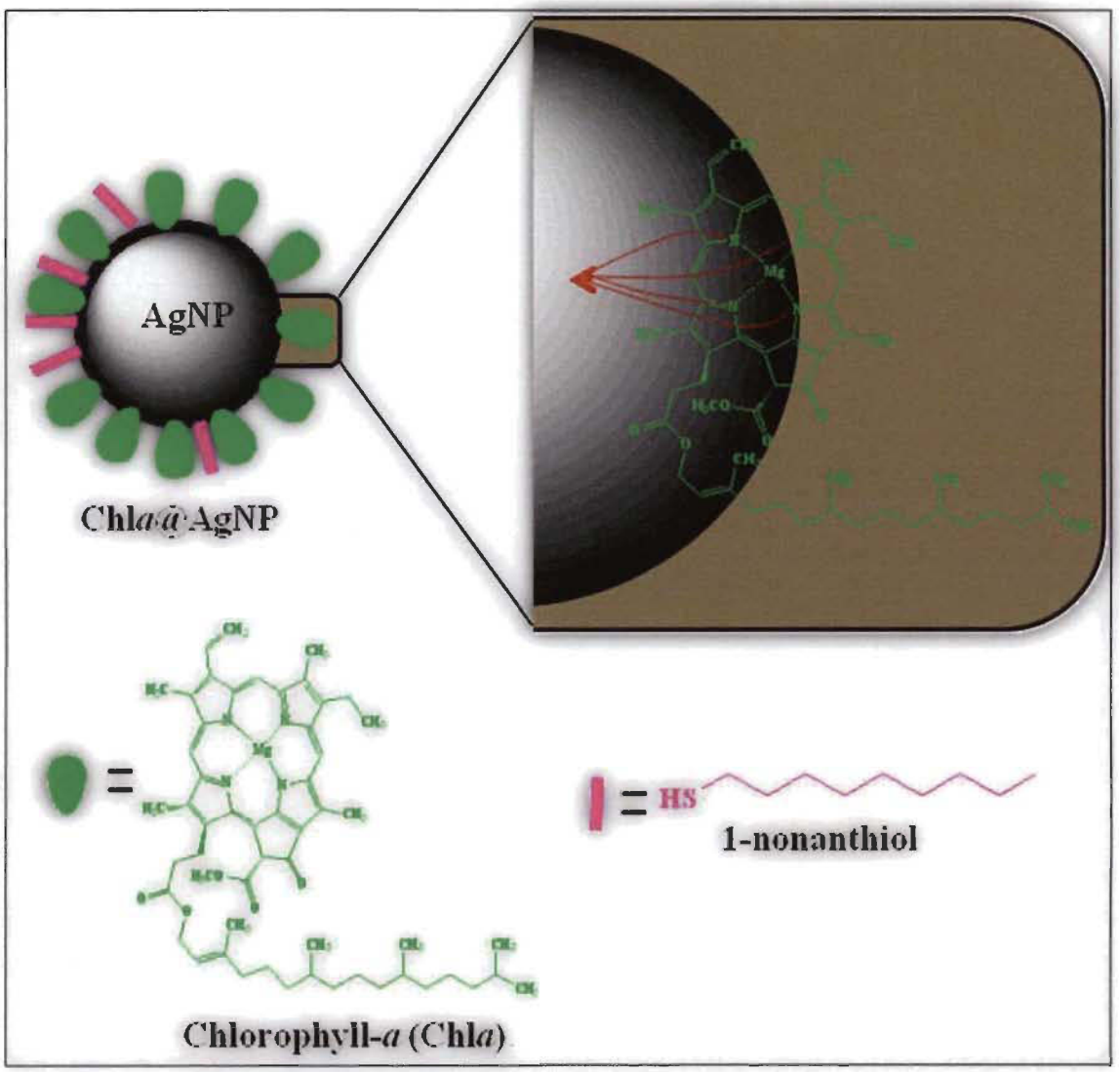

Scheme 1. Image of the complex consisting of Chl*a* and AgNP.

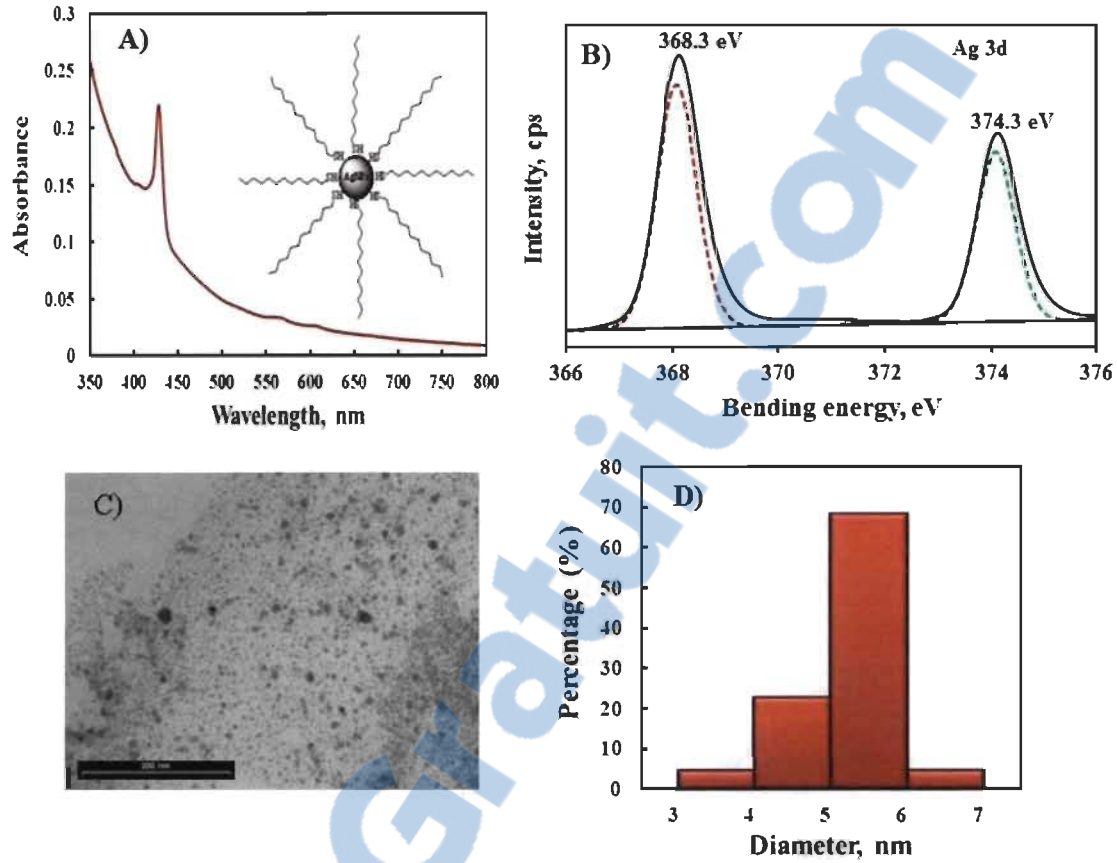

Figure 1. (A)Absorption spectrum of silver nanoparticles (AgNPs) in toluene (1.47 nM), (B) Ag 3d narrow scan XPS spectrum for AgNPs, (C) Transmission electron microscopic (TEM) image of AgNPs, and (D) size distribution of AgNPs; the mean particle size is 5.3 nm with standard deviation of 0.76 nm.

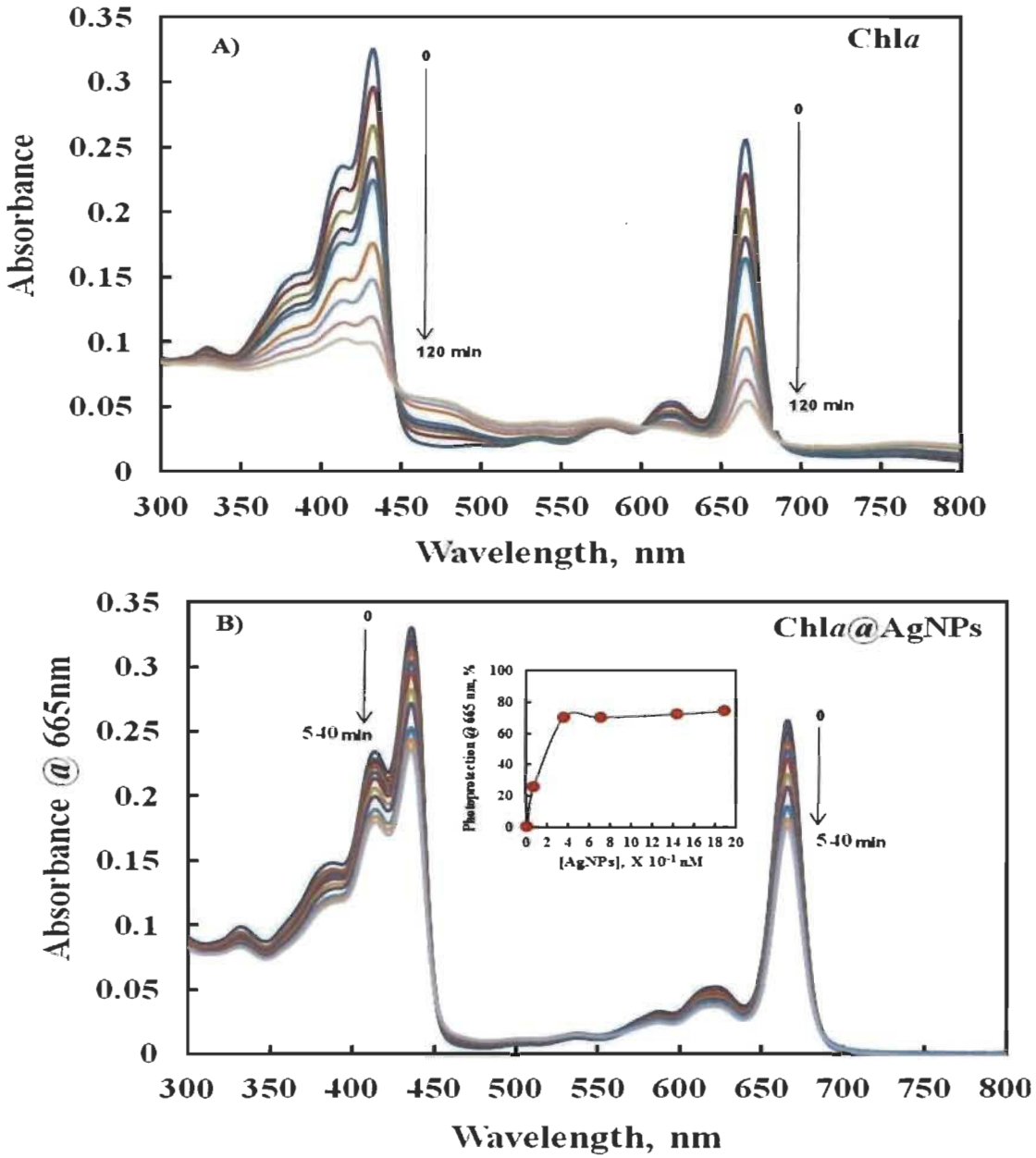

Figure 2. Changes in the Chl*a* (4.5 μM) absorption spectra following its exposure to red light irradiation (λ > 640 nm) in toluene at room temperature: (A) in absence and (B) in presence of AgNPs (0.36 nM). The exposure time periods were: 0, 5, 10, 15, 20, 40, 60, 90, 120 min for Chl*a* alone and 0, 5, 10, 15, 20, 40, 60, 90, 120, 190, 250, 360, 420, and 540 min for Chl*a* + AgNPs. The inset shows the effect of AgNPs concentration on the photoprotection of Chl*a* at 665 nm; red-light irradiation period is 540 minutes. The % photoprotection of Chl*a* was calculated from the variation of absorbance at 665 nm, using eq. 1.

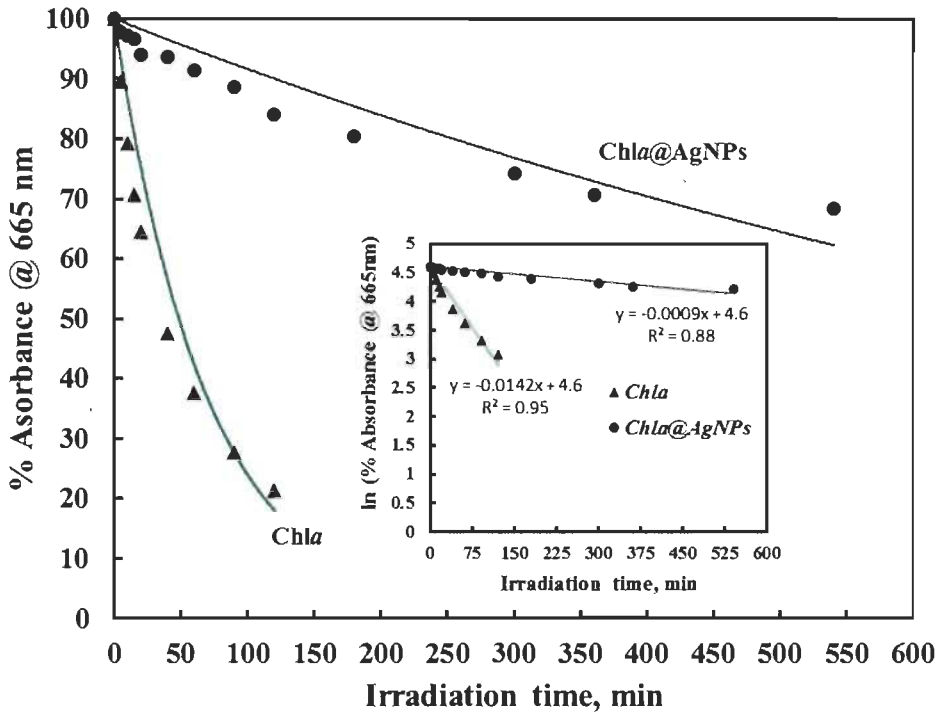

Figure 3. Photodegradation of Chl*a* in the absence and presence of AgNPs (0.36 nM) as a function of time under red-light irradiation ($\lambda > 640$ nm). The inset shows the first order photodegradation kinetics of Chl*a* in absence and presence of AgNPs (0.36 nM) (see eq. 4 in SI).

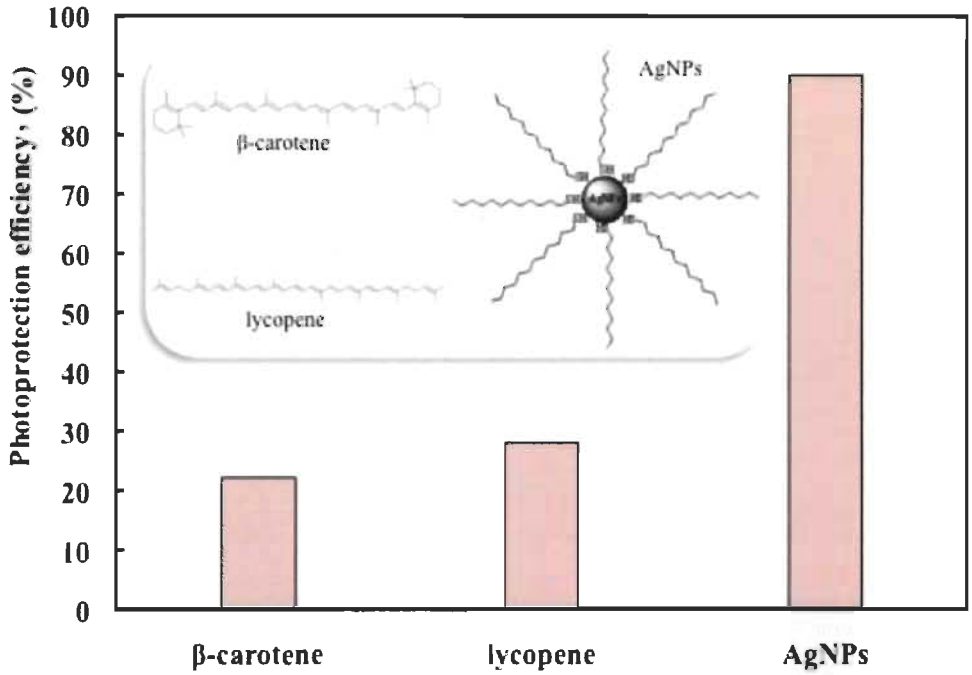

Figure 4. Comparison of the photoprotection efficiency provided to Chl*a* (4.5 μM) by various photoprotective agents in toluene: β-Carotene (22 μM), lycopene (22 μM) and AgNPs (0.36 nM). The molecular structures of the corresponding photoprotective agents are also shown.

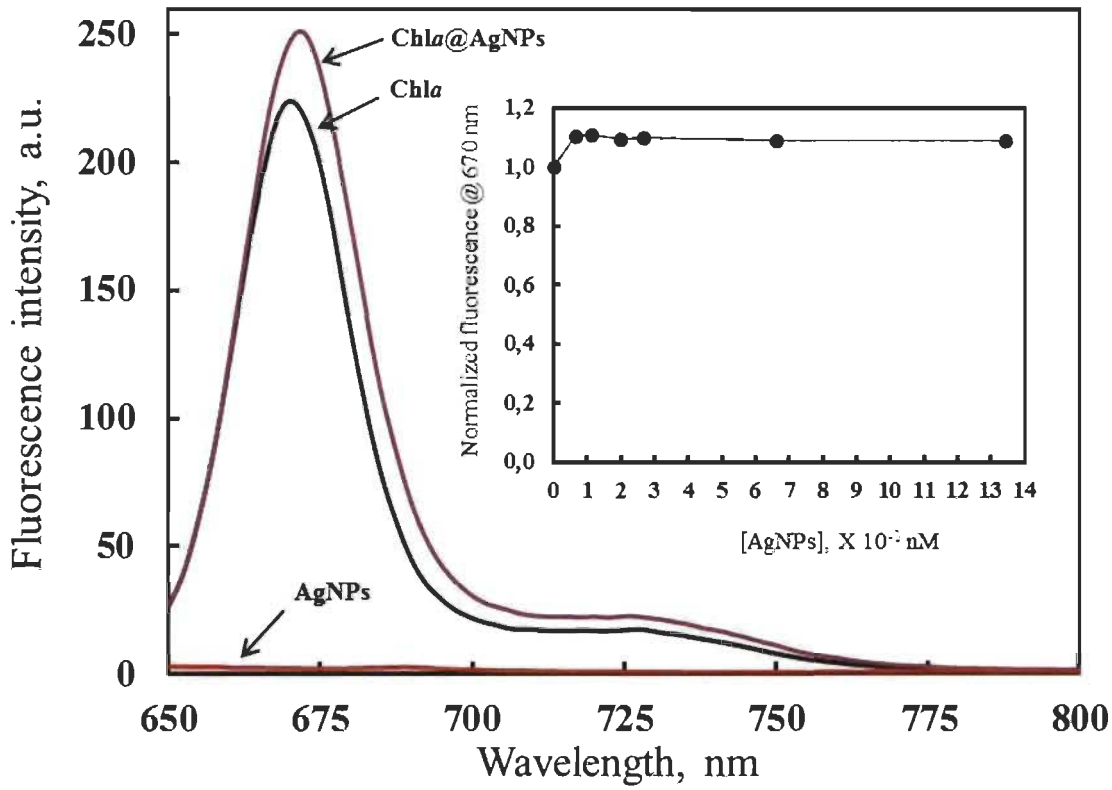

Figure 5. Fluorescence spectra of Chl*a* (4.5 μM) in the absence and presence of AgNPs (0.36 nM). The fluorescence spectrumof AgNPs is also shown. The excitation was at 625 nm. The inset shows the effect of AgNPs concentration on the metal enhanced fluorescence (MEF) of Chl*a*. MEF was measured as the ratio of fluorescence of Chl*a* in presence and absence of AgNPs. The fluorescence spectra given here are an average of the five replicate runs for Chl*a*, AgNPs, and their mixture.

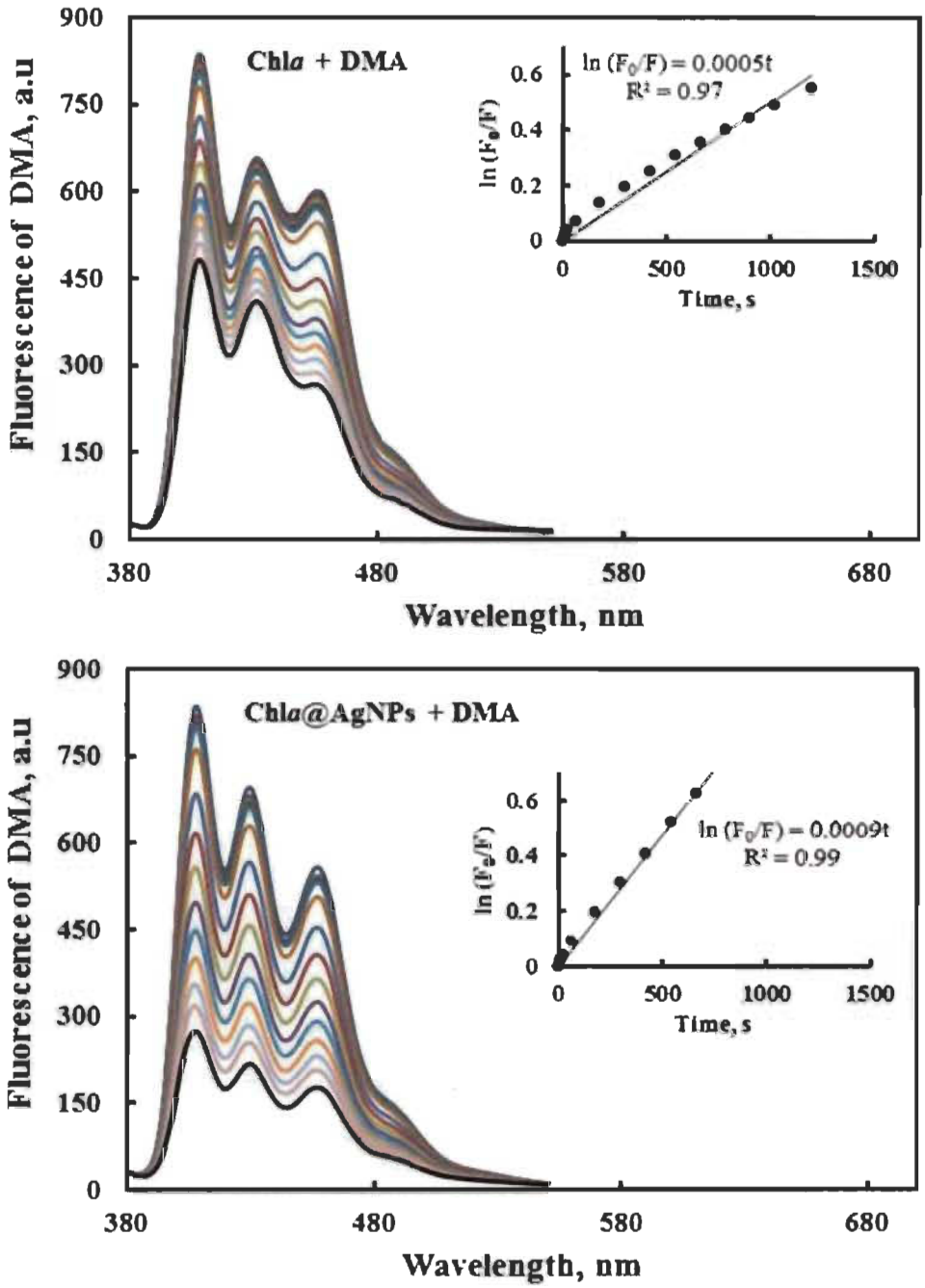

Figure 6. Fluorescence spectra of 9,10-dimethyl-anthracene (DMA): (A) in presence of Chl*a*, and (B) in presence of Chl*a* and AgNPs; λ_{exc} = 360 nm. The fluorescence spectra were recorded after red-light irradiation (λ > 640 nm) at room temperature for different time intervals: 0, 5, 10, 15, 20 s and 1, 3, 5, 7, 9, 11, 13, 15, 17 and 20 min. The insets show the plots of ln (F_0/F) as function of irradiation time; F_0 and F represent the fluorescence intensity of DMA before and after irradiation, respectively.

Table 1. First order kinetic data for irradiated Chl*a* and Chl*a*@AgNPs.

Photodegradation kinetic parameters	**Samples**	
	Chl*a*	Chl*a*@AgNPs
Rate constant (min^{-1})	1.4×10^{-2}	9×10^{-4}
Half-life time, $t_{1/2}$ (min)	49	770
Correlation coefficient (R^2)	0.94	0.87

SUPPORTING INFORMATION

Nanosilver Could Usher in Next-Generation Photoprotective Agents for Magnesium Porphyrins

Laurent Bekalé*, Saïd Barazzouk* and Surat Hotchandani*

Département de chimie, biochimie et physique, Université du Québec à Trois-Rivières, C. P. 500, Trois-Rivières (Québec), G9A 5H7, Canada

* To whom correspondence should be addressed. e-mail: bekale@uqtr.ca; hotchand@uqtr.ca; Said.Barazzouk@uqtr.ca

(A) Calculation of nanoparticles concentration:

It should be mentioned that 3 mL solution of the mixture of Ch*a* + AgNPs was used for all experiments. The concentration of Ag atoms in the stock solution of nanoparticles was 9 mM. The highest photoprotection imparted to Chl*a* by AgNPs was achieved after the addition of 7.33 μL of stock solution of AgNPs to 3 mL Chl*a* (4.5 μM) solution.

1) The total number of Ag atoms in 7.33 μL (9 mM) is given by:

$N_{Ag} = (9 \times 10^{-3}\ mol/L) \times (7.33 \times 10^{-6}\ L) \times (6.02 \times 10^{23}\ mol^{-1}) = 3.97 \times 10^{16}$

Since, 7.33 μL of 9 mM AgNPs are added to 3 mL solution of Chl*a*, the total number of Ag atoms present in 3 mL solution of the mixture (Ch*a* + AgNPs) will also be 3.97×10^{16}.

2) The number of Ag atoms, n_{atom}, in a single Ag nanoparticle (5.3 nm) is given by:

$n_{atom} = V_{NP}/V_{atom} = (R_{AgNP}/R_{atom})^3 = (2.65\ nm/0.145\ nm)^3 = 6104$ Ag atoms per AgNP,

Where V_{NP} and V_{aton} are, respectively, the volume of AgNP and Ag atom; R represents their corresponding radius.

3) The total number of AgNPs (N_{AgNPs}) in 3mL solution of mixture is, therefore, equal to:

$N_{AgNPs} = N_{Ag}/n_{atom} = (3.97 \times 10^{16})/(6104) = 6.50 \times 10^{12}$

4) The total number of mole of AgNPs in 3mL solution of mixture is given by:

Number of mole (AgNPs) $= N_{AgNPs}/ N_A = (6.50 \times 10^{12})/(6.02 \times 10^{23}) = 1.08 \times 10^{-12}$ mol

5) Concentration of AgNPs is, therefore, equal to

Concentration of AgNPs (mol/L) = (Number of mole (AgNPs))/(Volume of solution)

$= (1.08 \times 10^{-12}$ mol)/ $(3 \times 10^{-3}$L) $= 3.6 \times 10^{-10}$ mol/L = **0.36 nM**

(B) Calculation of the number of Chlorophylls on a silver nanoparticle

According to our experimental results, the concentration of AgNPs greater than 0.36 nM did not provide any additional protection. We can, therefore, safely assume that in 3 mL solution of the mixture of Ch*a* (4.5μM) and AgNPs (0.36 nM), all Chl*a* molecules are bound to the AgNPs surface. The ratio of Chl*a* to AgNP can be obtained as follows:

1) Since, AgNPs are spherical with an average diameter of 5.3 nm, the surface area of one AgNP, $\mathbf{A}_{(AgNP)}$, is:

$\mathbf{A}_{(AgNP)} = 4\pi \times R^2 = 4\pi \times (5.3/2)^2 = 88.25\ nm^2$, R is the radius of spherical AgNPs.

2) The total surface area (A_T) provided by 0.36 nM of AgNPs, therefore, is given by:

$A_{T(AgNP)}$ = Total number of AgNPs (N_{AgNPs}) in 3mL solution of mixture multiplied by the individual area of AgNP, $A_{(AgNP)}$.

Thus, $A_{T(AgNP)} = 6.50 \times 10^{12} \times 88.25\ nm^2 = 5.74 \times 10^{14}\ nm^2$

The calculations regarding total number of AgNPs ($N_{AgNPs} = 6.50 \times 10^{12}$) in 3mL solution of mixture has been described above in section (A).

It should be mentioned that the experimental results have revealed that Chl*a* binds with AgNP via its nitrogen atoms of porphyrin head while the phytol tail is not involved in the process of complex formation between AgNP and Chl*a*, i.e., Chl*a*@AgNP. It is thus reasonable to assume that only porphyrin head of chlorophyll covers the surface of AgNPs in the Chl*a*@AgNP complex. According to the literature, the chlorophyll molecule is depicted as follows.[1]

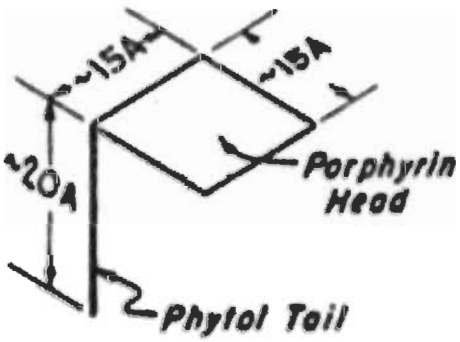

CHLOROPHYLL MOLECULE

3) The surface area of one porphyrin head of Ch*a*, $A_{(chl)}$, is, therefore, equal to:

$A_{(chl)} = (1.5\ nm)^2 = 2.25\ nm^2$

4) The total number of Chl*a* molecules (N_{Chla}) in 3mL solution of mixture (Ch*a* (4.5μM) + AgNPs (0.36 nM)) is given by:

$N_{Chla} = (3 \times 10^{-3}\ L) \times (6.02 \times 10^{23}\ mol^{-1}) \times (4.5 \times 10^{-6}\ mol/L) = 8.13 \times 10^{15}$

5) The total surface area of porphyrin heads of all Ch*a* molecules available is given by:

$\mathbf{A_{T(chl)}} = (N_{Chla}) \times (\mathbf{A_{(chl)}}) = 8.13 \times 10^{15} \times 2.25\ nm^2 = 1.83 \times 10^{16}\ nm^2$

6) The number of Chl*a* molecules per AgNP in 3mL solution of mixture (Ch*a* (4.5µM) + AgNPs (0.36 nM)) can then be obtained simply by dividing the total area $\mathbf{A_{T(chl)}}$ of chlorophyll molecules by the total surface area furnished by 0.36 nM of AgNPs, i.e., $A_{T(AgNP)}$.

Therefore, the number of Chl*a* molecules per Ag nanoparticle is equal to $(1.83 \times 10^{16}\ nm^2)/(5.74 \times 10^{14}\ nm^2) = \mathbf{32}$

In other words, the ratio of Chl*a* to AgNP is 32 : 1

Kinetics of photochemical reaction:

The photodegradation of Chl*a* in presence of O_2 can be described by the following equation:

$$Chla + O_2 \xrightarrow{h\nu} Chla\ [O_2] \qquad (1)$$

The photodegradation rate of Chl*a* was monitored by recording the absorbance at 665 nm as a function of irradiation time, and is:

$$-\frac{d[Chla]}{dt} = k[Chla]*[O_2] \qquad (2)$$

where [Chl*a*] denotes the concentration of Chl*a*, $[O_2]$ is the concentration of O_2, t is the reaction time, and k is the rate constant. Since $[O_2]$ remains constant as the reaction proceeds, the reaction can be considered pseudo-first-order because it depends on the concentration of Chl*a* only.

Thus, eq. (2) can be written as follows:

$$-\frac{d[Chla]}{dt} = k'[Chla] \tag{3}$$

where $k' = k[O_2]$

Solving eq. (3), one obtains eq. (4):

$$\ln([Chla]_t) = -k't + \ln([Chla]_0) \tag{4}$$

where [Chl*a*]$_0$ is the initial concentration of Chl*a* and [Chl*a*]$_t$ is the concentration of Chl*a* at any time *t*. Plotting ln ([Chl*a*]$_t$)/ ln ([Chl*a*]$_0$) *vs t* **(Fig. 3)**, the values of *k'* (from slope of the plot) and $t_{1/2}$ (= ln *k'*/2) are obtained.

Scheme 1: Reaction scheme of the photosensitized oxidation of 9,10-dimethyl-anthracene (DMA) by Chl*a*. This reaction can be described by the following simplified scheme:

(1) Chl*a* excited singlet state (^{1}Chl*a**) is formed upon photoexcitation of chlorophyll-*a* (Chl*a*)

$$Chla + hv \rightarrow {}^1Chla^* \tag{5}$$

(2) ^{3}Chl*a**, i.e., Chl*a* triplet state is formed by intersystem crossing (*ISC*) process

$${}^1Chla^* \xrightarrow{ISC} {}^3Chla^* \tag{6}$$

(3) ^{3}Chl*a**transfers it excitation energy to the ground state molecular oxygen ($^3O_2$) to produce singlet oxygen (^{1}O$_2$)

$${}^3Chla^* + {}^3O_2 \rightarrow Chla + {}^1O_2 \tag{7}$$

(4) Photooxidation of DMA by ^{1}O$_2$

$${}^1O_2 + DMA\,(flourescent) \rightarrow DMA\ endoperoxide\ (non\ fluorescent) \tag{8}$$

Figure S1. Image showing the photoprotection provided to Chl*a* (4.5 μM) by AgNPs (0.36 nM) under 540 min red-light irradiation ($\lambda > 640$ nm). As expected, a quick bleaching occurs after exposure of Chl*a* solution to light. No apparent change in color of Chl*a* solution is observed when AgNPs were added to it.

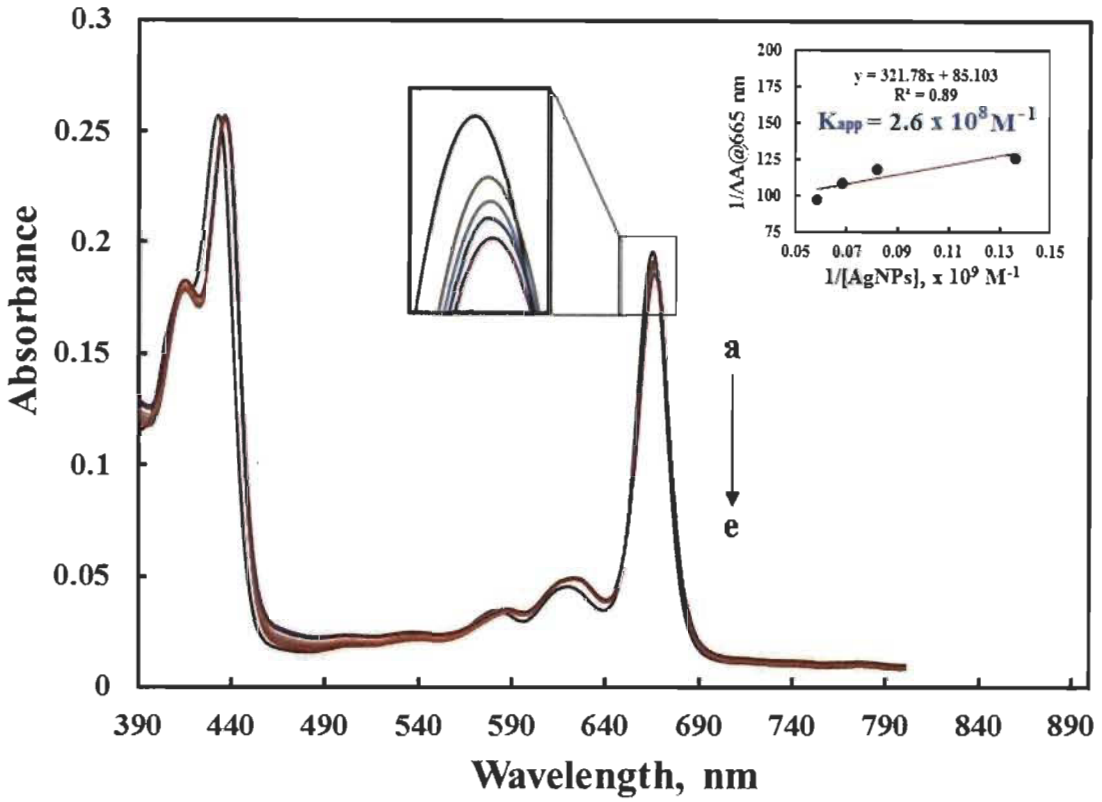

Figure S2. Effect of AgNPs on the absorption spectra of Chl*a* solution (4.5 μM) in toluene: (a) 0, (b) 0.26, (c) 0.73, (d) 1.22 and (e) 1.72 nM. The insert shows the plot of 1/ΔA(665 nm) vs 1/[AgNPs]. An apparent association constant (K_{app}) of 2.6×10^8 M^{-1} was obtained from the intercept-to-slope ratio of the plot.

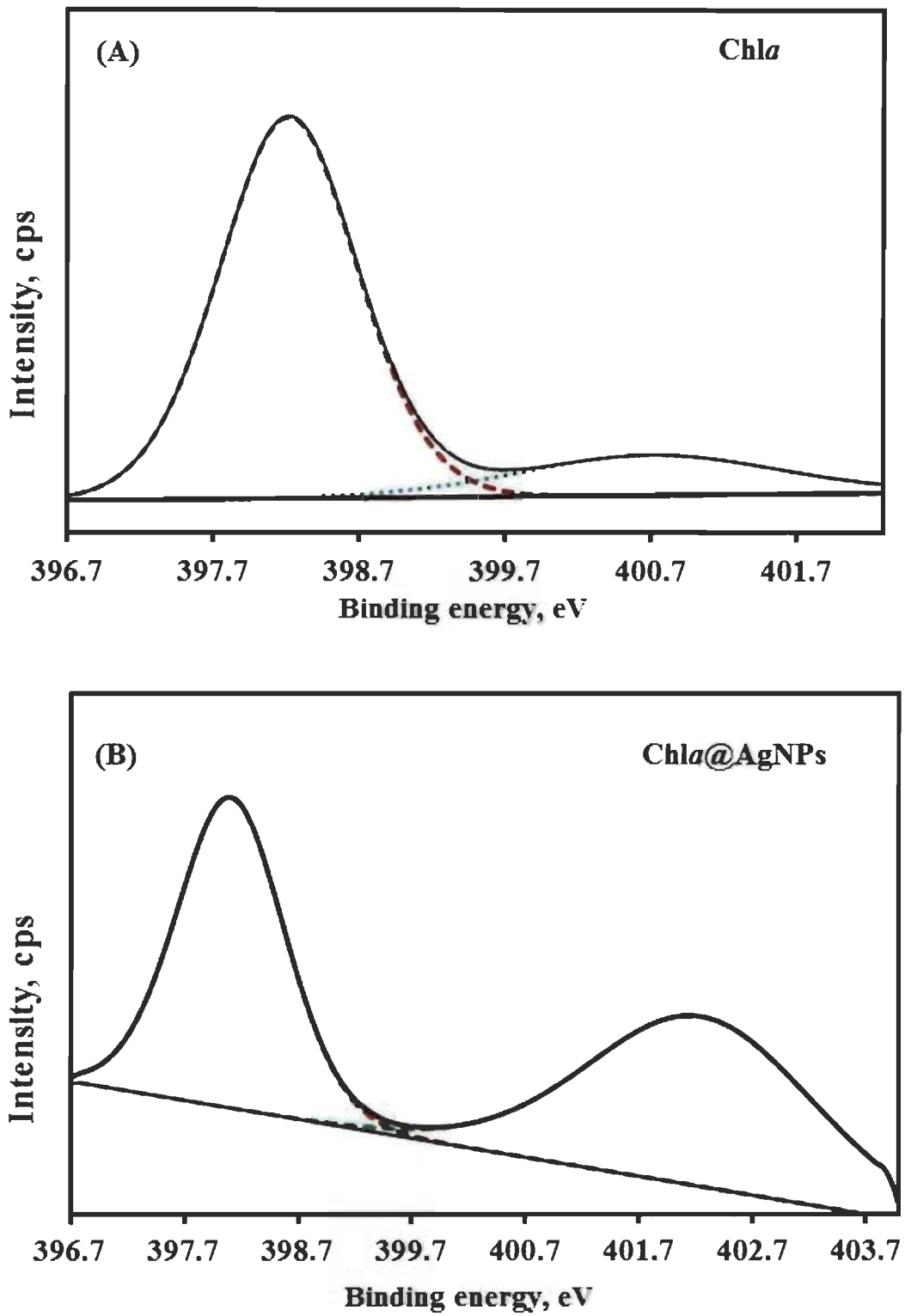

Figure S3. N1s narrow scan XPS spectra for: (A) Chl*a* and (B) Chl*a*@AgNPs. The comparison between these spectra supports that nitrogen atoms interact with AgNPs.

The high-resolution scans of the XPS spectra of O 1s levels of Chl*a* and Chl*a*@AgNPs with their decomposition into three components are shown in Figure S-4. The peak appearing at ~530.5 eV has been attributed to the molecular adsorbed oxygen, O_2. The most intense peak at 532.5 eV has been assigned to the carbonyl oxygen from ketone (>C=**O**) and ester groups (–O–C=**O**) of Chl*a*. Finally, the peak at 533.4 eV is attributed to the ether-type oxygen in the ester group (–**O**–C=O) of Chl*a*.

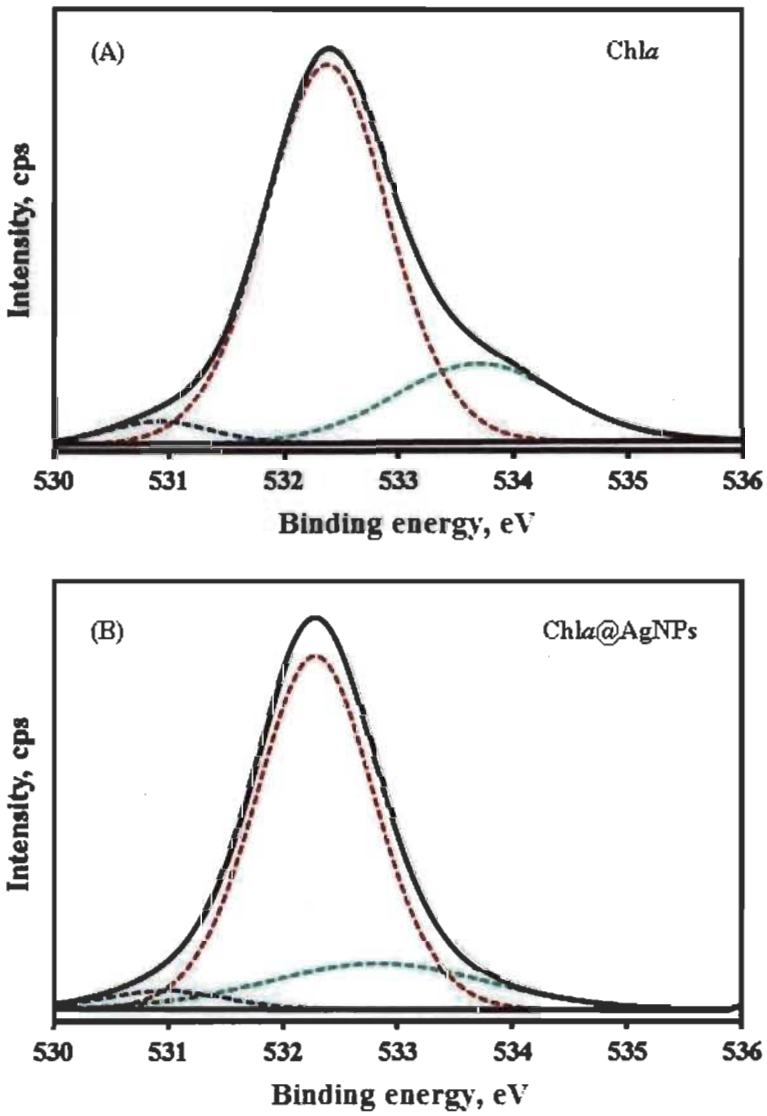

Figure S4. O1s narrow scan XPS spectra for (A) Chl*a* and (B) Chl*a*@AgNPs.

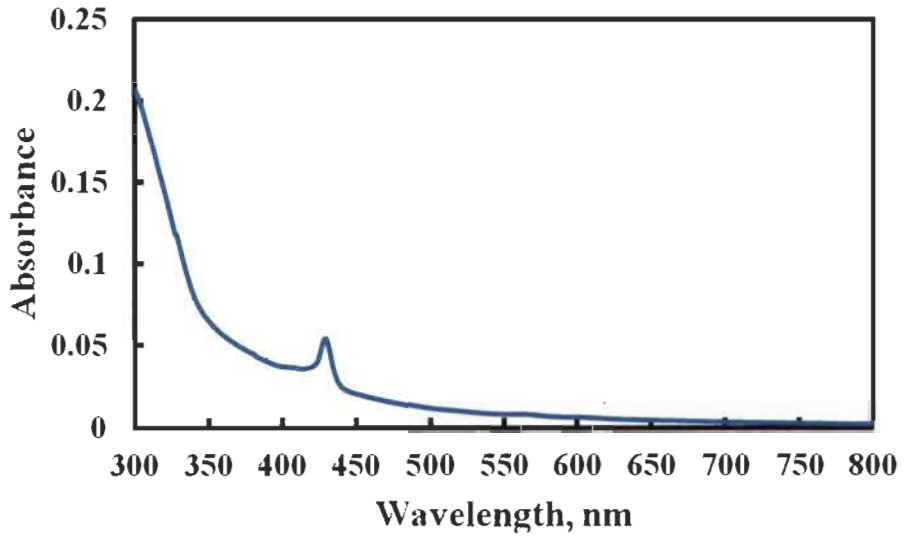

Figure S5. Absorption spectrum of AgNPs (0.36 nM) in toluene.

Références

[1] J. J. Wolken, F. A. Schwartz, *J. Gen Physiol.* **1953**, 37, 111.

CHAPITRE V

CONCLUSION ET PERSPECTIVES

5.1 Conclusion générale

Le but premier de cette thèse de doctorat était de développer une stratégie de photoprotection, reposant sur l'utilisation des nanoparticules de métaux nobles afin d'améliorer la stabilité des porphyrines de magnésium. De plus, nous voulions trouver une façon d'augmenter non seulement la photostabilité, mais aussi les autres propriétés photophysiques et photochimiques de ces porphyrines, à savoir : l'émission de fluorescence et la capacité de production d'oxygène singulet. Tous ces efforts visent la réduction de la photodégradation des porphyrines extraites du milieu naturel, pour la plupart des porphyrines de magnésium, connues pour être très instables si elles sont retirées des structures cellulaires hautement organisées qui les protègent naturellement contre la dégradation par la lumière visible. Le potentiel des porphyrines naturelles dépasse largement le cadre des processus physiologiques fondamentaux dans les cellules vivantes et adresse une panoplie d'enjeux scientifiques et technologiques majeurs en lien avec la biomédicale, l'optoélectronique, le photovoltaïque, la photocatalyse et l'élaboration de photopesticides. C'est pourquoi le développement d'une stratégie efficace de photoprotection, dans un contexte de recherche, constitue actuellement un enjeu de taille pour plusieurs secteurs d'activités.

Je conclus donc cette recherche en abordant successivement la synthèse des résultats obtenus, la contribution à l'avancement des connaissances et les pistes possibles d'investigation, nécessaires afin d'approfondir la compréhension de cette nouvelle méthode de photoprotection.

5.2 Bilan des résultats

La présente thèse établit la possibilité d'améliorer la photostabilité des porphyrines de magnésium par l'inhibition des sites azotés du macrocycle porphyrique. Cette approche se base sur le résultat d'analyse de différents mécanismes réactionnels détaillée, postulée dans la littérature pour expliquer la photodégradation des porphyrines de magnésium. En effet, cette analyse a permis de relever que le doublet libre des atomes d'azote, ne participant pas à l'aromaticité du macrocycle porphyrique, est sollicité lors de la réaction de photodégradation des porphyrines de magnésium. Ce bilan a été particulièrement important comme point de départ, en ce sens qu'il présuppose que, si les sites azotés (le doublet libre des atomes d'azote) du macrocycle porphyrique sont bloqués, avant l'illumination, alors il se produira une augmentation de la photostabilité.

Au chapitre II, ce mécanisme de photoprotection fut démontré expérimentalement par l'utilisation du tétraphénylporphyrine de magnésium (MgTPP) comme porphyrine modèle, et les nanoparticules d'or (AuNPs) comme agent de blocage des sites azotés du macrocycle porphyrique. Il a été observé que l'ajout dans l'obscurité, d'une faible quantité de AuNPs, dans une solution de MgTPP augmentait considérablement la photostabilité du MgTPP. En effet, avec une concentration appropriée de AuNPs, une efficacité de photoprotection quasiment de 100 % a pu être obtenue. L'analyse des interactions entre AuNPs et MgTPP a permis de relever qu'il se forme un complexe AuNPs@MgTPP après l'addition des nanoparticules. La constance de formation de ce complexe de l'ordre de 10^4 M^{-1} indique que le complex AuNPs@MgTPP est très stable. De plus, la démonstration établit que le complexe AuNPs@MgTPP est stabilisé par des liaisons organométalliques directes entre les atomes d'azote (-N) et l'or métallique (Au). De ce fait, la capacité photoprotectrice des AuNPs réside dans leur faculté à se lier aux sites d'azote du macrocycle, inhibant ainsi la formation de liaisons entre les espèces réactives de l'oxygène (ROS) à ces sites d'azote, connues pour causer la photodégradation de MgTPP et plusieurs autres porphyrines dans des conditions aérobies. En outre, la diminution de la formation d'états singulets excités du MgTPP, à la suite de sa liaison avec les AuNPs, supprime également la production de ROS,

améliorant considérablement la photostabilité du MgTPP. Ce résultat démontre clairement l'efficacité de notre approche et met en lumière la possibilité de développer de nouveaux types d'agents photoprotecteurs, qui ont comme principale propriété de bloquer le doublet libre d'atomes d'azote du macrocycle porphyrique, afin d'induire une augmentation de la photostabilité.

Effectivement, il est impossible de prédire, avec ce type d'agent photoprotecteur, s'il permettrait également d'accroître la stabilité des porphyrines de magnésium, possédant à la fois des doublets d'électrons libres sur les atomes d'azote du macrocycle et sur les groupes fonctionnels périphériques, n'étant pas conjugués au macrocycle.

Toutefois, au chapitre III, nos résultats sur l'emploi de nanoparticules d'or en tant qu'agent photoprotecteur pour améliorer la stabilité des chlorophylles-*a* (Chl*a*) ont démontré que la photodégradation de la Chl*a* est ralentie en présence de AuNPs. L'estimation du temps de demi-vie de la Chl*a* (c'est-à-dire le temps nécessaire pour que la quantité d'une substance soit diminuée de moitié de sa valeur initiale) a révélé une augmentation pouvant atteindre un ordre de grandeur en présence de AuNPs. Nous en déduisons que le rôle photoprotecteur des AuNPs est bien présent, c'est-à-dire que les nanoparticules se lient aux atomes d'azote de la Chl*a* dans l'obscurité, et ce, malgré la présence de groupes fonctionnels ester (-COO-R) et cétone (>C=O) porteurs de doublets libres sur l'oxygène.

Par ailleurs, il est important de mentionner que dans les conditions *in vitro*, les AuNPs sont de bien meilleurs photoprotecteurs que les molécules, comme la β-carotène ou les quinones, reconnues pour être très efficaces afin de protéger les chlorophylles dans des conditions *in vivo*, c'est-à-dire dans les plantes.

Étant donné la nécessité de trouver un procédé multifonctionnel très efficace pour l'amélioration simultanée de différentes propriétés photoniques des porphyrines naturelles, la méthode de photoprotection développée dans cette thèse se devrait d'être

ajustée, afin d'augmenter conjointement la photostabilité, l'émission de fluorescence et la production d'oxygène singulet.

Au chapitre IV, une observation sans précédent démontre que les nanoparticules d'argent (AgNPs) sont des additifs potentiels pour augmenter simultanément la photostabilité, l'émission de fluorescence, ainsi que la capacité de production d'oxygène singulet de Chl*a* *in vitro*. L'estimation du temps de demi-vie de la Chl*a* a révélé une augmentation pouvant atteindre un ordre de grandeur en présence d'une concentration d'AgNPs extrêmement faible, c'est-à-dire avec des valeurs de concentration dans la plage nanomolaire. De ce fait, ils sont actuellement les meilleurs agents photoprotecteurs connus. En plus de leur performance photoprotectrice surprenante, les AgNPs ont également permis d'améliorer l'émission de fluorescence et la capacité de production d'oxygène singulet de la Chl*a* respectivement de 1,2 et 2 fois. La forte efficacité photoprotectrice des AgNPs par comparaison aux AuNPs peut-être dû au fait que lors du processus photoprotection, nous effectuons un échange de ligand entre un tétraakyl ammonium et une amine tertiaire dans le cas des nanoparticules d'or. Les liaisons chimiques qui sont brisées (de nature électrostatique) et d'autres qui se contiuent, sont sensiblement de même force. Par contre, dans le cas des nanoparticules d'argent, nous brisons une liaison Ag-thiol pour former une liaison Ag-amine. Cette réaction est très favorable puisque la laison Ag-amine et plus forte que la liaison Ag-thiol. Ainsi, la réaction d'échange de ligand dans le cas l'argent un plus rapide. Cet aspect peut expliquer en partie la forte réactivité des nanoparticules d'argent. Toutefois, il est possible que les nouvelles propriétés émergentes à l'échelle du nanomètre soient aussi impliquées dans la différence de comportement entre les nanoparticules d'or et d'argent.

Enfin, ces résultats obtenus avec les AgNPs sont exceptionnellement intéressants et importants, car ils ont fait la preuve de l'amélioration simultanée de différentes propriétés photoniques des porphyrines. Ils constituent donc une solide raison de développer de nouveaux agents photoprotecteurs. Ainsi, le présent travail ouvrirait la voie au développement d'une nouvelle génération d'agents photoprotecteurs multifonctionnels, mieux adaptés à des applications des porphyrines naturelles dans le

théranostique (l'association d'une thérapeutique et d'un test diagnostique), l'imagerie et la thérapie photodynamique.

5.3 Contribution de la thèse à l'avancement des connaissances

Eu égard à tout ce qui précède, cette thèse de doctorat contribue, de façon originale, à l'amélioration des connaissances relatives à la photoprotection des porphyrines naturelles, et ce, en exploitant principalement les propriétés des nanoparticules de métaux nobles. Effectivement, la mise au point d'une méthode de photoprotection, reposant sur l'utilisation des nanoparticules de métaux nobles pour accroître la stabilité des porphyrines de magnésium, constitue une première dans le domaine de la protection des porphyrines contre la dégradation par la lumière. Les méthodes de photoprotection développées antérieurement s'intéressent davantage à augmenter la photostabilité, en supprimant tout simplement la production des espèces réactives de l'oxygène, plutôt que d'augmenter simultanément la photostabilité, l'émission de fluorescence et la capacité de production d'oxygène singulet. La découverte de cette nouvelle stratégie de photoprotection met en lumière la possible mise au point des photoprotecteurs multifonctionnels, pouvant non seulement pallier le problème de stabilité, mais aussi renforcer les autres propriétés intéressantes de porphyrines naturelles.

5.4 Perspectives

Dans le prolongement des résultats obtenus au cours de ce travail de thèse, il sera intéressant d'approfondir ces études, afin de mieux comprendre, optimiser et étendre cette méthode de photoprotection. Pour ce faire, la recherche, sur la photoprotection des porphyrines par des nanoparticules, gagnerait en s'orientant vers deux directions distinctes.

5.4.1 Analyser systématiquement l'effet de la taille et de la forme des nanoparticules sur l'efficacité photoprotectrice

Nous avons démontré dans cette thèse que les nanoparticules d'or (AuNPs) et d'argent (AgNPs) sont de bons photoprotecteurs, et peuvent ainsi être ulitisés pour améliorer la photostabilité des porphyrines par l'inhibition des sites azotés du macrocycle porphyrique. Cette découverte constitue une toute nouvelle possibilité afin de lutter contre la dégradation rapide des photosensibilisateurs à base de porphyrines naturelles. Ainsi, elle paverait la voie au développement d'une nouvelle classe d'agents photoprotecteurs à base de nanoparticules (NPs).

Il est bien établi que la taille et la forme des NPs ont une très grande influence sur les propriétés finales (activité catalytique, réactivité chimique, adhésion, etc.)[1,2]. Cette caractéristique est un effet du changement de la fraction d'atomes de surface des NPs. Lorsque la taille de la particule devient plus petite, son rapport surface/volume augmente considérablement. En outre, pour une nanoparticule de même taille, l'étendue de la surface dépend de la forme du matériau. Un exemple simple est de comparer une sphère et un cube ayant le même volume. Le cube a une surface totale plus grande que la sphère. Pour cette raison, dans la nanoscience, non seulement la taille d'un nanomatériau est importante, mais également sa forme. L'exemple parfait, pour illustrer l'influence du changement de rapport surface/volume à l'échelle nanométrique, est d'observer l'effet de la taille et de la forme des NPs sur les propriétés optiques[3,4]. Comme le témoigne la figure 5.1, selon la taille des AuNPs en suspension, la couleur de la solution varie du rouge vif (pour des particules de moins de 100 nm), au bleu-violet (pour les particules les plus grosses).

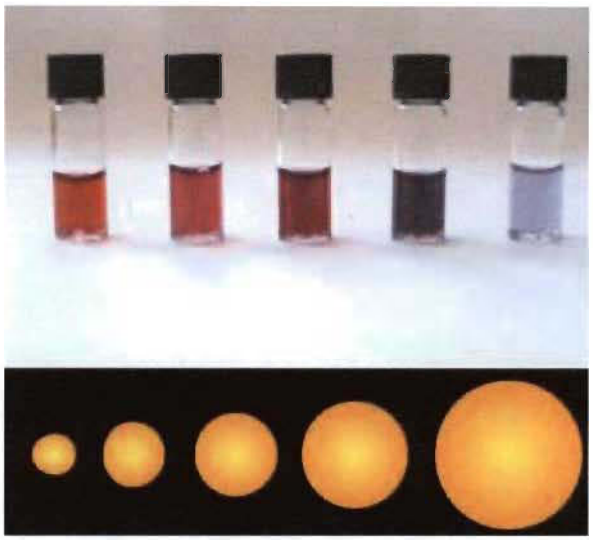

Figure 5.1 Solutions de nanoparticules d'or de différentes tailles. La différence de taille provoque la différence de couleur[3].

De même, Mock *et al.*[4], en élaborant par voie colloïdale des particules d'argent aux formes variées (sphérique, pentagonale, triangulaire), ont démontré que leur réponse optique était fortement corrélée à la forme des nanoparticules (Figure 5.2).

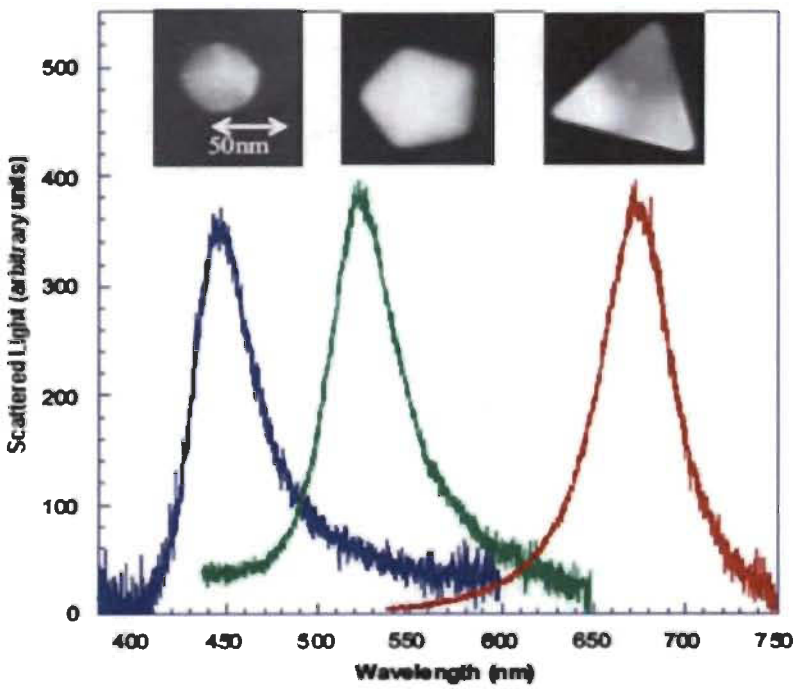

Figure 5.2 Spectres de diffusion de la lumière par des nanoparticules d'argent de différentes formes[4].

En vue de l'obtention d'une réactivité optimale des nanoparticules (d'or et d'argent) afin d'améliorer leur efficacité photoprotectrice, il serait souhaitable d'examiner les effets de la taille et de la forme sur le pouvoir photoprotecteur des nanoparticules. Une étude de cette nature revêt une importance particulière, déterminant ainsi la dimention et la morphologie idéales des nanoparticules photoprotectrices.

5.4.2 Examiner si la méthode de photoprotection mise en œuvre dans cette thèse peut être employée pour l'élaboration des nanoparticules fonctionnelles pour des applications médicales

Les résultats présentés aux chapitres II, III et IV sont encourageants et incitent à de nouvelles perspectives de recherche intéressantes. Cette stratégie de photoprotection permettrait le développement des agents photoprotecteurs magnétiques pouvant être utilisés en nanomédecine, particulièrement dans la thérapie photodynamique des cancers. Nous prévoyons que ces nanoparticules joueront un triple rôle dans le traitement photodynamique (PDT) :

(i) ils agiront comme photoprotecteurs pour accroître la photostabilité des photosensibilisateurs à base de porphyrines naturelles, afin de générer des $^1O_2$ pendant de plus longues périodes de temps,

(ii) ils opéreront en tant qu'amplificateurs additionnels de la production des $^1O_2$ *via* des interactions métal-photosensibilisatrices,

(iii) ils se comporteront comme agents de contraste en imagerie par résonance magnétique (IRM), visualisant clairement les tissus tumoraux, offrant par surcroît la possibilité de diriger les nanoparticules fonctionnalisées par les photosensibilisateurs vers des cellules tumorales, plutôt que vers les cellules saines.

Cette idée propose d'utiliser les nanoparticules d'oxyde de fer superparamagnétique (Fe_3O_4) recouvertes d'une couche d'or, soit une structure

cœur-coquille Fe_3O_4@Au (Figure 5.3). Le revêtement d'or aide à réduire l'agglomération des particules, améliorant ainsi la biocompatibilité[5,6].

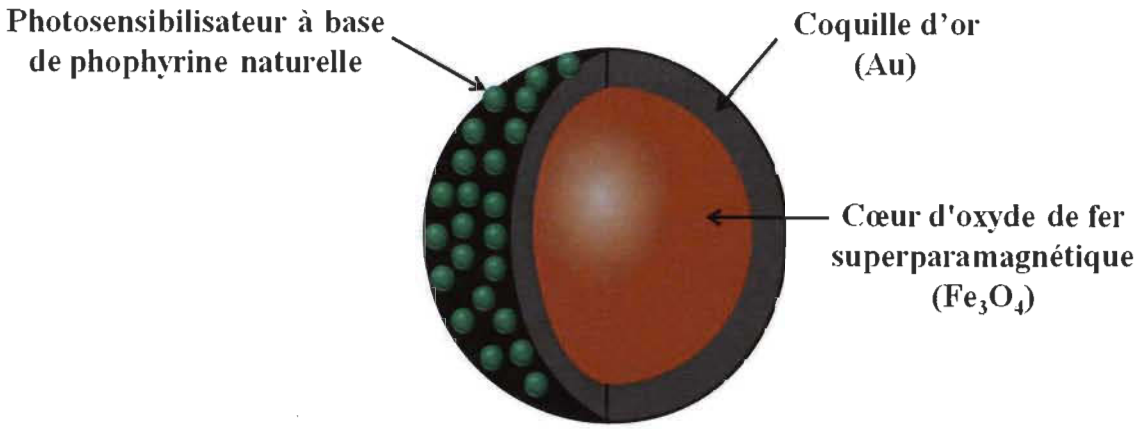

Figure 5.3 Représentation schématique de l'agent photoprotecteur magnétique de structure cœur-coquille Fe_3O_4@Au.

Récemment, les nanoparticules d'oxyde de fer superparamagnétique (Fe_3O_4) ont suscité beaucoup d'intérêt, en raison de leur application potentielle dans le domaine biomédical[7]. Effectivement, les nanoparticules (Fe_3O_4 NPs) sont utilisées en clinique humaine, comme agents de contraste d'IRM[8].

Actuellement, lors du traitement photodynamique, les photosensibilisateurs (PSs) se distribuent dans l'organisme de manière plus ou moins ciblée, c'est-à-dire que le PS ne sera pas forcément délivré sur les cellules concernées. On doit donc administrer d'importantes doses de PS, contraignant ainsi une petite proportion d'atteindre finalement sa cible. L'incorporation d'une propriété magnétique dans des nanoparticules photoprotectrices vise à contourner cet obstacle, rendant le traitement plus spécifique et plus efficace. Ainsi, les nanoparticules photoprotectrices, magnétiques, faciliteraient la livraison des PSs, du site d'injection vers les régions tumorales ciblées, se servant d'un champ magnétique externe (Figure 5.4)[9].

Enfin, la combinaison de l'IRM et de la PDT, sur un même agent thérapeutique, présente l'avantage de visualiser clairement les tissus tumoraux et de fournir des

informations importantes relatives à la réponse thérapeutique au traitement photodynamique, et, de ce fait, guider précisément l'irradiation de lumière aux tissus tumoraux, atteignant ainsi une efficacité maximale du traitement thérapeutique[10-12].

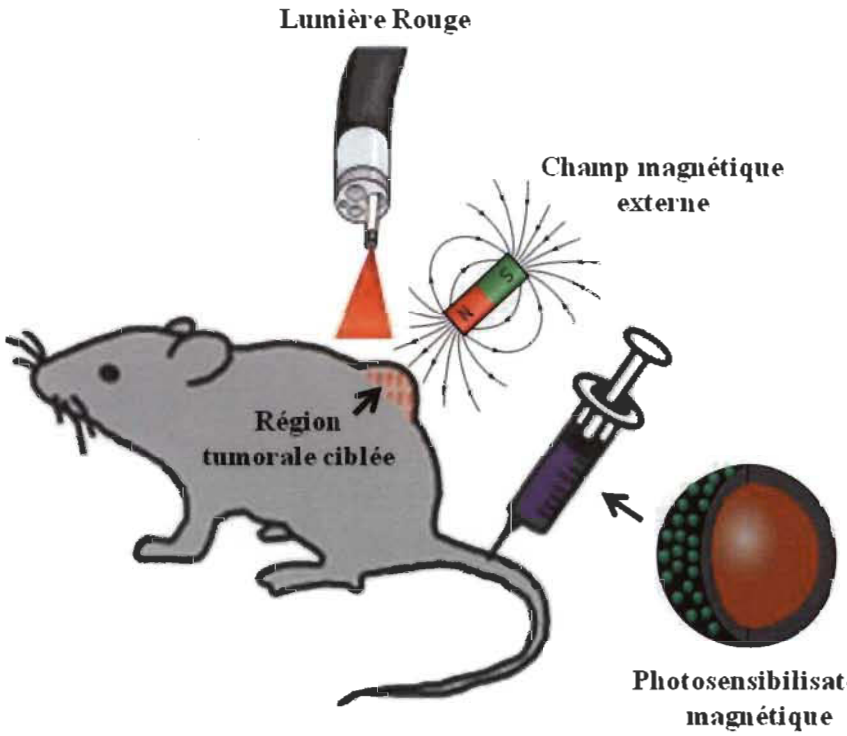

Figure 5.4 Schéma illustrant le ciblage *in vivo* de la tumeur par champ magnétique externe.

5.5 Références

(1) El-Sayed, M. A.; Some interesting properties of metals confined in time and nanometer space of different shapes. *Acc. Chem. Res.*, **2001**, 34, 257-264.

(2) Xu, R.; Wang, D.; Zhang, J.; Li, Y. Shape-dependent catalytic activity of silver nanoparticles for the oxidation of styrene. *Chem. Asian J.*, **2006**, 1, 888-893.

(3) http://en.wikipedia.org/wiki/Colloidal_gold

(4) Mock, J. J.; Barbic, M.; Smith, D. R.; Schultz, D. A.; Schultz, S. Shape effects in plasmon resonance of individual colloidal silver nanoparticles. *J. Chem. Phys.*, **2002**, 116, 6755-6759.

(5) Lyon, J. L.; Fleming, D. A.; Stone, M. B.; Schiffer, P.; Williams, M. E. Synthesis of Fe oxide core/Au shell nanoparticles by iterative hydroxylamine seeding. *Nano Lett.*, **2004**, 4, 719-723.

(6) Lo, C. K.; Xiao, D.; Choi, M. M. F. Homocysteine-protected gold-coated magnetic nanoparticles: synthesis and characterization. *J. Mater. Chem.*, **2007**, 17, 2418-2427.

(7) Hasany, S. F.; Abdurahman, N. H.; Sunarti, A. R.; Jose, R. Magnetic iron oxide nanoparticles: chemical synthesis and applications review. *Curr. Nanosci.*, **2013**, 9, 561-575.

(8) Corot, C.; Robert, P.; Idee, J. M.; Port, M. Recent advances in iron oxide nanocrystal technology for medical imaging. *Adv. Drug Deliv Rev.*, **2006**, 58, 1471-1504.

(9) Li, Z. W.; Wang, C.; Cheng, L.; Gong, H.; Yin, S. N.; Gong, Q. F.; Li, Y. G.; Liu, Z. PEG-functionalized iron oxide nanoclusters loaded with chlorin e6 for targeted, NIR light induced, photodynamic therapy. *Biomaterials.*, **2013**, 34, 9160-9170.

(10) Gross, S.; Gilead, A.; Scherz, A.; Neeman, M.; Salomon, Y. Monitoring photodynamic therapy of solid tumors online by BOLD-contrast MRI. *Nat. Med.*, **2003**, 9, 1327-1331.

(11) Vaidya, A.; Sun, Y.; Ke, T.; Jeong, E. K.; Lu, Z. R. Contrast enhanced MRI-guided photodynamic therapy for site-specific cancer treatment. *Magn. Reson. Med.*, **2006**, 56, 761-767.

(12) Vaidya, A.; Sun, Y. G.; Feng, Y.; Emerson, L.; Jeong, E. K.; Lu, Z. R. Contrast-enhanced MRI-guided photodynamic cancer therapy with a pegylated bifunctional polymer conjugate. *Pharm. Res.*, **2008**, 25, 2002-2011.

ANNEXE A

MÉTHODES EXPÉRIMENTALES, SYNTHÈSE ET INSTRUMENTATION

A.1 Synthèse générale des nanoparticules métalliques en solution

De façon très générale, on décrit les nanoparticules comme étant des amas d'atomes de diverses tailles, variant de 1 à 100 nm. En général, la synthèse en solution (aqueuse ou organique) des nanoparticules métalliques s'effectue principalement toujours de la même manière, soit par réduction des sels métalliques, dissous en solution avec un agent réducteur, sous agitation vigoureuse. Une fois réduits, les colloïdes métalliques à l'état d'oxydation zéro s'associent rapidement entre eux et forment alors des agglomérats de quelques atomes avant de former, par ajout successif d'atomes, des nanoparticules de plus en plus grandes (Figure A.1).

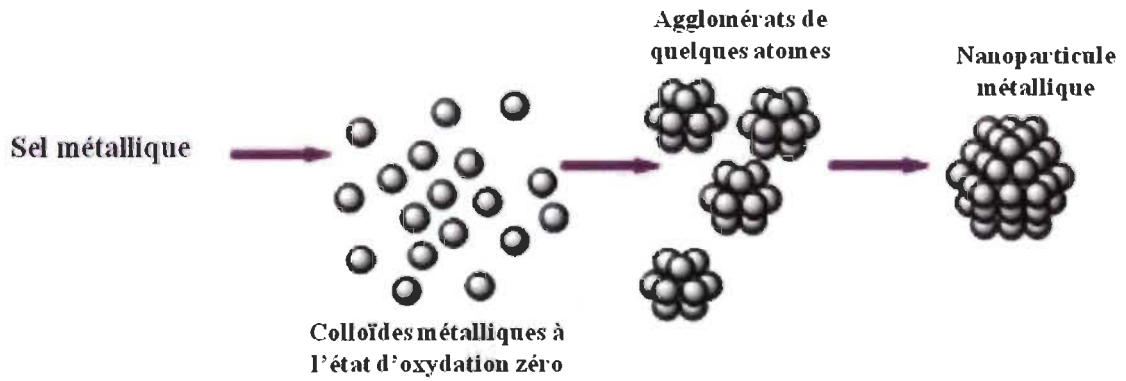

Figure A.1 Représentation schématique de la synthèse générale des nanoparticules métalliques en solution.

A.1.1 Préparation des nanoparticules d'or (AuNPs)

La procédure de préparation des nanoparticules d'or (AuNPs), dans un solvant organique, est une version modifiée[1] de celle proposée par Brust *et al.*[2], sans addition de thiols (Figure A.2). Cette méthode permet d'obtenir des nanoparticules monodisperses en tailles et de formes bien contrôlées. En général, les particules obtenues par cette méthode ont une taille inférieure à 10 nm. Sommairement, les AuNPs sont préparés par une procédure de réduction biphasique (H_2O + toluène) de l'acide tétrachloroaurique, ($HAuCl_4$) en présence d'un surfactant (le bromure de trétraoctylammonium $(C_8H_{17})_4NBr$ ou TOAB). La phase aqueuse contient du sel d'or ($HAuCl_4$, 30 mM), tandis que la phase organique, constituée de toluène, contient l'agent surfactant (TOAB, 0.1 M), étant aussi l'agent de transfert de phase des ions auriques ($AuCl_4^-$). Les ions $AuCl_4^-$, ainsi transférés dans la phase organique, sont par la suite réduits par addition, goutte à goutte, d'une solution aqueuse de borohydrure de sodium ($NaBH_4$, 0.4 M), formant ainsi les nanoparticules métalliques d'or (AuNPs). La phase organique, laquelle contient les AuNPs, est lavée, puis asséchée. Après filtration, les AuNP de couleur rose-rouge foncée sont conservées dans l'obscurité à température ambiante et sont très stables pendant plusieurs mois.

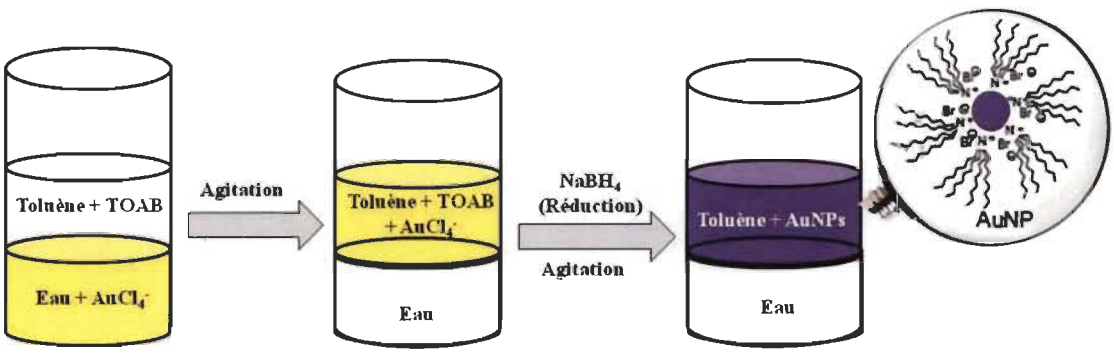

Figure A.2 Représentation schématique de la synthèse des nanoparticules d'or, par la procédure biphasique de réduction des ions auriques.

A.1.2 Préparation des nanoparticules d'argent (AgNPs)

La méthode de préparation des nanoparticules d'argent (AgNPs), dans un solvant organique, est une version modifiée de celle proposée par Korgel *et al.*[3] (Figure A.3). Brièvement, les AgNPs sont préparées par une procédure de réduction biphasique (H_2O + toluène) du nitrate d'argent ($AgNO_3$), en présence d'un catalyseur de transfert de phase (le bromure de trétraoctylammonium $(C_8H_{17})_4NBr$ ou TOAB). La phase aqueuse contient du nitrate de sodium ($NaNO_3$, 5 M), tandis que la phase organique, constituée de toluène, contient l'agent de transfert de phase (TOAB, 50 mM). Après avoir agité le mélange biphasique, une solution aqueuse de sel d'argent ($AgNO_3$, 30 mM) est alors ajoutée. Ensuite, on récupère la phase organique et on ajoute du nonanethiol (189 µL) à la solution. Après agitation, une solution aqueuse de borohydrure de sodium ($NaBH_4$, 416 M), utilisée comme agent réducteur, est injectée goutte à goutte à la solution organique, formant ainsi les nanoparticules métalliques d'argent (AgNPs). La phase organique, laquelle renferme les AgNPs, est lavée, puis asséchée. Après filtration, les AgNP de couleur jaune pâle sont maintenues dans la noirceur à température ambiante et sont d'une grande stabilité (plusieurs mois).

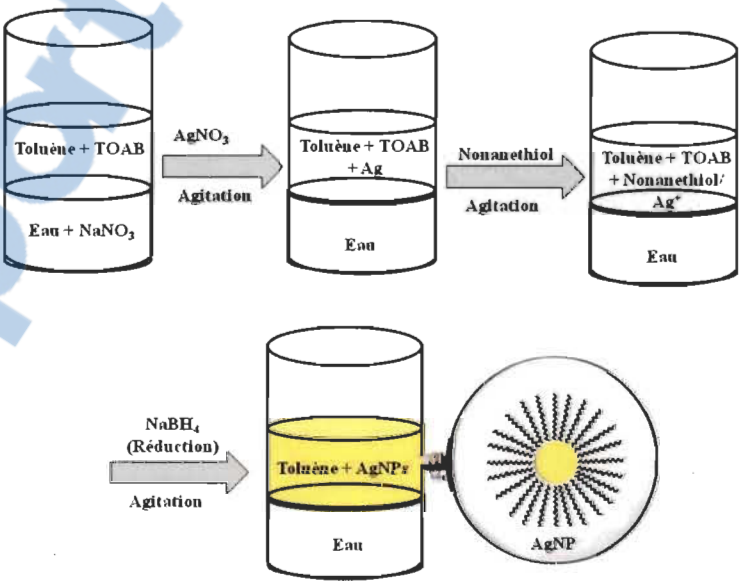

Figure A.3 Représentation schématique de la synthèse des nanoparticules d'argent, par la procédure biphasique de réduction des ions argent.

A.2 Caractérisation des nanoparticules

La caractérisation des nanoparticules (NPs) est nécessaire, établissant ainsi le contrôle de la synthèse. La caractérisation morphologique des NPs est faite en utilisant une variété de techniques différentes, principalement tirées de la science des matériaux. Les techniques courantes, exploitées dans cette thèse, sont la microscopie électronique à transmission (MET), la spectroscopie d'absorption UV-visible et la spectroscopie de photoélectrons X (XPS).

A.2.1 Microscopie électronique à transmission (MET)

La microscopie électronique à transmission est l'outil par excellence, pour caractériser la morphologie et la taille des NPs. Cette technique de microscopie consiste à placer un échantillon suffisamment mince sous un faisceau d'électrons, en utilisant un système de lentilles magnétiques projetant ainsi l'image de l'échantillon sur un écran qui transforme l'image électronique en image optique. Les effets d'interaction entre les électrons et l'échantillon donnent naissance à une image, dont la résolution peut atteindre 0,08 nanomètre, soit 1000 fois plus élevées qu'un microscope optique. Le mode d'imagerie le plus utilisé pour la visualisation des NPs est celui en champ clair. Dans ce procédé, on emploie un diaphragme, placé dans le plan focal, de manière à sélectionner uniquement le faisceau transmis en ligne droite par l'échantillon. Donc, seuls les électrons non diffractés formeront l'image sur l'écran. Conséquemment, les zones de l'échantillon diffractant fortement le faisceau (zones de fortes densités) apparaissent les plus sombres.

A.2.2 Spectrométrie d'absorption UV-visible

La spectrométrie d'absorption UV-Vis est une technique utilisant des photons, dont les longueurs d'onde sont comprises entre le domaine du spectre ultraviolet et celui du proche infrarouge. Cette technique spectroscopique est grandement utilisée, pour mettre en évidence la formation des NPs en solution par la mesure de leur spectre d'absorption.

A.2.3 Spectroscopie de photoélectrons X (XPS)

La spectroscopie XPS permet de mesurer les états électroniques dans un matériau, par irradiation d'un échantillon avec un rayonnement de rayons X monochromatique et en analysant les photoélectrons émis. Chaque élément chimique étant caractérisé par un spectre unique, cette méthode spectroscopique permet d'analyser précisément la nature chimique d'un matériau donné, c'est-à-dire qu'on peut déterminer l'état d'oxydation du matériau, ainsi que son environnement moléculaire (ou environnement chimique). En XPS, l'identification de l'état chimique d'un élément est obtenue à partir de la mesure exacte de la position des pics et de leurs séparations en énergie.

A.3 Références

(1) Jakob, M.; Levanon, H.; Kamat, P.V. Charge Distribution between UV-Irradiated TiO_2 and gold nanoparticles: determination of shift in the fermi level. *Nano Lett.*, **2003**, 3, 353-358.

(2) Brust, M.; Walker, M.; Bethell, D.; Schiffrin, D. J; Whyman, R. Synthesis of thiol-derivatised gold nanoparticles in a two-phase Liquid–Liquid system. *J. Chem. Soc, Chem. Commun.*, **1994**, **7**, 801-802.

(3) Korgel, B. A.; S. Fullam, Connolly, S.; Fitzmaurice, D. Assembly and self-organization of silver nanocrystal superlattices: ordered "soft spheres". *J. Phys. Chem. B.*, **1998**, 102, 8379-8388.